ACS Catalysis

Review

Cite This: ACS Catal. 2019, 9, 10812−10869

pubs.acs.org/acscatalysis

# Artificial Multienzyme Scaffolds: Pursuing *in Vitro* Substrate Channeling with an Overview of Current Progress

Gregory A. Ellis,*[,†] William P. Klein,[†,‡] Guillermo Lasarte-Aragonés,[†,§] Meghna Thakur,[†,§] Scott A. Walper,[†] and Igor L. Medintz*[,†]

[†]Center for Bio/Molecular Science and Engineering, Code 6900, U.S. Naval Research Laboratory, Washington, D.C. 20375, United States

[‡]National Research Council, Washington, D.C. 20001, United States

[§]College of Science, George Mason University, Fairfax, Virginia 22030, United States

**ABSTRACT:** Artificial multienzyme scaffolds are being developed for *in vitro* cascaded biocatalytic activity and, in particular, accessing substrate channeling. This review covers progress in this field over the last ∼5 years with a specific focus on the scaffold materials themselves and the benefits they can provide for assembling multienzyme cascades *in vitro*. These benefits include improving biocatalytic efficiency, bypassing potential cellular toxicity, directed catalysis, modularity, incorporating enzymes from different prokaryotic and eukaryotic sources, and potentially the ability to create *de novo* designer cascades. We begin with an overview of the strongest impetus currently driving the rapid development of this field, namely, biomanufacturing and cell-free synthetic biology. We then discuss in detail pertinent mechanisms responsible for the benefits of artificial multienzyme scaffolds. In particular, we focus on substrate channeling, including the evolving debate about what leads to substrate channeling in artificial systems—proximity, confinement, or both—and whether sequential enzyme order is really needed. How different scaffold materials/chemistries can in turn affect enzyme activity is also discussed. The bulk of the review then details progress in the development of different biotic (*e.g.*, cells) and abiotic (*e.g.*, nanoparticles) scaffolding materials and is divided up by class and subtype as needed. Within each material class of scaffolds, attention is given to their inherent chemical diversity, how they are engineered, how they allow for enzymatic attachment, their ease of use, their benefits (*e.g.*, inherent three-dimensional architecture) and liabilities where appropriate, and other relevant issues. For each scaffolding material, a detailed overview of current progress is provided using examples of multienzyme cascades and data/schematics reproduced from the literature. Special attention is also given to the use of DNA scaffolds, as they can potentially provide the most versatile designer three-dimensional scaffold architectures. Finally, a short perspective on how this rapidly moving field will evolve in the near and long terms is provided.

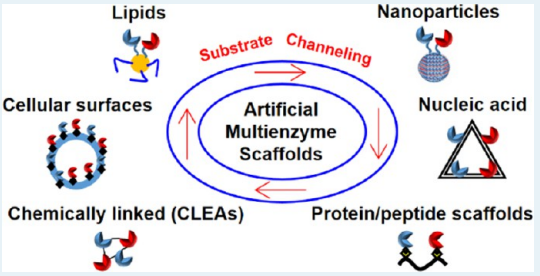


**KEYWORDS:** *enzyme, scaffold, biocatalysis, substrate channeling, nanoparticle, DNA*



## INTRODUCTION

Over the last few decades, individual enzymes have emerged as complementary catalysts to traditional organic or organometallic materials for chemical processes.[1] Despite misconceptions, these enzymes can be relatively inexpensive, fairly stable, and functional in partially organic solvent and can accept both natural and non-natural substrates.[2−4] Enzymes are currently used in the pharmaceutical, chemical, food, and detergent industries and have both degradative and synthetic uses (*e.g.*, proteases for laundry detergent and lipases for chiral resolution of pharmaceuticals and wax ester synthesis for cosmetics).[1,3] They can also act as biosensors and can be coupled to nanomaterials to endow them with bioresponsiveness or biocompatibility.[3,5] Enzymes enjoy many advantages as catalysts for these processes, including the ability to use water as a "green" solvent, the capability to perform reactions at ambient temperature and pressure, and the potential to engage in substrate and product regio- and stereoselective chemistries.[1,3]

For all of the benefits of enzymatic catalysis, currently we have only scratched the surface of its full potential. While industry typically uses single-enzyme processes, the inspiration for these catalysts—nature—typically employs enzymes in the form of multienzyme cascades, reflecting the vast bioprocess opportunities available if one can harness multiple enzymes simultaneously.[6] The use of "one-pot" multienzymatic cascades, particularly linear cascades, can generate multiple benefits: (1) as no processing steps (*e.g.*, purification) are needed between reactions, the overall process time and waste are decreased; (2) unstable/toxic intermediates do not accumulate but can immediately proceed to the next step, making processes safer

Received: June 10, 2019
Revised: September 6, 2019

  

DOI: 10.1021/acscatal.9b02413
ACS Catal. 2019, 9, 10812−10869

and minimizing the risk of side reactions; and (3) a reversible reaction can be driven forward by a proceeding irreversible reaction, increasing the yield.[7]

Multienzymatic cascades can be grouped into four categories: linear, orthogonal, parallel, and cyclic (see Figure 1 for a descriptive schematic).[7,8] In linear cascades, one substrate is ultimately converted to one product through multiple enzymes and intermediates. In orthogonal cascades, one substrate is converted to one product but requires a cosubstrate or cofactor or generates a byproduct; the cosubstrate or cofactor is generated by a second enzyme, or a second enzyme removes the undesired byproduct. In the closely related parallel cascades, two substrates are converted to two products, and the two reactions are coupled by cosubstrate or cofactor use; these cascades differ from orthogonal cascades in that both products are desired, though one could potentially consider the orthogonal cascade as just a combination of the linear and parallel cascades. Finally, in cyclic cascades, from a mixture of substrates (*e.g.*, D and L enantiomers), only one (*e.g.*, the D enantiomer) is selectively converted but then in the second reaction is converted back to a mixture of substrates (*e.g.*, D and L enantiomers); over multiple cycles, the nonreactive substrate (*e.g.*, the L enantiomer) accumulates. If this second step proceeds through a nonenzymatic chemical reaction, strictly speaking this is a chemo-enzymatic cascade. Importantly, in nature these multienzyme cascades are often structurally or functionally assembled together or encapsulated, which can enhance their benefits and endow other utility as discussed below.[6,9−15] Moreover, within cells multienzyme cascades are functionally interconnected with each other in many cases and thus can be subject to complex competition processes.

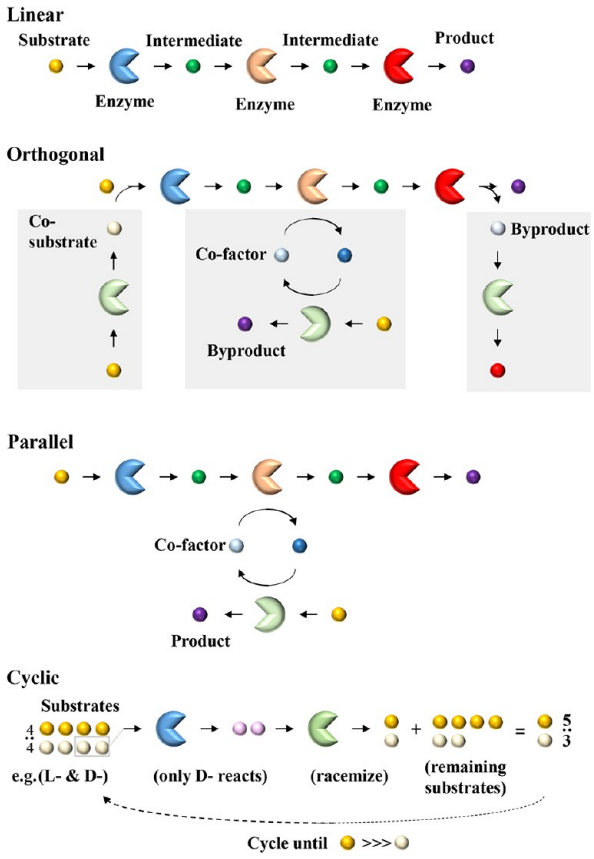


**Figure 1.** Multienzymatic cascades. The functionality or mechanism behind cascaded enzyme structures can be grouped into four primary categories: linear, orthogonal, parallel, and cyclic.[7,8] In linear cascades, one substrate is ultimately converted to one product through multiple enzymes and intermediates. In orthogonal cascades, a cosubstrate or cofactor is generated by a second enzyme or a second enzyme removes the undesired byproduct. In parallel cascades, two reactions are coupled by cosubstrate or cofactor use; importantly, in this case both products are desired, though one could potentially consider the orthogonal cascade as just a combination of the linear and parallel cascades. In cyclic cascades, from a mixture of substrates (*e.g.*, D and L enantiomers), only one type (*e.g.*, the D enantiomer) is selectively converted to an intermediate and subsequently converted back to a mixture of substrates (*e.g.*, D and L enantiomers); over multiple cycles, the nonreactive substrate (*e.g.*, the L enantiomer) accumulates. The second step can be chemical instead of enzymatic, making the process a chemo-enzymatic cascade. Adapted with permission from ref 7. Copyright 2011 Wiley-VCH Verlag GmbH & Co. KGaA, Weinheim.

In nature, two key examples of multienzyme cascades are natural product biosynthetic clusters and carbohydrate-degrading cellulosomes.[12] While natural product biosynthetic clusters, including nonribosomal peptide synthetases (NRPSs) and polyketide synthases (PKSs), do not have scaffolds *per se*, the enzymes are linked by protein−protein interaction domains that transfer linked intermediates using a "swinging arm" mechanism. This specifically allows for directed catalysis and minimizes off-target pathways, enabling a diverse set of natural products.[12,15] Cellulosomes use a protein scaffold made of cohesin domains residing at the bacterial outer cell membrane that binds degradative enzymes with complementary dockerin domains. This facilitates degradation of cellulose by bringing the multienzyme cascade close to the extracellular substrate, maintaining higher local concentrations of intermediates versus their loss by diffusion into the environment, and assembling the correct ratio and order of enzymes.[6,12]

Inspired by these and other natural scaffolds, researchers have sought to engineer both biotic and abiotic artificial multienzyme scaffolds. Among the strongest impetuses currently driving the rapid development of this field are cell-based biomanufacturing and cell-free synthetic biology. In cell-based biomanufacturing, microorganisms (*e.g.*, bacteria, yeast) are engineered to produce a desired product through incorporation of heterologous pathways, metabolic engineering of endogenous pathways, or a combination of the two.[12,16] One seminal example of research toward improving cell-based biomanufacturing by application of artificial multienzyme scaffolds, albeit intracellularly, is the assembly of three enzymes in the cascade for production of the artemisinin precursor artemisinic acid by the Keasling laboratory, as shown in Figure 2.[17−19] To improve upon the *in vivo* pathway, the authors engineered a protein-based scaffold to assemble the enzymes acetoacetyl-CoA thiolase (AtoB, *Escherichia coli*), hydroxyl-methylglutaryl-CoA synthase (HMGS, *Saccharomyces cerevisiae*), and hydroxyl-methylglutaryl-CoA reductase (HMGR, *S. cerevisiae*) toward increased production of the artemisinic acid precursor mevalonate (Figure 2A). The authors reasoned that this heterologous pathway was causing a high metabolic load on the cell; to alleviate this, they could scaffold this part of the cascade together at the correct enzyme ratios to enhance the efficiency of the pathway, which would allow for decreasing enzyme expression (and therefore metabolic load) while maintaining (or increasing) product titers (Figure 2B). Scaffolding these enzymes at a ratio of 1:2:2 enhanced the


DOI: 10.1021/acscatal.9b02413
ACS Catal. 2019, 9, 10812−10869

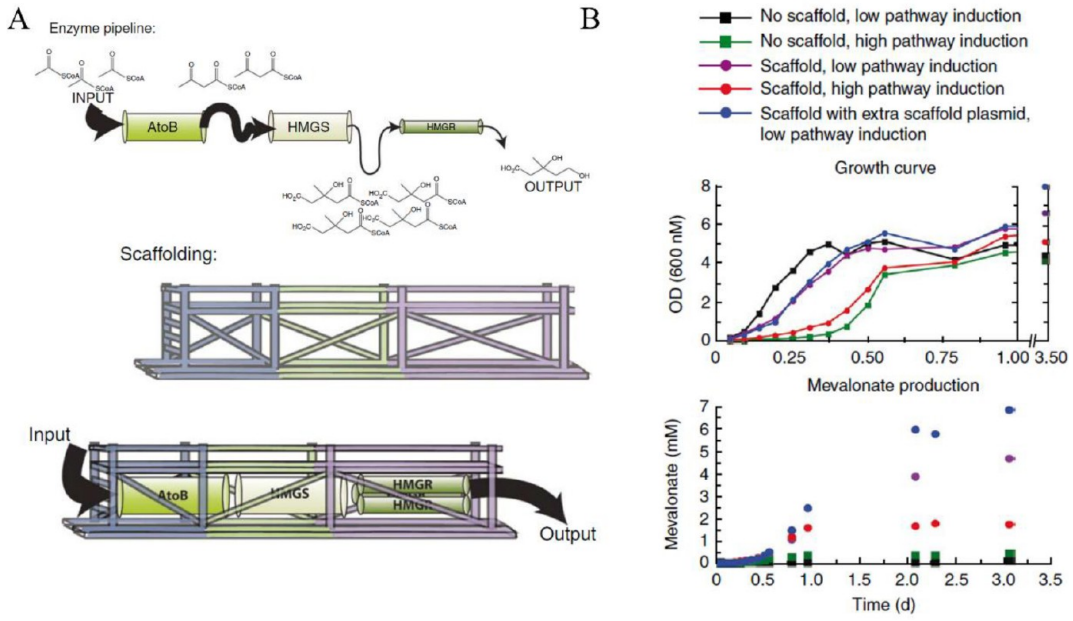


**Figure 2.** Mevalonate biosynthetic cascade. (A) The genes encoding the mevalonate pathway enzymes (HMGS and HMGR) were taken from yeast (*S. cerevisiae*) and inserted into *E. coli* along with the *E. coli* gene encoding AtoB. These enzymes have different levels of activity, creating a bottleneck that results in accumulation of the intermediate HMG-CoA, which is toxic to *E. coli* at high concentrations.[18] Fluxes through each enzymatic step can be compared to pipes of different cross-sectional areas put together to make a pipeline. The thicknesses of the arrows connecting these enzymes represent the fluxes through these respective steps, and the resultant relative accumulations of intermediates are also depicted. The scaffolded pathway is more efficient as a result of colocalization of the mevalonate enzymes to the same complex as well as optimization of the enzyme stoichiometry to balance the units of activity at the complex. (B) Expression of the scaffold (G1S2P2) allows more mevalonate to be produced at low pathway induction. At this low induction, the growth rate of *E. coli* is dramatically increased over strains with the pathway highly induced. A high-copy plasmid expressing additional scaffold (G1S2P2) did not hinder the growth but further improved the titer. Reproduced with permission from ref 17. Copyright 2009 Springer Nature.

intracellular production of mevalonate by 77-fold relative to free tagged enzymes.[17]

Cell-free synthetic biology is a more minimalistic equivalent of cell-based biomanufacturing. Products are produced either in cell lysate (*e.g.*, transcription−translation (TX-TL) systems) or using purified enzymes in buffer. Cell lysate systems come with the advantage of producing reaction enzymes from added DNA *in situ* but can require several exogenously added components besides cell lysate, including buffer, salts, dithiothreitol, nucleotides, a tetrahydrofolic acid derivative (*e.g.*, folinic acid), tRNAs, amino acids, nicotinamide adenine dinucleotide ($NAD^+$), coenzyme A, spermidine, putrescine, oxalate, phosphoenolpyruvate, and optional exogenous T7 RNA polymerase.[20,21] "Bare-bones" purified enzyme systems, sometimes called synthetic biochemistry,[22] require a buffer (and/or solvent) that allows for enzyme function as well as substrate, intermediate, and product solubility; they also require any cofactors needed for the reaction (*e.g.*, $NAD^+$). Regardless of the cell-free system, advantages of this approach can include (1) the ability to produce intermediates and products that would be toxic to cells; (2) the ability to minimize or remove off-target pathways, including those involving host metabolism, a competing branch point, or those occurring during purification from cells; (3) increased options for engineering methods to minimize product inhibition; (4) increased options for solvent conditions to facilitate solubility of substrates, intermediates, and products; (5) wider flexibility in controlling reactions; and (6) no requirement for substrates or products (and importantly for this discussion, scaffolds) to cross cell membranes.[12,23] However, cell-free synthetic biology can also be limited by (1) reduced kinetics due to farther diffusion of substrates and intermediates in reaction vessels compared with the small femtoliter to picoliter confines of a cell; (2) forced "one-pot" reactions where all of the enzymes are required to be compatible with regard to pH, temperature, and cofactor utilization; (3) cross-reactivity between substrates, intermediates, and products (although flow reactions may help mitigate some of these concerns); and (4) in the case of purified enzymatic systems a lack of automatic enzyme regeneration.[12]

Herein we review recent efforts to engineer artificial scaffolds to assemble multienzyme cascades that are meant to empower next-generation bioprocesses. Our focus is on *in vitro* scaffolded systems only, and therefore, we do not discuss enzyme encapsulation in particular, as this approach tends to be mechanistically quite different. However, we do discuss some systems that do manifest an encapsulation process, including metal−organic frameworks (MOFs), hydrogels, and carbon nanotubes. For an excellent overview detailing enzyme encapsulation techniques with their own pertinent mechanisms for enzymatic enhancement, we direct the reader to a recent review by Kuchler *et al.*[11] Furthermore, while our review focuses largely on non-intracellular systems to avoid complications of cellular processes and effects due to encapsulation in the cell, in selected cases we do include these examples to highlight specific systems of interest. Specifically, we cover progress over the last ∼5 years in the development of artificial multienzyme scaffolds in pursuit of *in vitro* cascaded biocatalytic activity, with an eye in particular toward those that are capable of demonstrating or have potential for accessing substrate channeling. We especially focus on the scaffold materials themselves, covering research on biotic scaffolds including cellular surfaces, natural and engineered proteins, peptide


DOI: 10.1021/acscatal.9b02413
*ACS Catal.* 2019, 9, 10812−10869

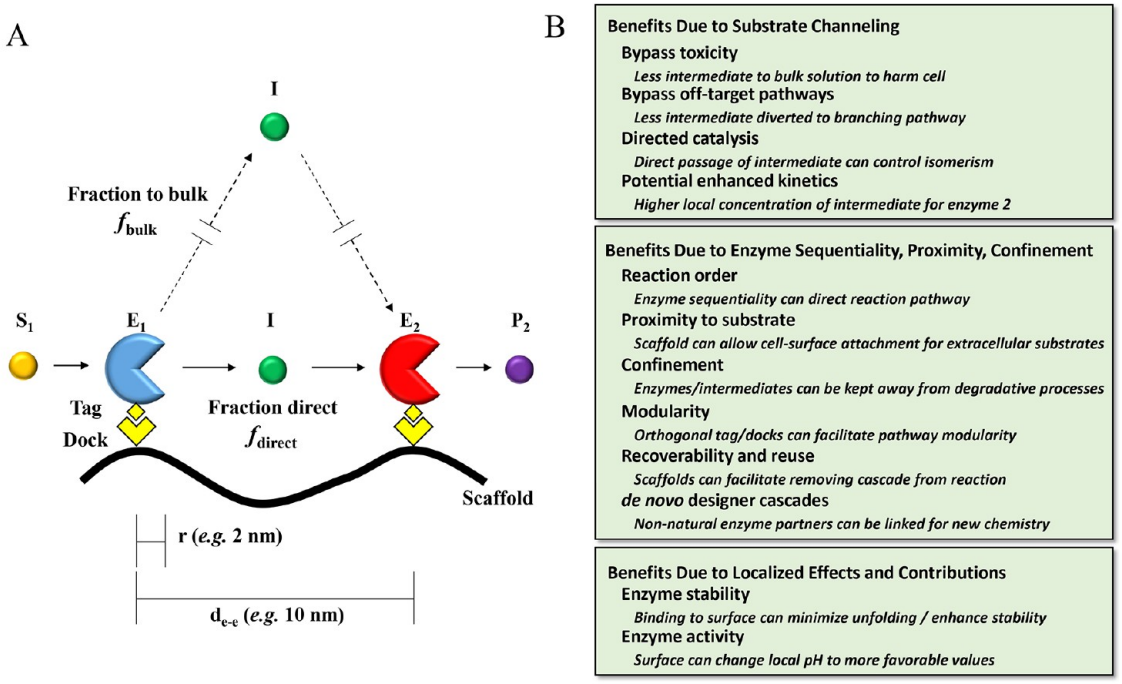


**Figure 3.** Potential benefits suggested from artificial multienzyme scaffolds. (A) In this example of an artificial multienzyme scaffold, enzyme 1 ($E_1$), with its substrate (S) and product (the "intermediate", I), is in a cascade with enzyme 2 ($E_2$), which takes the intermediate as its substrate and makes the final product (P). The intermediate can either travel directly between the enzymes ($f_{direct}$) or diffuse from $E_1$ into bulk solution before encountering $E_2$ ($f_{bulk}$) The radius of the enzyme ($r$), the distance between enzymes ($d_{e-e}$), the type of scaffold, and the type of attachment (*e.g.*, tag/dock) can all play a role in the benefits from artificial multienzyme scaffolds.[10,27,28,30−32] (B) Overview of some potential mechanisms responsible for the benefits of artificial multienzyme scaffolds.[29]

scaffolds, multienzyme fusions, chemically linked enzyme aggregates, DNA and other nucleic acid scaffolds, and other biopolymers. We also cover abiotic scaffolds including nanoparticles (NPs), polymers, MOFs, and others. We utilize selected examples for our discussion and extend our apologies for any and all omissions. Our hope is that this discussion will facilitate future engineering efforts for both novices and those experienced with artificial multienzymatic scaffolds. Demonstrating the high interest in this field, we also point the interested reader to other excellent recent reviews of related subject matter.[24−26] We begin by providing a short overview of the mechanisms underlying the functional benefits of artificial multienzyme scaffolds, in particular enzyme channeling processes, and some of the continuing debate surrounding how they may actually function. This is meant to provide a context for interpreting the examples highlighted in the subsequent sections.

## POTENTIAL MECHANISMS UNDERLYING THE FUNCTIONAL BENEFITS OF MULTIENZYME CASCADED SCAFFOLDS

Utilizing scaffolds for multienzyme assembly brings with it access to several potential functional benefits, which fall under three loosely grouped and related mechanisms: (1) substrate channeling; (2) enzyme sequentiality, proximity, confinement, or some combination thereof; and (3) localized scaffolding effects (for an overview, see Figure 3).[10,27−32] Understanding these pertinent mechanisms, especially some of the debate that still surrounds them, allows for both the full potential and challenges of artificial enzyme scaffolds to be appreciated.

**Substrate Channeling.** The first mechanism potentially provided by a multienzyme scaffolded cascade is that of substrate channeling. In the strictest terms, this is the direct transmission of substrate/intermediate from one enzyme to the next, bypassing diffusion into the bulk medium; leaky or probabilistic substrate channeling still enhances the overall catalytic flux through the cascaded enzymes but also allows for some diffusion to the bulk medium (Figure 3A).[10,30−32] Four key benefits can be anticipated from minimizing the bulk diffusional loss of an intermediate from a source enzyme to that of a direct downstream enzyme: (1) bypassing cellular toxicity of intermediates; (2) curtailing reactive intermediates from participating in off-target pathways; (3) directed multistep catalysis; and (4) enhanced kinetics under specific conditions (Figure 3B, top panel).[29]

The primary example epitomizing substrate channeling in nature is the tryptophan synthase complex, where a hydrophobic channel facilitates transport of indole from one active site to another and increases the reaction rates by 1−2 orders of magnitude.[12] The distance of substrate channeling in the tryptophan synthase complex case is very short (~2.5 nm) and also is chemically facilitated *via* the hydrophobic nature of the channel itself.[12,31−35] Intuitively, it seems that substrate channeling and the benefits thereof could be extended to artificial multienzyme scaffolds when enzymes are placed close together (Figure 4A).[14]

However, while most agree that substrate channeling in artificial multienzyme scaffolds can bypass toxicity and off-target reactive pathways,[12] the idea of significantly enhancing the kinetics solely on the basis of bringing enzymes into close proximity (*e.g.*, ≤10 nm) is contested. Other methods of


DOI: 10.1021/acscatal.9b02413
ACS Catal. 2019, 9, 10812−10869

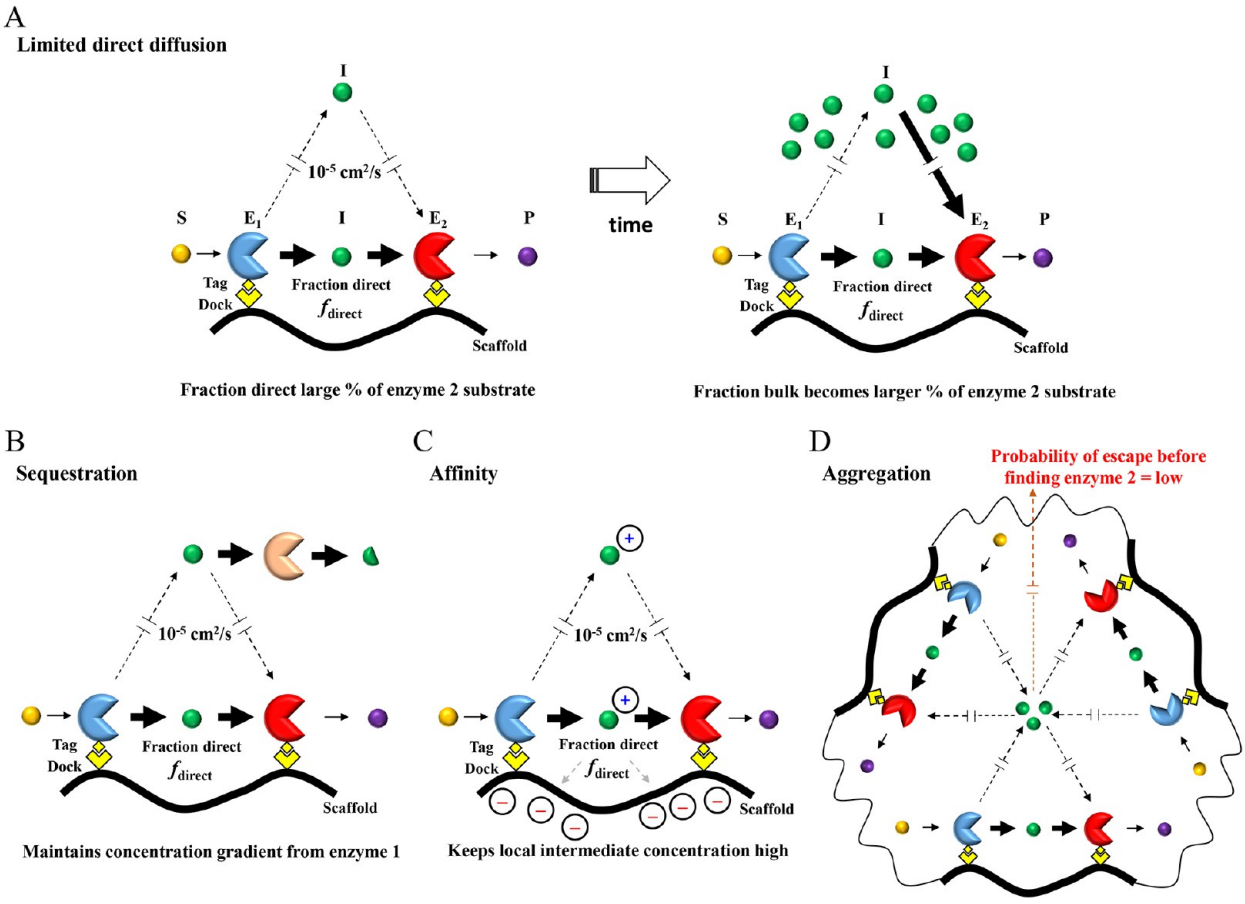


**Figure 4.** Mechanisms behind the beneficial effects of substrate channeling. The four mechanisms of substrate channeling that can benefit multienzyme cascades are (A) limited direct diffusion, (B) sequestration, (C) affinity, and (D) aggregation.[28] Limiting direct diffusion by proximity typically enhances the kinetics transiently, as intermediate accumulates in the bulk solvent and becomes the dominant contributor to enzyme 2. Sequestration protects intermediates from alternative reactions; these alternative reactions limit the accumulation of intermediate in the bulk solvent, which allows for sustained benefit from scaffolding. Affinity between the scaffold and intermediate keeps the local concentration of intermediate high by creating a barrier to diffusion and can enhance the kinetics relatively long-term. Aggregation increases the likelihood that intermediate escaping from one reaction pair will react with another reaction pair rather than diffuse to the bulk solvent; this effect is anticipated to occur with multiple enzymes scaffolded onto a nanoparticle as well. $E_1$ = enzyme 1 with substrate $S_1$ and product I (the "intermediate"); $E_2$ = enzyme 2 with substrate I and product $P_2$.

substrate channeling, such as creating barriers to diffusion, will be discussed further below.[12,32,36] Two similar yet distinct counterarguments have been made against invoking substrate channeling as a mechanism for increased kinetics on artificial multienzyme scaffolds, as iterated in depth by Hess, Fernie, and others:[28,37] (1) for typical enzyme scaffolded distances and the high rate of diffusion, bulk-diffused intermediate quickly accumulates and becomes the dominant contribution to the reaction rate within seconds;[28] (2) the diffusion rate (*e.g.*, $1 \times 10^9$ nm$^2$/s)[28,38] is orders of magnitude higher than most enzyme reaction rates (*e.g.*, $k_{cat}/K_M = 10^5$ M/s),[9,14,39] and therefore, channeling cannot contribute significantly to the overall reaction rate since it will not be the rate-limiting step.[9,14,37,39] The exception where channeling could contribute would be during the lag-phase buildup to the steady state. It is worth delving briefly into each of these arguments.

For the following, we assume a two-enzyme reaction cascade, in which enzyme 1 ($E_1$) converts a substrate (S) into an intermediate (I), which is then used as the substrate for enzyme 2 ($E_2$) and converted into the final product (P), as shown in eq 1:

$$E_1 + S + E_2 \overset{K_{M,2}}{\rightleftharpoons} E_1S + E_2 \underset{v_1;V_{max,1}}{\overset{k_{cat,1}}{\rightleftharpoons}} E_1 + I + E_2$$
$$\overset{K_{M,2}}{\rightleftharpoons} E_1 + E_2I \underset{v_2;V_{max,2}}{\overset{k_{cat,2}}{\rightleftharpoons}} E_1 + E_2 + P \quad (1)$$

Under Michaelis–Menten kinetics, $K_{M,1}$ and $K_{M,2}$ are the Michaelis constants, $k_{cat,1}$ and $k_{cat,2}$ are the turnover rates, $v_1$ and $v_2$ are the velocities, and $V_{max,1}$ and $V_{max,2}$ are the maximum velocities for $E_1$ and $E_2$, respectively.[28] We also assume that $E_1$ is the rate-limiting enzyme since if $E_2$ were rate-limiting the intermediate would accumulate regardless of channeling.[32,40]

The first question in this context concerns the fraction of the intermediate that is directly channeled between $E_1$ and $E_2$ ($f_{direct}$). This can be estimated using eq 2,

$$f_{direct} = \frac{r}{d_{e-e}} \quad (2)$$

where $r$ is the radius of $E_2$ and $d_{e-e}$ is the distance between enzymes.[27,28] Assuming a radius of 2.5 nm for $E_2$ (*e.g.*, for horseradish peroxidase, which is close to that estimated for a 50



DOI: 10.1021/acscatal.9b02413
ACS Catal. 2019, 9, 10812−10869

kDa enzyme, ~2.4 nm)[28,41,42] and a scaffolded separation distance of 10 nm between enzymes, a calculated 25% of the intermediate flows directly to $E_2$, yet 75% escapes to bulk solvent! How does this compare to the nonscaffolded case? The distance between free-floating enzymes decreases as the their concentrations increase; this distance ($d_{e-e}$ in nm) can be estimated using eq 3,

$$d_{e-e} \approx \frac{1.18}{C^{1/3}} \tag{3}$$

where $C$ is the molar concentration (also see Figure 5 for a quantitative plot).[41]

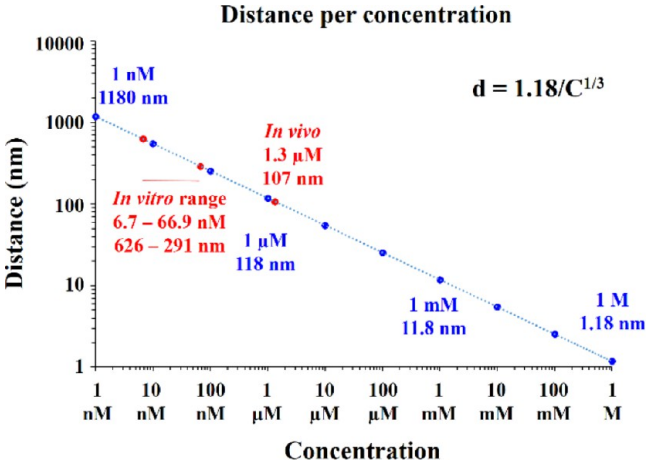


**Figure 5.** Enzyme concentration directly influences the substrate channeling efficiency. To estimate the distance between protein molecules, their molar concentration $C$ can be converted to units of molecules/nm$^3$ as $CN_A/(10^{24}$ nm$^3$/L) = 0.6$C$ molecules/nm$^3$. The reciprocal of this, 1.66/$C$ nm$^3$/molecule, can be used as an estimate of the volume per molecule. Estimating the average separation between molecules as the cube root of the volume per molecule gives $d = 1.18/C^{1/3}$ nm.[41] In the graph, red values highlight the average concentration of proteins in bacterial cells ("*in vivo*", *e.g.*, cell-based manufacturing)[23,43] and the range of concentrations of proteins for cell-free synthetic biology ("*in vitro*");[23,43] the "*in vivo*" value gives a shorter distance between proteins than the "*in vitro*" values. The fraction directly channeled can be determined as the ratio of the enzyme radius ($r$) to the separation distance ($d_{e-e}$); radii can be estimated on the basis of enzyme size.[27,28,41]

Within cell-based biomanufacturing (*i.e.*, intracellular or cytosolic enzyme catalysis), free-floating enzymes (assumed to have a concentration of ~1.3 $\mu$M)[23,43−46] would have a distance of ~107 nm, giving $f_{direct} \approx 2.3\%$. For cell-free synthetic biology, a given free-floating endogenous enzyme (assumed to have a concentration of ~36.8 nM)[23,43−46] would have a distance of ~458 nm, giving $f_{direct} \approx 0.6\%$. Both of these $f_{direct}$ percentages are significantly lower than for the scaffolded example above (25%). However, given the possible high amount of production of heterologously expressed proteins (*e.g.*, 20% of total cellular protein),[47] the amount of enzyme could increase significantly, decreasing the distance and putting $f_{direct}$ on the order of ~6−22% for cell-free and cell-based systems, respectively, close to that found on the scaffolded example. Therefore, using a scaffold could increase $f_{direct}$ substantially for endogenous enzymes but would have less effect for highly expressed heterologous enzymes. It should be noted that these values are rough approximations and are given here simply to put these issues in proximate context.

The first counterargument to the contention that artificial multienzyme scaffolds enhance the reaction rate through close-proximity-based substrate channeling is that any kinetic benefit would occur only transiently, as the fraction of intermediate that is directly channeled gets overwhelmed by the accumulating intermediate fraction that escapes to the bulk solvent.[28,29,40,48,49] To determine the time in which scaffolding may improve the kinetics, Idan and Hess detailed an elegant mathematical derivation to describe the channeling time ($\tau_{ch}$):

$$\tau_{ch} \approx \frac{V}{4\pi D d_{e-e}} \tag{4}$$

where $V$ is the volume of the container, $D$ is the diffusion coefficient of the substrate, and $d_{e-e}$ is the distance between enzymes (eq 4).[28,48] This equation was derived under the assumptions that [S] ≫ $K_{M,1}$ (*i.e.*, Briggs−Haldane conditions) and [I] ≪ $K_{M,2}$, as would be the case for initial reaction rates. Importantly, one can see that this equation is not dependent on the rates of the enzymes themselves.[28]

How would this apply to practical examples? For cell-based manufacturing, assuming a bacterial volume of 1 fL (i.e., $1 \times 10^9$ nm$^3$),[44,46,50,51] a diffusion coefficient of $1 \times 10^9$ nm$^2$/s (*i.e.*, $H_2O_2$ in $H_2O$ at 25 °C),[28,38] and a scaffolded distance of 10 nm, the time over which the scaffold will improve the kinetics is only ~8 ms. This intuitively makes sense if 75% of the intermediate is escaping to the bulk solvent in a fairly limited volume like a cell, where it will quickly accumulate and dominate the reaction. Conversely, for cell-free synthetic biology, a much larger reaction volume could be assumed (*e.g.*, 1 mL); for the same diffusion coefficient and scaffolded distance, the time over which the scaffold will improve the kinetics increases to *years*. However, both of these examples assume only one reaction pair in the reaction volume. In reality, reaction pairs could be in the micro- to millimolar range, and presumably, intermediate from one reaction pair that is escaping to "bulk solvent" will react with the second enzyme of another reaction pair upon encountering it; this would then act to greatly decrease the time over which channeling is important as well. Given the presence of multiple reaction pairs, it would be difficult to experimentally measure the amount of intermediate that reacts within a given reaction pair ($f_{direct}$) versus going to bulk solvent versus reaction with another reaction pair. Most experimental setups would require conditions that may change the conditions (*e.g.*, microfluidics with each pair in a separate channel; mutated second pairs that covalently capture intermediates versus turning them over; competitive enzymes). Therefore, the best information can be expected from well-designed and validated theoretical simulations in conjunction with experimental confirmation.

The second counterargument to the idea that artificial scaffolds enhance the reaction kinetics through close-proximity-based substrate channeling is that the diffusion rates are orders of magnitude higher than the enzyme rates and therefore should not be the rate-limiting step.[9,14,28,37−39] To investigate this counterargument, one would first like to know how the concentration of the intermediate changes with distance from the active site of $E_1$. This can be calculated using eq 5:[32,36]

$$c(r, t) = \sum_{i=0}^{(t/\tau)-1} \frac{1}{4\pi D(t - i\tau)^{3/2}} \exp\left[-\frac{r^2}{4D(t - i\tau)}\right] \tag{5}$$



DOI: 10.1021/acscatal.9b02413
ACS Catal. 2019, 9, 10812−10869

where $c(r, t)$ is the concentration at radial distance $r$ at time $t$, $D$ is the diffusion coefficient, and $\tau$ is the time between reaction events ($\tau = 1/k$, where $k$ is the turnover frequency). Once the system reaches steady state (estimated as $t = 10^4\tau$), for $k = 10$ $s^{-1}$ and $D = 1 \times 10^9$ $nm^2/s$, the concentration of intermediate is approximately the same between 0 and 5 $\mu$m from the active site of $E_1$.[32,36] It should be noted that this time frame selected for steady state, estimated as $10^4\tau$ with $k = 10$ $s^{-1}$ and $\tau = 1/k \approx 16.7$ min, is in line with the point referenced by Idan and Hess that enzyme kinetics analyses need to be done long enough that they go beyond the lag time to the steady state.[28] Only when the enzyme is very quick (turnover frequency of 1000−10000 $s^{-1}$) at the same $D$ is there a large difference in intermediate concentration but only between 1 and 5 $\mu$m distance (small difference at 100 $s^{-1}$).[32] Since a distance of 1 $\mu$m would correspond to ∼1.64 nM enzyme (using $C = (1.18/d)^3$),[41] this would indicate that scaffolding would only really affect the kinetics if the analogous scaffold-free reaction were conducted at <1.64 nM.[32,36] This is much lower than typical values for cell-based manufacturing (∼1.3 $\mu$M enzyme), somewhat less than for cell-free synthetic biology (∼36.8 nM enzyme), and even lower for a highly expressed heterologous protein.[23,43] However, if one did work in this dilute regime, scaffolding may certainly help improve the kinetics over that for freely diffusing enzymes.[14] Furthermore, if one is working with "catalytically perfect" enzymes with $k_{cat}/K_M$ at or above the diffusion rate, scaffolding may help even more.[14] Finally, it is interesting to note that while enzymes may be attached at scaffold distances of 10 nm, if they are tethered *via* flexible linkages, then depending on the active-site orientation they may be able to move much closer to each other than 10 nm, which could improve the effect of scaffolding.[36,52]

Interestingly, this concept of the difference between enzymatic reaction rate and diffusion rate was also addressed by Buchner *et al.*[53] In their theoretical analysis, they addressed the idea of determining how much an intermediate is subject to "enzyme exposure" and determined a factor $\alpha$ that correlates the enzymatic reaction rate to the diffusion rate. They surmised that for $\alpha < 1$, i.e., when the enzymatic reaction time is much greater than the diffusion time (the reaction is relatively slow), clustering enzymes is better to maximize exposure of the intermediate to the second enzyme before it escapes and quickly diffuses away. Conversely, for $\alpha \gg 1$, i.e., when the enzymatic reaction time is much less than the diffusion time (the reaction is relatively fast), distributing some or all of the second enzyme is a "bet-hedging" strategy that helps to capture/react with intermediate before it diffuses away. The authors also derived equations that can help direct what fraction of the second enzyme should be clustered versus distributed in a one-dimensional system, which will be qualitatively related to higher-dimensional systems. Importantly, in this work, the authors described a boundary where intermediates are "absorbed/lost" if they encounter it, whereas the Idan and Hess analyses focus on boundaries that allow reflection and accumulation of the intermediate.[28,29,48,53] With this said, the Buchner *et al.* boundary could be seen to approximate degradation of the intermediate over time/travel or an encounter with a competitive/degradative enzyme.

Given these arguments, are there situations in which substrate channeling using artificial scaffolds CAN enhance multienzyme cascade kinetics? There are three situations outlined by Idan and Hess where substrate channeling can improve the overall kinetics, as illustrated in Figure 4B−D. The first is by sequestration, where there is an off-target reaction (*e.g.*, the intermediate undergoes oxidative degradation, causes a toxic effect on the cell, or is consumed by another reaction or the reaction is highly reversible; see Figure 4B).[28,54] It has been shown that there can be protection of intermediates due to channeling; furthermore, Idan and Hess showed that there is a long-term kinetic enhancement if the reaction is competing against an off-target reaction.[12,28,31,55] This can be described by eq 6:

$$\frac{k_{2,scaf}}{k_{2,free}} = 1 + \frac{V}{4\pi D d_{e-e}} R \tag{6}$$

where the $k_{2,scaf}/k_{2,free}$ ratio represents the benefit of the scaffold and $R$ is the rate of the off-target reaction.

For the reaction examples used above with $R = 10$ $s^{-1}$ and $V$ set equal to the volume occupied by an enzyme pair at the concentration for cell-based/cell-free systems, the ratio does not increase beyond 1.04.[9,14,28,39,56] This is due to the relatively high enzyme concentrations and therefore small volumes. However, the ratio can become substantial when the occupied volume is decreased (*i.e.*, the concentration of enzymes is decreased), $R$ is increased (*i.e.*, the competing reaction is very fast), the distance between enzymes on the scaffold is decreased (*e.g.*, 1 nm), or the rate of diffusion is decreased (*e.g.*, with viscogens or using a high-concentration environment like a cell).[28]

The second way in which substrate channeling can cause enhanced kinetics is if the scaffold itself (or the assembled enzymes) have affinity for the intermediate and present a barrier to diffusion (Figure 4C).[28,56,57] This could be the case for enzymes scaffolded onto anionic DNA with a cationic intermediate.[57] It has been shown that this affinity has to be moderate and can be considered as mimicking the Sabatier principle, which makes intuitive sense; if the affinity is too high, the scaffold would prevent the intermediate from binding to enzymes, while too-low affinity would not matter overall.[57,58] This effect can last from minutes to hours.[28]

Finally, the third way in which substrate channeling can enhance the kinetics is through aggregation of the scaffold (Figure 4D). If scaffolds encourage aggregation of enzyme pairs (as has been suggested for some systems),[28,56,59] then the chance that the intermediates heading toward the bulk solution (*e.g.*, ∼75%) will encounter another $E_2$ before fully diffusing dramatically increases, thereby increasing the overall reaction rate moderately long-term; this can be considered as a type of probabilistic substrate channeling.[28] In these cases, it is thought that the dimensions of the scaffold itself actually matter less than the presence of the scaffold and aggregation.[28,56] Models have shown that under selected conditions the optimal size of aggregates is ∼260 nm and the optimal separation between coclusters is 6.5 $\mu$m and that the flux could increase by 6-fold (for a two-step cascade) to over 100-fold (for a three-step cascade) compared with free enzymes in a cell.[12,14,60]

In view of the complexity of the substrate channeling issue, conducting experiments on emergent artificial multienzyme scaffolds to determine whether they are engaging in substrate channeling is important. Spivey and Ovádi[31] and Wheeldon *et al.*[32] have provided excellent reviews that incorporate experimental procedures to investigate substrate channeling by proximity. These methods include (1) transient-time analysis, where the focus is on measuring any shortening of the lag time; (2) isotope dilution or enrichment, where the



DOI: 10.1021/acscatal.9b02413
ACS Catal. 2019, 9, 10812−10869

substrate is labeled and the subsequent labeled intermediate competes with unlabeled intermediate; (3) addition of a reaction that competes for use of the intermediate; (4) use of enzyme buffering, where one uses the first enzyme (without substrate) to bind a cofactor to "buffer out" the amount of free cofactor and tests whether this changes the activity of the second enzyme; (5) transient-state kinetic analysis of enzyme forms, where enzyme concentrations approximate the same as substrate concentrations; and (6) using a reaction inhibitor, which is added to the second reaction to test whether there is resistance to inhibition due to channeling. There are advantages and limitations to each method and circumstances where one method is preferred over another; the interested reader is directed to the reviews mentioned above[31,32] and the references therein for a thorough treatment of these methods. Interestingly, some of these methods incorporate aspects that may enhance the channeling effect (*e.g.*, addition of a competing reaction leading to enhancement due to sequestration); therefore, caution when interpreting these results is necessary and requires a caveat that the observed substrate channeling is seen for those specific conditions.

Besides these experiments, additional measurements can help delineate the effect of channeling. Since the distance between enzymes decreases with increasing concentration, if a given cascade's enhancement is due to proximity channeling, it should decrease and approach zero as enzyme concentration is increased and the distance between free enzymes approaches the distance between enzymes on the scaffold. Furthermore, microscopy can be used to monitor aggregate formation of scaffolds. Shaking and/or the addition of viscogens can modulate the ability of intermediates to "escape" a scaffold and/or affect the rate of diffusion of intermediates.[61] Changing the ionic strength and/or pH of the buffer can give insight into whether electrostatics help to form a barrier to diffusion (away from the cascade).[62] Use of stopped-flow kinetics can enable rapid measurements providing additional information that can then be coupled with the experiments outlined above. Moreover, the application of theoretical simulations, such as those used by Idan and Hess, Vranish *et al.*, and others, can provide useful insight into the underlying processes.[28,29,48,61,63]

With all of these potential methods and experiments, it can still be difficult to determine the extent of substrate channeling, particularly as cascades become longer. For example, it may be difficult to know the rates of nonenzymatic degradation of all intermediates under given buffer conditions (pH, cofactors, *etc.*) or the extent of reversibility of enzymes in a cascade, which may affect channeling through the addition of sequestration. Furthermore, multiple factors may confound one another, for example, addition of enzyme stability (see below) with changes in kinetics upon immobilization; the extent of aggregation with different multimers of enzymes; the change in local pH due to the scaffold environment; the movement of intermediates near the scaffold surface (*i.e.*, "hydration layers");[64] and changes in viscosity/cofactor concentration/metal concentration with changes in enzyme concentration. This is particularly true for less well studied cascades. Additional advances in theoretical simulations and analytical techniques, coupled with new channeling examples, should help deconvolute some of these factors and illuminate these issues.

**Enzyme Sequentiality, Proximity, and Confinement.** The second putative mechanism by which scaffolds could benefit multienzyme cascades is derived from enzyme sequentiality, proximity, confinement, or some combination thereof (Figure 3B, middle panel). In terms of sequentiality, being able to control the sequence of enzymes along a multienzymatic cascade can affect the activity, though not always in obvious ways. The Keasling laboratory examined different orderings of the three enzymes they scaffolded from the mevalonate pathway (*vide supra* and Figure 2) and found that while their best scaffold showed 77-fold improvement over free identically tagged-only enzymes, ordering the enzymes in other ways showed only 10- or 22-fold improvement.[17] The Keasling laboratory system used different orthogonal tags/docks to be able to arrange their enzymes on the scaffold, based on the domains used, namely, the GTPase binding domain from the actin polymerization switch N-WASP (GBD), the Src homology 3 domain from the adaptor protein CRK (SH3), and the PSD95/DlgA/Zo-1 domain from the adaptor protein syntrophin (PDZ). In addition, specific placement can be accomplished with other systems, such as using orthogonal pairs of cohesin/dockerin domains from cellulosome systems or using DNA scaffold systems guided by sequence complementarity, both of which are addressed in later sections of this review.[6,65−69] Unfortunately, the Keasling laboratory did not determine why sequentiality had the effect it did.[17] However, the effect is expected to be complex and confounded by other issues. For example, intuitively it would make sense to place two enzymes that work in adjoining steps of a cascade together, especially for a long cascade; however, if those enzymes (and perhaps their intermediate) are both highly negatively charged it may actually be better to have them slightly separated. Further, it is acknowledged that the Keasling laboratory example was done *in vivo*, which may complicate the results regarding the importance of sequentiality because of the complex interactions in the cell.[17] Even with these caveats, the results are at least demonstrative that sequentiality may be important and should be considered. It would be interesting to see similar systems examined *in vitro* to examine this effect, and some examples in this vein are detailed below. Along with sequentiality come the benefits of modularity, which can contribute to the construction of *de novo* designer cascades; specific tags/docks can allow one enzyme to be swapped out for another easily without redesigning the entire scaffold, regardless of whether the cascade is producing a natural compound or a novel non-natural compound.[17,65,66,68]

Proximity refers to the close distance of the enzymes to the substrate. Again, the cellulosome system can be invoked as an example; the cell places all of the cellulase enzymes outside of the cell closer to the extracellular cellulose substrate, yet these scaffolded enzymes are still tethered to the cell to facilitate internalization of the product (digested sugars).[6,12] Confinement refers to using scaffolds to keep enzymes in a certain location, away from off-target pathways or degradative conditions, as well as coupled together. This can be illustrated by nature's placement of associated Krebs cycle enzymes in mitochrondria.[9−11,13,14] Another benefit of confinement is the ease of recoverability and reuse of artificial multienzyme cascades; one can engineer a system to recover the scaffold assembly for reuse instead of trying to recover a series of individual enzymes. This can be accomplished using magnetic NPs that can be easily separated from a reaction solution.[1,4,8,23,70]

**Localized Scaffold Effects.** Finally, the third mechanism by which scaffolds could provide benefits is by localized scaffold effects and contributions (Figure 3B, bottom panel); this is also perhaps the least understood and most contentious of all the



DOI: 10.1021/acscatal.9b02413
*ACS Catal.* 2019, 9, 10812−10869

**Table 1. Selected Examples of GOx−HRP Multienzyme Cascades[88,a]**

| entry | scaffold | scaffold name | highest fold enhancement observed[b] | enzyme separation distance (nm)[b] | ionic strength[c] | pH | ref |
|---|---|---|---|---|---|---|---|
| 1 | DNA | single DNA helix | 3 | 8 | 0.6 | 7.4 | 72 |
| 2 | DNA | DNA origami rectangle | 3.4 | 10 | 0.203 | 7.5 | 36 |
| 3 | DNA | DNA tweezer | 1.9 | 6 | 0.203 | 7.5 | 78 |
| 4 | DNA | DNA-origami-based nanoreactor | 25 | 30 | 0.0035 | 5 | 79 |
| 5 | DNA | flexible DNA triangle prism | 2.1 | 7 | 0.103 | 7.5 | 80 |
| 6 | DNA | DNA origami rectangle | 10 | 10 | 0.156 | NE | 81 |
| 7 | DNA | cocaine aptamer | 13 | 5 | 0.16 | 7.4 | 82 |
| 8 | DNA | circular DNA with cocaine aptamer | 6 | 10 | 0.6 | 7.4 | 83 |
| 9 | DNA | dsDNA with AZB moieties | 25 | 5 | 0.28375 | 7.8 | 84 |
| 10 | DNA | Y-shaped DNA | 7 | 5 | 0.16 | 7.4 | 85 |
| 11 | DNA | RCA-prepared long DNA | 18 | 22 | NE | NE | 69 |
| 12 | DNA | hexagon-like strips | 15.8 | 5 | 0.06 | 7.5 | 56 |
| 13 | DNA | rectangular and tubular origami | 8 | 15 | NE | 7.4 | 86 |
| 14 | DNA | nanocage origami | 8 | 5 | 0.203 | 5 | 64 |
| 15 | chemical linker | sSMCC linker | ∼0 | NE | 0.2105 | 8 | 49 |
| 16 | CLEA | combi-CLEA | 1.5 ($k_{cat}/K_M$), 0 ($k_{cat}$) | NE | 0.6 | 7.4 | 73 |
| 17 | NP | QD | ∼3 | NE | 0.2105 | NE | 63 |
| 18 | MOF | metal−organic framework | 7.5 | NE | 0.61 | NE | 87 |
| 19 | NP | $SiO_2$ NP | 2 | NE | NE | NE | 87 |
| 20 | NP | acrylamide hydrogel | 2.5 | NE | NE | NE | 87 |

[a]Abbreviations: CLEA = cross-linked enzyme aggregate; NP = nanoparticle; MOF = metal−organic framework; AZB = azobenzene; RCA = rolling circle amplification; sSMCC = sulfosuccinimidyl 4-(*N*-maleimidomethyl)cyclohexane-1-carboxylate; QD = quantum dot; NE = not evaluated/not recorded. [b]Interenzyme distances and turnover rates were estimated using the reported data when not specifically listed or given in the corresponding papers. When multiple configurations of the same DNA template were investigated, only the most substantial reported turnover rate is listed. [c]Ionic strengths were calculated as $I = 0.5\sum_i C_i z_i^2$, where $C_i$ and $z_i$ are the concentration and charge of ion $i$, respectively. Values are estimates.

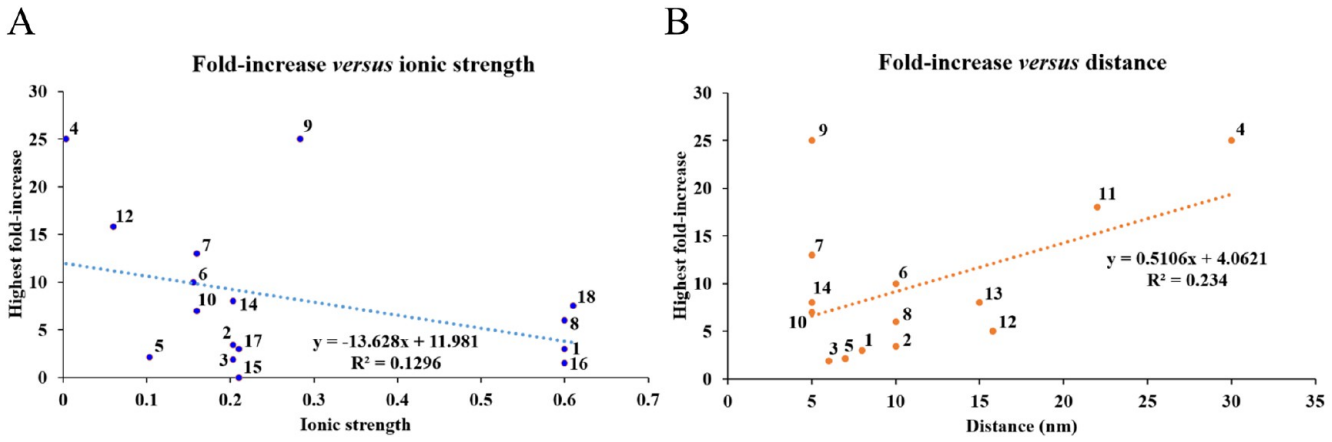


**Figure 6.** GOx−HRP system factors. No strong correlation is seen between the fold increase in activity and either the ionic strength or distance, as shown in Table 1. This illustrates the complexities of the system and the difficulties in assigning the factors that are responsible for an increase in activity. Numbers correspond to entry numbers in Table 1.

potential enhancement processes. The prime example of this mechanism was delineated by the Hess laboratory in their investigation of a common multienzyme pairing tested with artificial scaffolds, namely, that of glucose oxidase (GOx) and horseradish peroxidase (HRP), especially as displayed on DNA scaffolds. GOx oxidizes glucose to D-glucono-$\delta$-lactone and $H_2O_2$; HRP uses the $H_2O_2$ to oxidize a dye such as 2,2′-azinobis(3-ethylbenzothiazoline-6-sulfonic acid) (ABTS), 3,3′,5,5′-tetramethylbenzidine (TMB), or Amplex/resorufin.[71−73] They demonstrated that the enhanced kinetics of these enzymes scaffolded on DNA likely was not due to substrate channeling, as conjugating the same two enzymes directly to each other using a small heterobifunctional linker (sulfosuccinimidyl 4-(*N*-maleimidomethyl)cyclohexane-1-carboxylate, sSMCC) did not improve the kinetics. They hypothesized that instead the negatively charged DNA lowered the local environment pH of the enzymes, improving their activity (both activities increase as the pH is lowered, although the HRP activity increases significantly more).[49] The use of this enzyme pair with DNA scaffolds is discussed further below. There are other potential issues with this coupled enzyme system that may arise from the low molecular weight of $H_2O_2$ and its diffusion rate along with its viable lifetime and other species with which it interacts. Even though the GOx−HRP


DOI: 10.1021/acscatal.9b02413
ACS Catal. 2019, 9, 10812−10869

pair is perhaps one of the most commonly used for investigating scaffolds and biosensing devices, this finding suggests that the results need to be carefully analyzed for localized environmental and other effects. Specifically with regard to assays with DNA, one needs to consider the potential for changes in activity due to (1) changing local pH as referenced above,[49] (2) interactions between the substrate/intermediate and negatively charged DNA (*i.e.*, barrier to diffusion),[49,57,74] (3) aggregation,[28,48,49] and (4) stabilization of enzymes by hydration layers.[49,64] With regard to (4), it should be noted that this layer could only be a few angstroms thick, and increased stability would be expected to increase the enzyme activity only if, for example, the assay were conducted below the $K_d$ for quaternary structure/subunit association.[49,61,64,75,76] As an example of how prevalent this enzyme pair is, especially as displayed on DNA scaffolds, see Table 1. As can be seen from Table 1 and Figure 6, the convoluted effects of electrostatics (presumably as modulated by different ionic strengths of buffers and pH values used in experimental activity assays) and $d_{e-e}$ on the fold enhancements of cascade activity illustrate the complexities of the system and the difficulties in assigning the factors that are responsible for an increase in activity.

Another localized scaffold effect that is sometimes observed is improvement of long-term enzyme stability. Several laboratories have shown improved stability when enzymes are linked onto scaffolds.[8,40] Importantly, not only can enhanced enzyme stability enable reactions to occur at elevated temperatures or for longer time-scales, but some scaffolded enzymes can even have improved recoverability from lyophilization, allowing for improved transport and storage.[77] Perhaps the most interesting phenomenon in this genre is that of kinetic enhancement when enzymes are attached to an NP scaffold. This is discussed in more detail in later sections. These localized scaffold effects make it important to, if within the scope of the project, determine the rates of all enzymes in the cascade individually when they are attached to a scaffold versus free in solution. This can highlight the difference between localized scaffold effects enhancing the overall reaction versus proximity-based substrate channeling.[49] If individual enzymes are enhanced on the scaffold, additional insight can be garnered by using (1) techniques such as circular dichromism to monitor conformation/stability, (2) different ionic strengths/pH buffers or different scaffolding materials to test for enhancements due to local pH,[49,62] and (3) concentrations above and below the dissociation constant of a multimeric enzyme to determine whether the scaffold is supporting the quaternary structure.[61] Regardless of the potential mechanism, the benefits of artificial multienzyme scaffolds on cascade reactions will depend on both the scaffold material and the chemistry used to link enzymes to the scaffold. We will now address aspects of the latter.

## ■ ENZYME–SCAFFOLD LINKAGE CHEMISTRIES

The chemistry utilized to attach or associate the enzymes with the scaffolding material is usually a secondary consideration in many experimental plans. However, given its importance to both the resulting structure and its intended function, we suggest that this should perhaps be a primary consideration. Bioconjugation chemistry can be quite vast, complex, and nuanced[89] and remains mostly beyond the scope of this review. However, it is still worth discussing several important points since this chemistry can directly influence or even dictate the achievable catalytic efficiency (or lack thereof) in an enzymatic cascade, especially as assembled on a scaffold.

What is ideally desired from such bioconjugation chemistry is that any desired enzyme be attached to the scaffold with intimate control over several key properties, including: (1) the orientation of the enzyme on the scaffold with the reaction site clearly available, (2) the ratio or attachment density per scaffold, (3) the separation distance from the scaffold, (4) the affinity of the attachment chemistry, (5) the choice of attachment sites on the scaffold and the enzyme, and most importantly (6) equal applicability of these chemistries to most enzymes and also most scaffold materials.[90] Unfortunately, the state of bioconjugation chemistry is far from achieving such a capability for any experimental format let alone having any technique that displays a plurality of these properties.[91,92] This issue is further complicated by the paucity of functional chemical groups available on both the enzymes and the scaffold materials described here. For the enzymes themselves, these chemical groups include the ubiquitously available carboxyls typically found on acidic residues and the C-termini and amines found on lysines or N-termini along with thiols on cysteine residues, which are quite often part of structurally critical disulfide bridges.[93] These choices are sometimes supplemented by engineered motifs such as hexahistidine ($His_6$) tags introduced to expressed proteins for purification and, to a much lesser extent, unique functional groups from incorporation of non-natural amino acids.[94,95] Although the scaffold materials described herein are quite structurally diverse, including cells, vesicles, DNA, proteins, MOFs, polymers, lipids, NPs, *etc.*, the actual chemical groups available within a given material can in fact be quite limited. As described in the examples below, the three primary superfamilies of enzyme–scaffold bioconjugation chemistry are based on covalent, non-covalent, and electrostatic approaches, each of which has several subtypes as well. More pertinently, each conjugation chemistry comes associated with a set of benefits and liabilities, and these must be carefully parsed and considered for both planning and interpreting data from a desired experimental format.

As an example of a covalent attachment approach, the most common method for attaching enzymes to NPs and other surfaces is to utilize carbodiimide chemistry to form an amide bond between either an available carboxyl or amine on the protein and the cognate target on the other participant.[89,96] This approach benefits from relatively facile and amenable chemistry (*i.e.*, aqueous reaction conditions). However, the presence of both groups on an enzyme can and often does lead to cross-linking, while the short viable half-life of carbodiimides in aqueous solutions means that a vast excess must be used, which then leads to the requirement for extensive purification and cleanup.[89] Introducing biorthogonal groups such as azides and alkynes into an enzyme for targeted click chemistry, for example, very often relies on an initial nonspecific labeling that targets available amines.[92] Targeting thiols in a protein can be very site-specific, but as mentioned, if these are part of a critical disulfide bond, protein function can be lost.[97]

In terms of non-covalent approaches, biotin–streptavidin is one of the most popular non-covalent chemistries and enjoys an extremely high affinity binding constant ($K_D \sim 10^{-15}$ M). However, one participant must be modified to display a biotin group, and as the streptavidin is tetravalent, the possibility of cross-linking and undesirable orientations again remains.[96] Another popular non-covalent approach is to utilize $His_6$ motifs appended to enzyme termini to coordinate to $Ni^{2+}$-nitrilotriacetic acid (Ni-NTA) groups attached to a scaffold. This takes advantage of the fact that the $His_6$ motif may already have been


DOI: 10.1021/acscatal.9b02413
*ACS Catal.* 2019, 9, 10812–10869

## Table 2. Representative Types of Biological Scaffolds

| type | functional requirements | advantages | disadvantages | examples | refs |
|---|---|---|---|---|---|
| cellular surfaces | genetically fuse enzymes to anchor proteins | (1) all components can be expressed together in one cell; (2) access to substrates that cannot be internalized into the cell; (3) renewable enzymes; (4) potential increased stabilization; (5) relatively accessible to engineer; (6) no need to purify enzymes | (1) exporting/maintaining enzyme outside cell; (2) achieving correct enzyme ratios; (3) limited number of anchor proteins, resulting in a limited number of different enzymes; (4) must maintain cell health (*i.e.*, limited toxicity allowance); (5) enzyme must still be active when fused; (6) potential dissociation from surface if non-covalently attached | display on yeast, bacteria, and bacterial spores | 104−111 |
| protein/peptide scaffolds | genetically fuse enzymes to tag; coexpress scaffold with docks if *in vivo* | (1) scaffolds genetically encoded with enzymes; (2) able to engineer user-defined order/ratios; (3) control over the enzyme distance; (4) ability to branch (with scaffold); (5) tag can be smaller than the anchor protein for cell surface display; (6) enzymes can be swappable | (1) limits on the number of enzymes attached per scaffold (branching can help); (2) limited number of tags/docks, resulting in a limited number of different enzymes; (3) time/resources to construct scaffold (human input and microbial input); (4) depending on the system, must maintain cell health; (5) enzyme may be less active when fused; (6) high production cost; (7) potential dissociation from scaffold if non-covalently attached | the cellulosome, affibodies, display on microcompartments, inclusion-body-based scaffolds, use of coiled coils and leucine zippers, protein crystalline inclusions, multienzyme fusions | 104, 112−123 |
| lipids | chemically attach lipid or tag to enzyme | (1) may be good for processes involving hydrophobic intermediates; (2) can attach many enzymes to a lipid droplet | (1) limitations when hydrophobicity or large size not desired; (2) enzyme must still be active when fused; (3) potential dissociation from lipid if non-covalently attached | intracellular lipid/protein-based, lipid droplets | 124, 125 |
| cross-linked enzyme aggregates (CLEAs) | precipitate enzymes, chemically aggregate enzymes with or without site selectivity | (1) easy preparation, no genetic modifications needed (if non-site-specific); (2) potential increased stability; (3) reusability; (4) packing enzymes densely may facilitate aggregation-based channeling; (5) multiple attachment points per enzyme; (6) can use with crude cell extracts | (1) enzyme must still be active when chemically modified (high risk of lower activity with non-site-specific cross-linking); (2) lack of control over orientation and homogeneity | precipitation followed by glutaraldehyde cross-linking | 12, 14, 29, 59, 60, 73, 104, 126−128 |
| nucleic acids | genetically construct nucleic acid scaffold (*e.g.*, rolling transcription); chemically attach complementary DNA to enzyme | (1) site-specific = very good order/ratio/distance control; (2) multiple enzymes can be attached; (3) can do 2D and 3D architectures; (4) cofactor retention | (1) relatively difficult to modify; (2) stability; (3) high production cost; (4) potential nuclease degradation; (5) requires very specific skills; (6) potential dissociation from scaffold if non-covalently attached | DNA origami | 36, 104 |



DOI: 10.1021/acscatal.9b02413
ACS Catal. 2019, 9, 10812−10869

appended to the enzyme (utilized for purification purposes), and therefore, a further modification of the enzyme is not needed for attachment onto the scaffold. A limitation of this approach is the low-micromolar dissociation constant of this interaction, which can preclude achieving the right concentrations for true Michaelis–Menten analysis (*i.e.*, Briggs–Haldane criteria with low enzyme concentrations and a vast excess of substrate),[98] while the $Ni^{2+}$ can affect or even inhibit other metal-dependent enzymes.

Meanwhile, electrostatic interactions between polymers or DNA and oppositely charged species, for example, can be quite strong and very easy to implement. However, this approach comes with a strong likelihood of significant loss over any desired orientation and again the possibility of cross-linking. Also, as will be repeatedly shown in the discussion below, localized charge can increase enzyme activity by sequestering substrate, for example, making the exact source of enhancement quite complex. There are of course many more examples of potential enzyme–scaffold conjugation chemistries with corresponding sets of benefits and liabilities, but these few should suffice to make the necessary points.

It is also important to note that in principle any type of modification to an enzyme can hinder its activity depending upon how sensitive its structure is to allosteric interactions. This can lead to a loss of activity in comparison with the native or parent construct. Moreover, in many cases attaching an enzyme to a surface results in a loss of activity, presumably due to the reduction of the enzyme's freedom of movement.[61,99,100] Cumulatively, extrapolating from the above, it becomes readily apparent how critical a consideration enzyme–scaffold bioconjugation chemistry is, as it can affect subsequent activity in a detrimental manner. For example, nonspecific amine–carboxyl chemistry can occur at the expense of modifying key residues in the enzyme's active site, causing a loss of activity. If the enzymes are attached in a heterogeneous manner to the scaffold or cross-linked to some extent, then some of the enzymes in the sample may not be active. Relying on specific protein–protein binding motifs such as cohesin–scaffoldin or enzyme fusions, as described below for scaffolds assembled on cell surfaces, requires extensive initial engineering and usually cannot be applied in a direct repeated sequence if sequentially arranged enzymes are desired. While the issues illustrated here highlight the need for continuing research into novel bioconjugation methods, current approaches can often be sufficient to demonstrate improvements of multienzyme cascades *via* artificial multienzyme scaffolds. The main point is that these issues may need to be taken into account when analyzing data and considering why a given multienzyme construct did or did not demonstrate optimized activity or function as efficiently as expected. The interested reader is referred to more focused treatises on bioconjugation chemistry.[89,91,101] The bulk of the remainder of this review will focus on the other major factor for the success of an artificial multienzyme scaffold, namely, the scaffold itself and a survey of what has already been accomplished to date with various different scaffolding materials.

## BIOTIC SCAFFOLDS

A variety of biological scaffolds have been explored for their ability to assemble multienzyme cascades. A succinct overview of some representative types of biological scaffolds, their requirements, advantages, and disadvantages, and some examples of their use are highlighted in Table 2. Biological scaffolds can range from live cell surfaces to proteins or other biopolymers, with each exploited for their unique architecture. In some cases, they self-assemble, driven by programmed biochemistry; other times, exogenous chemistry is used to bind them together. It is important to consider the properties of these scaffolds for the subsequent function of the cascade. Biological scaffolds have inherent benefits that are different from artificial scaffolds like synthetic surfaces, NPs, and MOFs. These benefits include natural compatibility with biologically derived enzymes and programmability through genetic engineering. Depending on the particular system, enzymes can be placed site-specifically or randomly on biological scaffolds. The method of this attachment is a critical consideration for all biological scaffolds, in terms of both the location of the attachment point(s) on the enzyme itself and the flexibility/rigidity and length of any linker between the enzyme and the scaffold.[102,103] This section explores different biological scaffolds, including significant aspects to consider in their use, starting with the display of multienzyme cascades directly on the cell surface of living microbes.

**Cellular Surfaces.** Using a cellular surface as a biological scaffold requires a method to display the enzymes on that surface. The desired enzymes are often fused to tags that must (1) export the protein outside the cell yet (2) keep it anchored to the cell surface.[110] Alternatively, a secondary protein-based binding moiety/scaffold that in turn recruits the desired enzymes is fused to the tags;[110] the use of secondary scaffolds is discussed in Naturally-Derived Protein and Peptide Scaffolds below. Tags may have different signal sequences for the two tasks, ideally with minimal interference of the target protein's function (see below).[110] This allows the entire cell membrane to act as a biological scaffold. Perhaps the most well-known use of this type of technology (albeit not on a cell/membrane) is phage display, where peptides or proteins are displayed on the outside of phages and can be rapidly screened for affinity to given targets.[110,129,130] However, this system can face limitations on how large the displayed peptides/proteins can be before steric effects restrain phage assembly.[110]

Display on cellular surfaces such as yeast/fungi and bacteria endows advantages and, of course, comes with its own set of limitations. All of the components can be expressed together in one live cell, which is particularly advantageous if the cascade utilizes other aspects of cellular machinery, such as displaying enzymes to degrade cellulose to glucose and then using internal enzymes to convert glucose to ethanol.[108,110] Additional advantages of this system can include access to nonconventional substrates that do not have to be internalized into the cell, self-immobilized enzymes that are renewable from the cell, and increased enzyme stabilization.[105,109−111] Limitations of this approach can include difficulties in exporting and maintaining fusion of enzymes outside a cell, difficulty in engineering/identifying cells displaying correct enzyme ratios, and other limitations inherent with using live cells (*e.g.*, pathways producing toxic intermediates or products and maintaining optimal environmental conditions). The use of both yeast and bacteria for cell surface display is highlighted below.[108,110]

*Yeast Cell Surface Display.* Using yeast for cell surface display has been colloquially described as "whole-cell biocatalysis", "yeast surface display", "yeast surface engineering", "arming technology", and "arming yeasts".[110,111,131,132] Multiple yeast hosts have been investigated for this purpose, including *Aspergillus oryzae*, *Pichia pastoris*, *Yarrowia lipolytica*, and the common baker's yeast *S. cerevisiae*.[106,108,110,111,131−141]



DOI: 10.1021/acscatal.9b02413
*ACS Catal.* 2019, 9, 10812−10869

To perform yeast cell surface display for multienzyme cascades, enzymes are typically fused to an anchor protein that in turn ideally contains two signal sequences, one targeting the cell surface and another for glycosylphosphatidylinositol (GPI) attachment to transiently anchor the protein to the cell membrane. There are a range of known anchor proteins (*i.e.*, "tags") from which to select for enzyme attachment, depending on which one maintains the target enzyme's activity. Tsai and colleagues and Kondo and colleagues have published excellent reviews that list these anchor proteins, including SED, Cwp2, Flo428p, and the $\alpha$-agglutinin system.[106,110,142−145] Of importance to multienzyme cascades, researchers have also identified several auxotrophic markers that can facilitate site-specific codisplay of enzymes on yeast.[111] In this subsection, we focus on direct yeast surface display (DYSD), specifically codisplay (CD), where multiple enzymes are displayed on each yeast cell. This contrasts from formats where multiple enzymes are displayed in a coculture of single yeasts, each displaying a separate enzyme (single enzyme display consortium or SEDC); for more information on this method, see Tabañag *et al.*[110]

One of the main applications of yeast cell surface display that has been investigated is the display of enzymes for the degradation of complex biological feedstocks.[110] This is largely due to the focus of using yeast for biofuel/ethanol production, where one of the main bottlenecks for production is the breakdown of feedstocks such as cellulose, which can be particularly difficult to degrade.[106,110,146] Given this focus, here we provide a brief introductory background on different types of cellulose and cellulose-degrading enzymes before delving into specific application examples. Polymerized glucose makes up cellulose, which can have disordered amorphous domains and ordered crystalline domains. In plant-based fibers, crystalline cellulose makes up 90−100% of the mass.[106,147,148] Cellulases are enzymes that can break down cellulose, but unfortunately, crystalline cellulose is particularly recalcitrant to cellulase degradation.[146] Given the inherent differences in the ability of different types of cellulose to be degraded, researchers typically specify the cellulose source when describing degradation systems: carboxymethyl cellulose (CMC), a soluble cellulose that can be degraded by some organisms that cannot degrade other types of cellulose;[149] phosphoric acid-swollen cellulose (PASC), an insoluble, mostly amorphous cellulose; and Avicel, which is nearly pure cellulose that has been treated with dilute acid to remove hemicelluloses and more extensive amorphous cellulose regions, though it still contains a significant amount of amorphous cellulose.[106,147,150−152] Figure 7 illustrates how three different types of cellulases can degrade cellulose: an endoglucanase and cellobiohydrolase can cleave cellulose to smaller pieces, and a $\beta$-glucosidase can hydrolyze cello-oligosaccharides into glucose.[106,153]

One recent example of the use of yeast cell surface display for cellulose degradation was reported by Liu *et al.*[106] This approach focused on surface display of four enzymes on *S. cerevisiae* for degradation of crystalline cellulose into glucose: an endoglucanase, two cellobiohydrolases, and a $\beta$-glucosidase.[106,153] To display these enzymes, they used a Sed1 anchoring domain, which is a stress-induced structural GPI-cell wall glycoprotein.[106,110,142,143] The authors desired to optimize the ratio of these enzymes to maximize the overall activity; however, modulating the ratio of enzymes in yeast cell surface display has traditionally been quite difficult. To address this issue, a cocktail $\delta$-integration method the laboratory had developed was used to generate a pool of yeast that expressed different copy numbers of genes encoding three of the cellulases/anchoring proteins in the genome; thus, these yeasts would display different ratios of the desired enzymes.[110,154,155] A screening strategy was then implemented to determine which ratios were best at degrading cellulose.[106,156] With this technique, the best strain identified (A26) was found to have 57% of the equivalent of the theoretical maximum yield from Avicel. The authors also noted that this yield from Avicel generated by cellulolytic yeast is among the highest reported. The A26 strain also had a 60% increase in ethanol yield from rice straw relative to the single-integrated strain displaying the four enzymes. The setup of the technique and the transcription ratios of the enzymes in A26 can be seen in Figure 8.[106,110] While this report did not specify whether substrate channeling improved the performance of the scaffolded cascade, it does highlight the importance of modulating the enzyme ratio and illustrates one technique for selecting cells displaying an optimized ratio of enzymes.

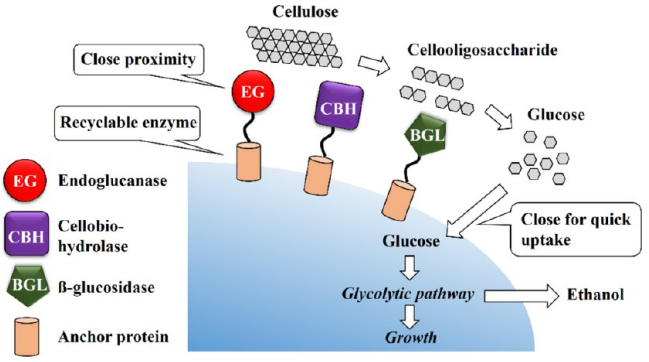


**Figure 7.** Schematic illustration of cellulose assimilation by cellulase surface-displaying microorganisms. Three different types of cellulases work together to degrade cellulose: an endoglucanase and cellobiohydrolase to cleave cellulose into smaller pieces and a $\beta$-glucosidase to hydrolyze cello-oligosaccharides into glucose, which is then taken up into the cell preferentially because of its close proximity.[106,153] Adapted with permission from ref 153. Copyright 2013 Elsevier Inc.

*Bacterial Cell/Spore Surface Display.* Similar to yeast cell surface display, enzymes can also be displayed on bacteria or even on bacterial spores. Schüürmann *et al.* published an excellent review detailing different anchor proteins and their use in Gram-negative and Gram-positive bacteria.[108] They described three general categories for Gram-negative bacteria. First are autotransporters, which typically contain a signal peptide for inner membrane translocation, a passenger domain (*i.e.*, targeted enzyme or a secondary scaffold), and a translocation domain enabling the passenger domain to be displayed on the cell surface. Second are ice nucleation proteins (INPs), which contain a C-terminal hydrophilic domain, a repetitive, large internal domain, and an N-terminal domain that binds to the outer membrane. Third are a collection of other outer membrane proteins such as OprF from *Pseudomonas aeruginosa*, OmpW from *E. coli*, and bacterial lipocalins. Three general categories for Gram-positive bacteria were also described. First is the use of the PgsA anchor motif from the membrane-associated poly-$\gamma$-glutamate synthetase complex PgsBCA from *Bacillus subtilis*. The second is the use of the NCg11221 anchor motif from *Corynebacterium glutamicum*, a channel protein that may be used for L-glutamate secretion. Third, and unique in that it is a display not on the mature cell surface itself, is the use of endospores made by *Bacillus* spp.,


DOI: 10.1021/acscatal.9b02413
ACS Catal. 2019, 9, 10812−10869

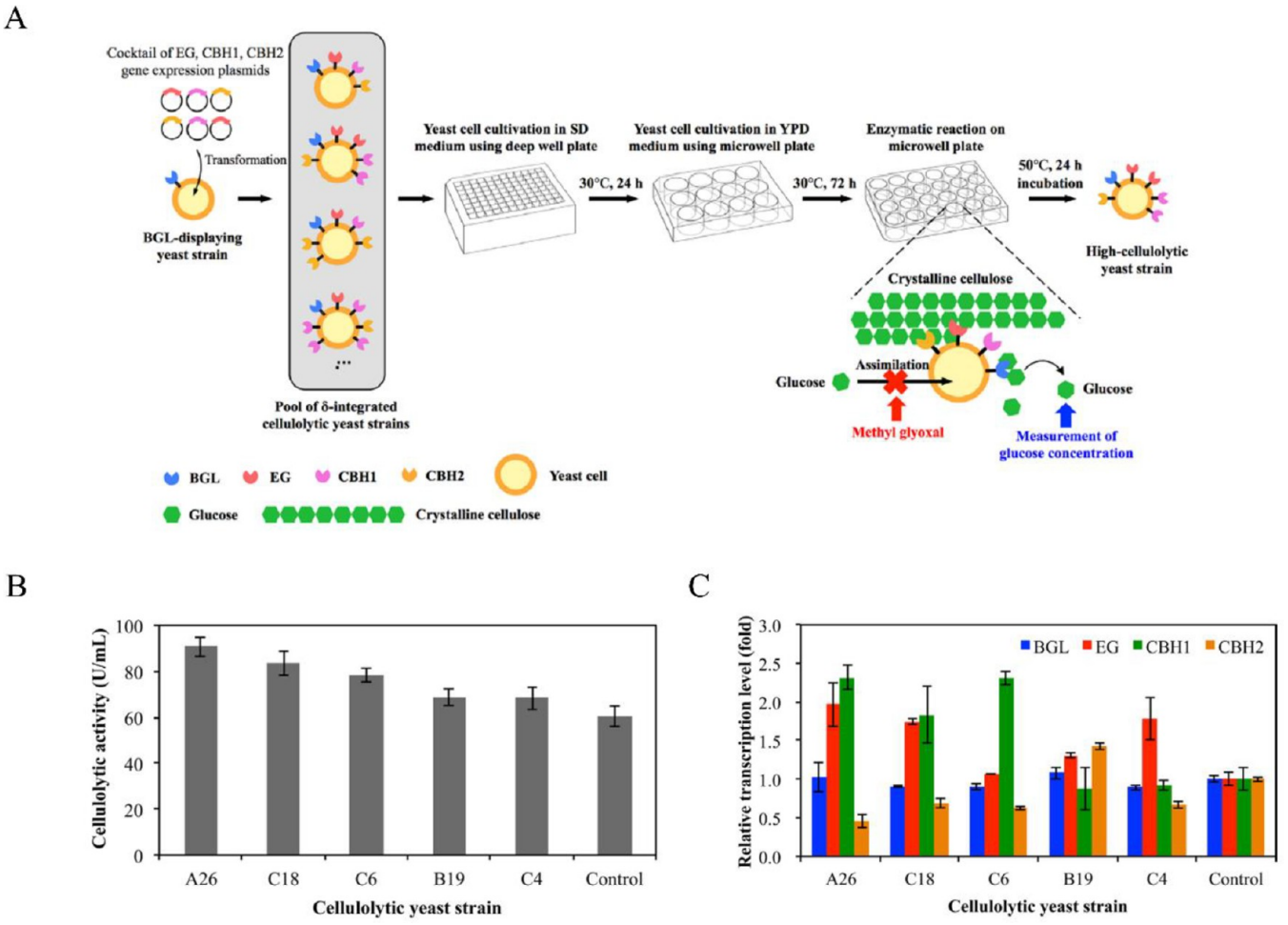


**Figure 8.** Yeast cell surface display of cellulolytic enzymes. (A) Schematic flow diagram of a novel screening method for high-cellulolytic yeast strains toward the degradation of crystalline cellulose. (B) Cellulolytic activity toward Avicel. (C) Relative transcription levels of cellulase genes *via* real-time PCR. The single-integrated strain EG-D-CBH1-D-CBH2-D was used as the control. Gene ACT1 was used as the internal standard. The relative transcription levels are shown as the fold of the level in the control strain. Data are means of three independent experiments; error bars represent SDs. BGL = $\beta$-glucosidase; EG = endoglucanase; CBH1 = cellobiohydrolase 1; CBH2 = cellobiohydrolase 2. Reproduced from ref 106. Copyright 2017 Wiley Periodicals, Inc.

where proteins are displayed by C-terminal fusion to inner and outer spore coat proteins. One benefit of this latter approach is that since spores are made inside the bacteria (and then released by lysis), membrane translocation of heterologous passenger domains is not an issue.[108]

For some of these systems, it has been reported that up to $10^3$–$10^5$ enzymes can be displayed on a given cell surface.[157−159] It has been speculated that Gram-positive bacteria may be better for cell surface display because of their rigid cell walls in view of the possible disruption of outer membranes caused by anchored enzymes.[160,161] With this said, there still have been several reports of displayed enzymes on Gram-negative bacteria.[108] For additional mechanisms of surface display on lactic acid bacteria in particular, the reader is referred to a review by Michon *et al.*[162] Two considerations to keep in mind when using bacterial cell/spore display and that may require trial and error are the choice of anchor/carrier and the choice of linker, since it was shown that the choice of carrier affected enzyme expression in one system[163] and the flexibility of the linker affected successful utility in another system.[102,103]

While much work has been done on bacterial cell/spore surface display using single enzymes,[108] one example of the use of a multienzyme cascade was reported by Ryu and Karim.[107] Similar to the goal of the yeast cell surface display highlighted above, they aimed to display three cellulases to degrade cellulose to glucose on *E. coli* LY01. Previous systems based on fungal enzymes and yeast display suffered from some incompatibility since the optimal temperature for the fungal enzymes was 55 °C, whereas the optimal yeast growth occurred at 30 °C. In the current example, enzymes came from the bacterium *Clostridium cellulolyticum*, and *E. coli* was used for display; the optimal temperature and pH for both are approximately 35 °C and 6.8, respectively.[164] The three cellulases utilized were the endoglucanase Cel5A,[164] the exoglucanase Cel9E,[165] and a $\beta$-glucosidase, and these were all fused to the anchor protein PgsA.[166,167] Different cellulose sources were degraded by displaying the three enzymes, followed by conversion to ethanol by the same bacteria; in particular, ethanol was produced from 10 g/L PASC at a yield of 3.59 g/L for an impressive 95.4% of the theoretical yield. The authors note some advantages and disadvantages to this approach. One advantage is that glucose can be used by the microbe immediately, thereby reducing product inhibition of the cellulases.[168] One disadvantage, however, is that the enzymes may not colocalize with each other in close proximity on the surface, limiting overall hydrolysis. While each biological


DOI: 10.1021/acscatal.9b02413
ACS Catal. 2019, 9, 10812−10869

scaffold has its own pros and cons, some of the limitations of cell-surface scaffolds could potentially be addressed by using naturally derived protein and peptide scaffolds, which is addressed in the next section.

**Naturally-Derived Protein and Peptide Scaffolds.** In contrast to using an entire cell surface directly as a scaffold, proteins and peptides can be engineered to assemble multiple enzymes together using a variety of methods, some of which are highlighted below. Advantages of using naturally derived proteins and peptide scaffolds are that they can be genetically encoded along with the desired enzymes and that the enzymes can be further assembled in user-defined ratios and order. Disadvantages can include limits on the number of enzymes attached per scaffold (in some systems branching can alleviate this to some extent) and added time/resources to construct the scaffold (in terms of both human input and microbial input).

*The Cellulosome.* The cellulosome can for all intents and purposes be considered nature's model scaffold for self-assembly of enzymatic cascades. These extracellular complexes are usually found either attached to the cell wall of bacteria such as *Clostridium thermocellum* or existing free in solution after being excreted from cells.[112,147,169−171] The native cellulosome core consists of a multicomponent scaffoldin protein that serves to organize and display the cellulolytic enzymes around the complex, such as the various cellulases described for cell surface display above. These cellulolytic enzymes include a variety of degradative enzymes such as xylanases, cellobiohydrolases, and endoglucanases that work together in a synergistic manner to "digest" insoluble cellulosic substrate into simple sugars.[147,170] Enzymes destined for use in cellulosomes typically display dockerin binding protein modules that bind to a cognate cohesin protein module on the scaffoldin when $Ca^{2+}$ ions are present.[119,172] The latter class of high-affinity binding partner proteins ($K_D$ in the nM to pM range)[66,116] have now been extensively cloned and studied to allow for attachment of appropriate fusion proteins to each other, to designer scaffolds, or around another large scaffold protein.[66,116,169−171] Cellulosomes even have cellulose-binding domains (CBDs) that allow for attachment to the substrate while undergoing digestive reactions. This complexity and organization is believed to have arisen by selection during evolution to optimize the kinetic efficiency, as cellulases are among the slowest-acting enzymes known.[146,173]

The beauty and innate evolutionarily derived organization of the cellulosome, whose structure imbues and amplifies its intended function, have led researchers to try to assemble similar systems as artificial multienzyme scaffolds in a variety of contexts. In particular, this strategy has been used to (1) display cellulosic enzymes on yeast for cellulose degradation, (2) investigate a mixture of covalent docking strategies, again for display of cellulases on yeast, (3) explore another orthogonal cascade on yeast; and (4) display enzymes on a surface other than yeast. These examples are highlighted below.

Instead of directly scaffolding enzymes on the cell surface as described in the previous section, researchers have investigated displaying artificial multienzyme scaffolds based on cellulosomes on yeast. The overarching goal driving this research is to develop new ways of processing cellulosic feedstock into simple reducing sugars for ethanol production as a key biofuel.[112,115] For example, Fan *et al.* cloned a variety of cellulases from *C. cellulolyticum* for assembly and display in minicellulosomes on the surface of *S. cerevisiae*.[112] As shown in Figure 9, the minimally functional minicellulosome was composed of a

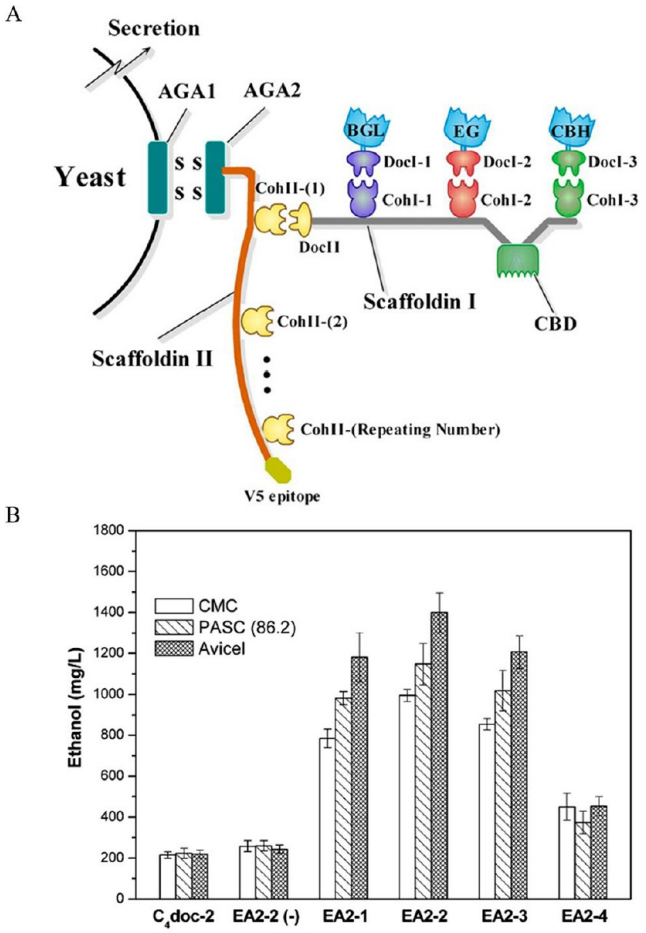


**Figure 9.** Self-surface assembly of minicellulosomes on the yeast cell surface. (A) Scaffoldin II was displayed through AGA1 and AGA2 (a yeast display system); the V5 epitope was used as a tag for immunodetection. CBD = cellulose-binding domain; BGL = $\beta$-glucosidase; EG = endoglucanase; CBH = cellobiohydrolyase (a.k.a. exoglucanase); DocI = exogenous or native type I dockerin, CohII = type II cohesins. (B) Functionality of the different versions of the minicellulosomes with various scaffoldin II lengths. PASC (86.2) means the cellulose was prepared using 86.2% phosphoric acid (phosphoric acid-swollen cellulose), CMC is soluble cellulose, and Avicel is another crystalline cellulosic substrate. Reproduced with permission from ref 112. Copyright 2012 reference authors.

scaffoldin and three attached catalytic subunits.[112] Scaffoldin I contained a C-terminal type II dockerin (DocII), a CBD, and three type I cohesins (CohI-1, CohI- 2, and CohI-3). The catalytic units included an endoglucanase (EG), an exoglucanase (cellobiohydrolase; CBH), and $\beta$-glucosidase (BGL), which cumulatively allowed the enzyme complex to meet the minimum requirement for crystalline cellulose hydrolysis. Scaffoldin II contained type II cohesins (CohII) to bind to scaffoldin I and an AGA2 domain to bind the cognate AGA1 domain on the yeast surface (AGA1 and AGA2 are components of a commercial yeast display system); the proteins were all secreted by the yeast, assembled extracellularly, and then displayed on the yeast cell surface.[174,175] Exploiting the benefits inherent to this design approach, the authors displayed multiple copies of scaffoldin I on the scaffoldin II protein again using dockerin−cohesin interactions. By optimizing the scaffoldin II length and its corresponding number of repeats, they were able to demonstrate simultaneous saccharification and fermentation


DOI: 10.1021/acscatal.9b02413
ACS Catal. 2019, 9, 10812−10869

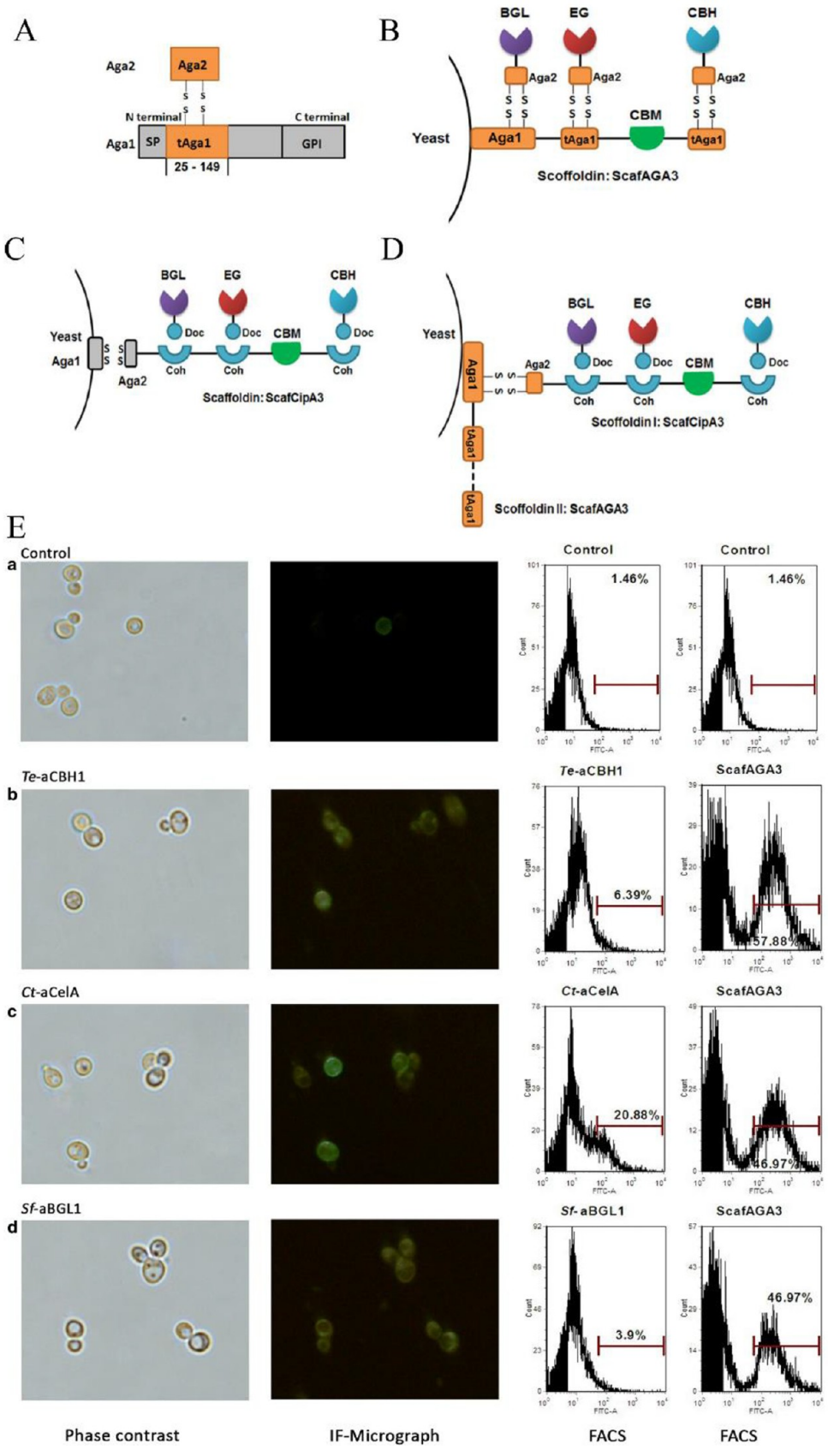


**Figure 10.** Self-assembling cellulosome designed for yeast surface display. (A) Interaction between Aga1p and Aga2p *via* disulfide bonds. (B) Assembly of cellulases on the surface-displayed synthetic scaffoldins through covalent disulfide bonds. AGA2s, used as dockerins; tAGA1s, used as cohesins; GPI, the glycosyl phosphatidylinositol anchor; SP, signal peptide; BGL, *β*-glucosidase; EG, endoglucanase; CBH, exoglucanase; CBM, carbohydrate-binding module. (C) Assembly of the cellulosome using scaffoldins from *C. thermocellum*. (D) Assembly of complex cellulosomes with two scaffoldins through covalent disulfide bonds. (E) Immunofluorescence micrographs and FACS analysis of each enzyme self-assembly through



DOI: 10.1021/acscatal.9b02413
*ACS Catal.* 2019, 9, 10812−10869

**Figure** 10. continued

covalent disulfide bonds. (a) Control strain with expression of empty plasmids. (b) Assembly of *Talaromyces emersonii* exoglucanase fused with Aga2p (*Te*-aCBH1) onto synthetic scaffoldin using the repeated N-terminus of Aga1p (ScafAGA3) on yeast cell wall. (c) Assembly of *Chaetomium thermophilum* endonuclease fused with Aga2p (*Ct*-aCelA) onto ScafAGA3 on yeast cell wall. (d) Assembly of *Saccharomycopsis fibuligera* β-glucosidase fused onto Aga2p (*Sf*-aBGL1) onto ScafAGA3 on yeast cell wall. Anti-DDDDK antibody was used to detect the assembly of BGL1 and CBH1, and anti-Myc tag antibody was used to detect the assembly of CelA (endoglucanase). The control is the strain without staining. Results are representative of two independent repeat experiments. Reproduced from ref 119 under a Creative Commons license (https://creativecommons.org/licenses/by/4.0/).

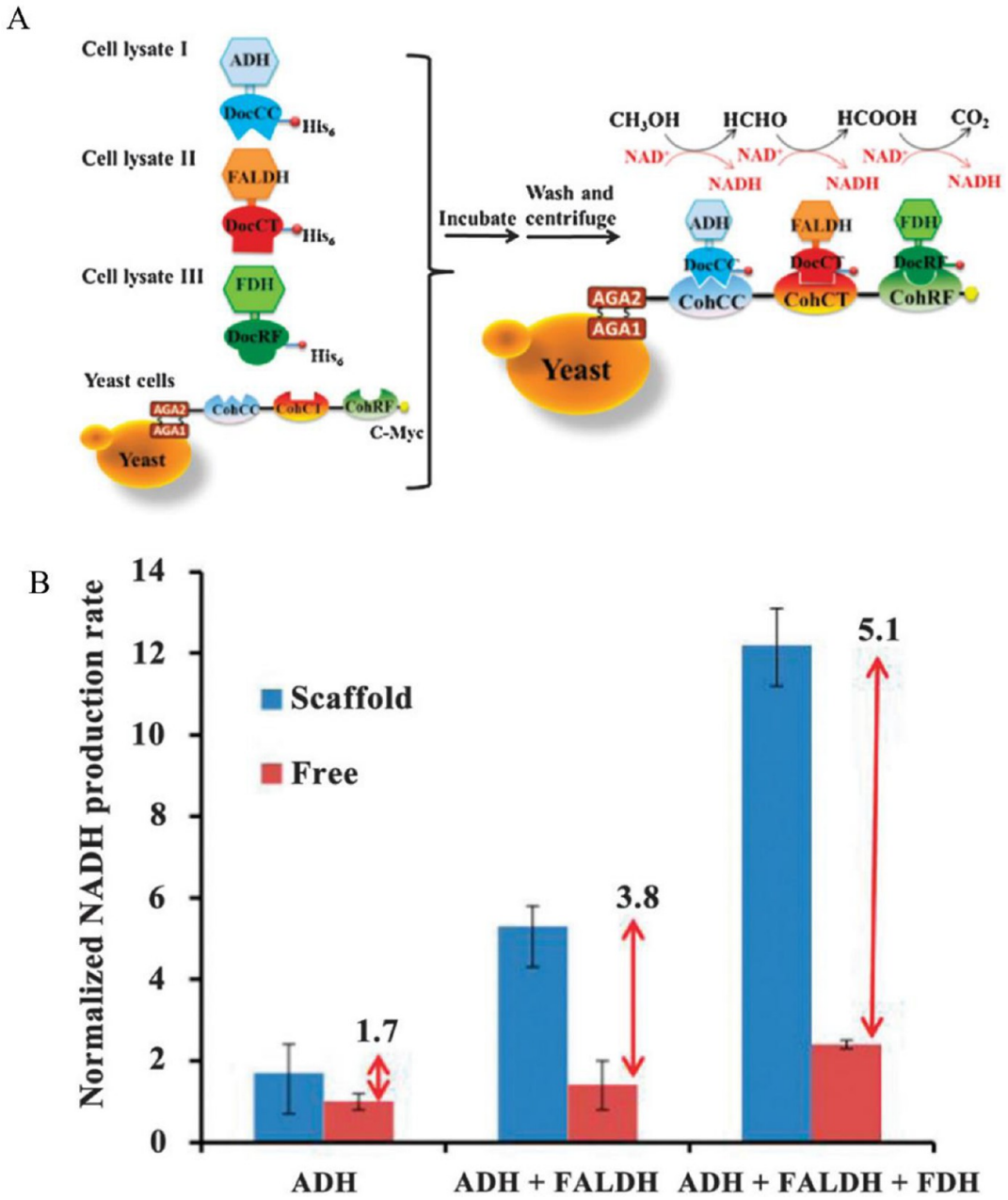


**Figure 11.** Trifunctional scaffold displayed on the yeast surface. (A) Schematic representation of the coimmobilization of three dehydrogenases (alcohol dehydrogenase (ADH), formaldehyde dehydrogenase (FALDH), and formate dehydrogenase (FDH)) on a trifunctional scaffold displayed on the yeast surface using Aga1/Aga2 components. Three orthogonal cohesin (Coh)−dockerin (Doc) pairs from *Clostridium cellulolyticum* (CC), *Clostridium thermocullum* (CT), and *Ruminococcus flavefaciens* (RF) were used for the assembly. With this system, methanol was fully oxidized to $CO_2$, resulting in three molecules of NADH. (B) NADH production rates generated by the dehydrogenase multienzyme cascade and the same amount of free enzymes. Using all three dehydrogenases on the scaffold resulted in a 5.1-fold increase in NADH production rate. Reproduced with permission from ref 116. Copyright 2013 Royal Society of Chemistry.



DOI: 10.1021/acscatal.9b02413
*ACS Catal.* 2019, 9, 10812−10869

of cellulose into ethanol directly from crystalline cellulose substrate, yielding an ethanol titer of 1.4 g/L (Figure 9B). More importantly, the constructs demonstrated a 1.3-fold increase in cellulose hydrolytic ability which was ascribed to proximity-based synergy and a 3.2−3.6-fold increase in ethanol titer for the optimized construct over unifunctional minicellulosomes. Overall, this example serves as a key proof that cellulosome-derived enzyme cascades can be assembled in a designed heterologous manner on other cell surfaces and still provide the benefit of a close-packed enzyme scaffold. Liang *et al.* built upon this approach to create analogous yeast minicellulosomes that further included lytic polysaccharide monooxygenases, which are believed to cleave cellulose oxidatively.[115] This minis-caffoldin cascade increased the ethanol titer to 2.7 g/L and allowed the yeast strain to use PASC as its sole carbon source.

While cellulosome assembly on yeast using the display of scaffoldin with cohesin−dockerin domains can be effective, it relies on the non-covalent interaction between these two domains and can face limitations including (1) a low number of cells displaying the scaffold efficiently, (2) high-affinity yet still non-covalent docking of cellulase−dockerin fusions onto the scaffold, and (3) the low activity of the cellulase−dockerin fusions.[119] To address these limitations, Tang *et al.* investigated using subunits of the *S. cerevisiae* cell adhesion protein $\alpha$-agglutinin as a docking pair instead.[119] This protein has been used previously as a yeast surface display system,[176−178] and in fact, AGA1/AGA2 was the basis for anchoring scaffoldin II to the yeast surface in the above example from Fan *et al.* but was not investigated with regard to the docking/pairing system. This protein consists of an Aga1p subunit that anchors to the surface cell wall and an Aga2p subunit that binds two cells together; these two subunits are attached using two disulfide bonds.[174,175] The N-terminus of Aga1p, called tAga1p, contains 149 amino acids and is the region that binds Aga2p. Three yeast-displayed systems were compared by the authors: (1) a scaffold using only the $\alpha$-agglutinin system docking pairs (Figure 10A,B), (2) a scaffold using the cohesin−dockerin pairs (Figure 10C), and (3) a complex scaffold using the $\alpha$-agglutinin system as the primary scaffold with the cohesin−dockerin system as branching secondary scaffolds (Figure 10D). A $\beta$-glucosidase, exoglucanase, and endoglucanase multienzyme cascade was used to test degradation of PASC followed by yeast conversion to ethanol. The display of each fusion enzyme, especially that of the endoglucanase, was significantly improved using the $\alpha$-agglutinin system versus the cohesin−dockerin system. The display percentages using the $\alpha$-agglutinin system versus the cohesin−dockerin system were 3.90% versus 1.58% for $\beta$-glucosidase, 6.39% versus 1.80% for exoglucanase, and 20.88% versus 1.58% for endoglucanase (see Figure 10E for $\alpha$-agglutinin percentages). Importantly, the display of the cohesin−dockerin system was seen only when those secreted fusion enzymes were concentrated and added to cells displaying the scaffold; for the $\alpha$-agglutinin system, the fusion enzymes could be coexpressed with the scaffold with no concentration step needed. Tang *et al.* also explored additional modifications, including placing linkers between the dockerin domain and enzymes to improve the activity (no activity increase was seen for the endoglucanase) and expressing select aspects of the yeast secretory pathway to improve yeast display of the scaffold. Ultimately, they showed 0.89 g/L ethanol production from PASC at 72 h using the $\alpha$-agglutinin system, while the cohesin−dockerin system produced 3-fold less, and 1.7-fold more was produced using the optimized complex scaffold, which was also optimized for enzyme ratios. Overall, the use of a covalent docking pair seems to come with functional advantages; however, one limitation is the inability to control the enzyme ratio in the simple system due to a lack of orthogonal docking pairs, requiring the use of complex scaffolds with the cohesin−dockerin system, though this limitation may be addressed with future research.

The use of the yeast-displayed cellulosome system is not limited to cellulose degradation; it can also be used for a completely orthogonal multienzyme cascade, as demonstrated by Liu *et al.*, who focused on assembling a system that could fully oxidize methanol to $CO_2$ (Figure 11A).[116] The goal was to fully oxidize the fuel, resulting in an improved current density for enzymatic biofuel cells.[116,179−181] The cascade reaction results in three molecules of NADH, proportional to the number of electrons that would go to a biofuel cell anode.[116] To improve upon a previously constructed scaffold,[68,182] the authors deleted the internal CBD in order to move the attached enzymes into closer proximity, leaving three divergent cohesin domains from *C. cellulolyticum*, *C. thermocullum*, and *Ruminococcus flavefaciens* to bind three different dockerins.[68,116,182] Three dehydrogenases were recombinantly expressed in *E. coli*—alcohol dehydrogenase (ADH; tetrameric) from *B. stearothermophilus*, formaldehyde dehydrogenase (FALDH; tetrameric) from *Pseudomonas putida*, and formate dehydrogenase (FDH; dimeric) from *S. cerevisiae*—each fused at the C-terminus with a separate dockerin domain that matched the species-specific cohesin domain referenced above.[68,179,182,183] The fusions did not need purification to attach onto the yeast surface; the use of just cell lysates was sufficient. Ultimately, this trifunctional scaffold on the surface of yeast cells increased the NADH production rate by 5.1-fold compared to the same amount of free enzymes (Figure 11B). This was attributed to substrate channeling and the ability to minimize product inhibition of formate on FALDH by conversion of formate to $CO_2$.

The cellulosome system has also been used without being displayed on yeast. Park *et al.* investigated using the cellulosome scaffold displayed on bacterial-derived outer membrane vesicles (OMVs).[117] OMVs are produced by some Gram-negative bacteria and consist of 20−200 nm proteoliposomes made as part of these bacteria's normal growth.[117,184−186] Displaying cellulosome scaffolds on OMVs instead of on yeast cells may be advantageous in the case of multienzyme cascade reactions for which the use of living cells could be difficult (*e.g.*, for reactions that produce toxic products or species that are substrates for competing reactions).[12,23] Furthermore, using OMVs may be less complicated than using liposomes or polymerosomes, necessitating only molecular biology methods and cell growth.[117] A potential problem in displaying the cellulosome scaffold on bacterial membranes was that the scaffold is large (>100 kDa). To solve this problem, the authors used the INP anchor to display the scaffold, as this anchor has previously been used to display proteins up to 119 kDa on *E. coli*.[187] They used *E. coli* JC8031 because this strain overproduces OMVs in comparison with *E. coli* BL21(DE3), which does not produce many OMVs under the same growth conditions.[117,188] A multienzyme cascade reaction was tested on the OMV-scaffolded system using three cellulases (an endoglucanase, an exoglucanase, and a $\beta$-glucosidase) fused to three dockerin domains that were bound to the scaffold with three cohesin domains (the scaffold also contained the cellulose-binding module in this case) (Figure 12A). This reaction catalyzes the


DOI: 10.1021/acscatal.9b02413
*ACS Catal.* 2019, 9, 10812−10869

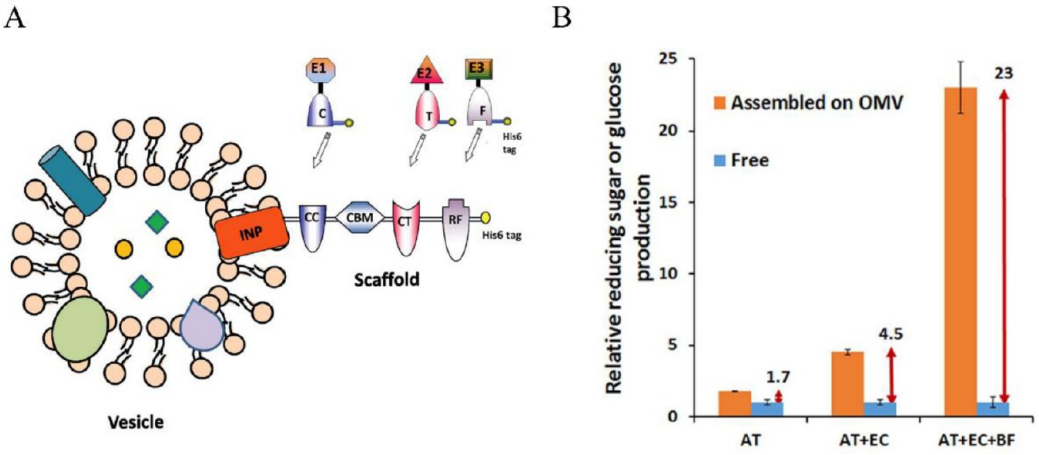


**Figure 12.** Multiple enzymes functionally assembled on engineered bacterial outer membrane vesicles (OMVs). (A) A trivalent scaffold containing three orthogonal cohesion domains, DocC (from *C. cellulolyticum*), DocT (from *C. thermocellum*), and DocF (from *R. flavefaciens*), and one cellulose-binding module was displayed on OMVs using the ice nucleation protein (INP) anchor. The specific interaction between each cohesin−dockerin pair enabled the sequential assembly of three dockerin-tagged cellulases (E1, E2, and E3) onto the OMVs at the corresponding positions (C, T, and F). With this system, PASC was degraded to glucose. CMB = cellulose-binding module. (B) Reducing sugars (AT = endoglucanase and AT+EC = endoglucanase + exoglucanase) or glucose (AT+EC+BF = endoglucanase + exoglucanase + $\beta$-glucosidase) were produced from PASC by enzyme-assembled OMVs or the same amount of free enzymes. Using all three cellulases on the scaffold resulted in a 23-fold increase in glucose compared with free enzyme. Reproduced with permission from ref 117. Copyright 2014 reference authors.

conversion of PASC to glucose, facilitating the use of common feedstocks for biosynthesis. The OMV scaffold system produced 23-fold more glucose than the free enzyme system (Figure 12B). Importantly, this system was better than a yeast display system with the same scaffold, and this was attributed to increased cooperative action between enzymes due to the smaller bacterial structure and better enzyme proximity.[117]

*Affibodies.* Another strategy to dock enzymes onto scaffolds is through the use of affibodies and their cognate binders.[120] Affibodies are based on a 58-residue three-helix bundle from the Fc-binding Z domain of *Staphylococcus aureus* protein A, where helix 2 can be engineered for increased stability and the Fc binding face can be randomized in order for affibodies to bind to other targets.[189−192] Affibodies can be paired with other affibodies that are anti-idiotypic (*i.e.*, that bind to the equivalent of an antigenic determinant of an affibody) to form a docking pair. One part of the pair can be linked to form a scaffold, and the other can be attached to the enzyme of interest (Figure 13A).[120,193] Some of the selected anti-idiotypic affibody−affibody pairs include $Z_{Taq}$:anti-$Z_{Taq}$ ($K_D$ = 0.7 $\mu$M), $Z_{IgA}$:anti-$Z_{IgA}$ ($K_D$ = 0.9 $\mu$M), $Z_{HER2}$:anti-$Z_{HER2}$ ($K_D$ = 0.3 $\mu$M), and $Z_{WT}$:anti-$Z_{WT}$ ($K_D$ = 0.05 $\mu$M).[120,189] Importantly, there are many known affibody/anti-idiotypic pairs that are orthogonal, so this system could be used to dictate enzyme ratios and/or positions on scaffolds similarly to the previous cohesin−dockerin systems.[120,189,194]

Tippmann *et al.* examined the use of affibody pairs to associate enzymes with scaffolds because of their small size, stability, and fast folding kinetics.[120] In addition to a two-enzyme cascade for farnesene production, they also examined a three-enzyme cascade to produce polyhydroxybutyrate (PHB) from *Synechocystis* sp. PCC 6803, since this compound can be used as a bioplastic (Figure 13A).[195] Importantly, the first step is thermodynamically unfavorable (under standard conditions), and thus, channeling the product (acetoacetyl-CoA) forward could improve the overall reaction (Figure 13B). The N-terminus of the enzymes were fused to $Z_{WT}$, $Z_{HER2}$, and $Z_{IgA}$; the scaffold contained the cognate antiaffibodies separated by $(SSSSG)_4$ linkers (Figure 13A). Production of PHB by the fusion enzymes was increased 3-fold even in the absence of scaffold; using this scaffold, production was increased another 2.5-fold, but only at low enzyme and scaffold levels (Figure 13C). The authors indicated that along with placement of the affibody, the affibody-pair $K_D$ values could affect the efficiency of the system. The $K_D$ values indicate a half-life of 3−50s for the complex, while enzyme−substrate complex lifetimes can be estimated as 35−270 ms (based on median enzyme turnover numbers for central and secondary metabolism);[39] therefore, the lifetime of the complete scaffold may be short compared with the kinetics of the multienzymatic reaction. A further way to improve the efficiency could be scaffold aggregates based on multimeric enzymes.[12,14,28,56,59,60,196,197]

*Display on 2D/3D Architectures.* While the previous examples have focused on a scaffold of linked binding domains, Zhang *et al.* recently developed a system using a shell protein from the ethanolamine utilization (Eut) microcompartment of *Salmonella enterica*, as shown in Figure 14A.[123] EutM forms hexamers that self-assemble into arrays, which then assemble *in vivo* into microcompartment shells.[198−200] The authors showed that EutM purified from *E. coli* self-assembled *in vitro* into large crystalline arrays (not shells) and envisioned this as a scaffold for multienzyme assembly. To attach enzymes to this scaffold, the authors chose to use the SpyTag/SpyCatcher system,[201] where the ∼1.5 kDa SpyTag peptide would be fused to the enzyme and the ∼9.5 kDa SpyCatcher would be fused to EutM. Upon encountering each other, the SpyTag/SpyCatcher pair forms an autocatalytic isopeptide bond. Using green fluorescent protein (GFP) and mCherry in place of enzymes, the authors showed that the SpyTag/SpyCatcher system could associate proteins with the EutM scaffold *in vivo* and found that the C-terminal fusion of SpyCatcher to EutM only slightly altered self-assembly. On this basis, an N-terminal His-tagged EutM−SpyCatcher fusion was overexpressed in *E. coli*, purified in one-step, and found to self-assemble at room temperature at pH 7.4 into micrometer "nests" formed from long, flexible protein fibrils with widths of ∼40 nm width and lengths of several


DOI: 10.1021/acscatal.9b02413
ACS Catal. 2019, 9, 10812−10869

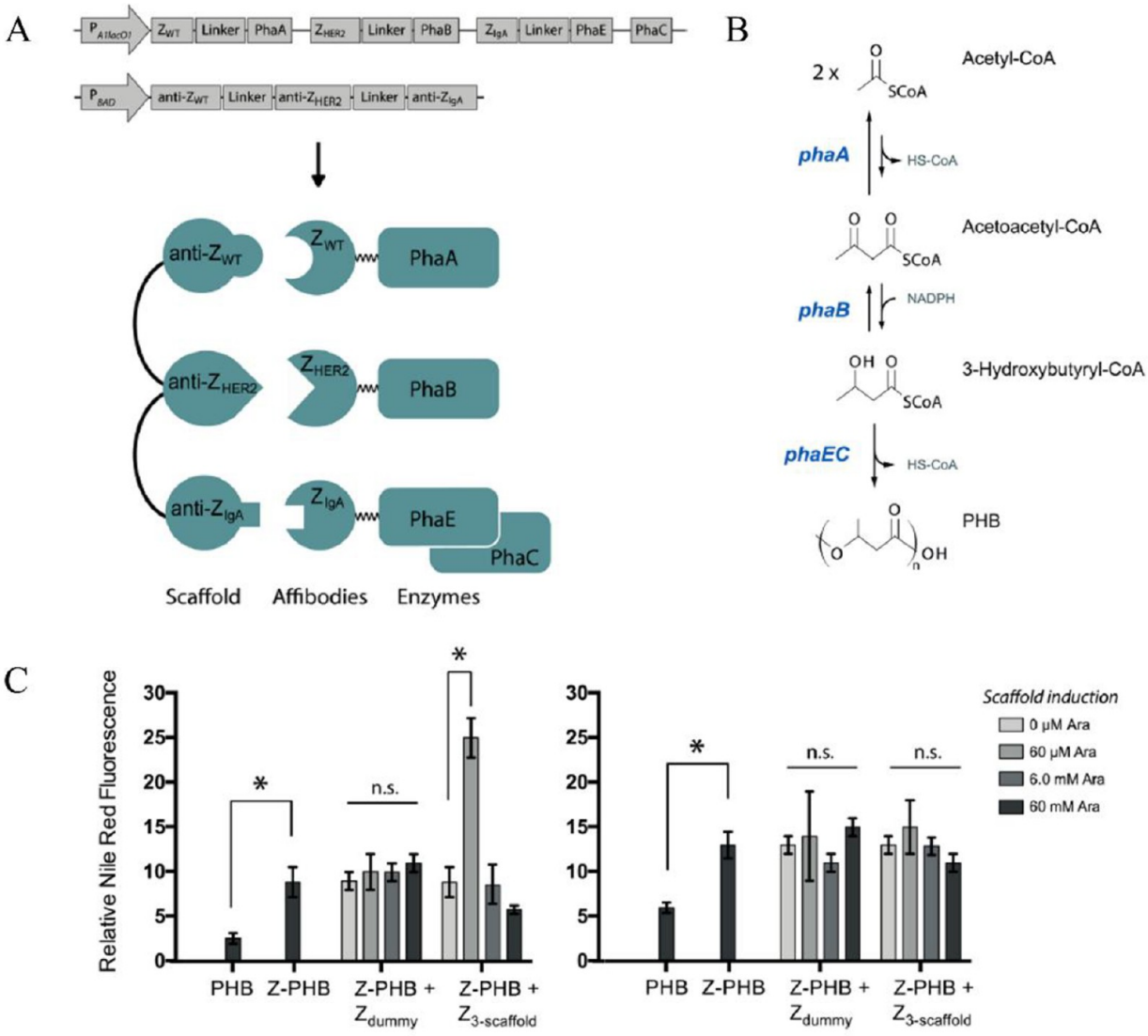


**Figure 13.** Affibody scaffold for improved production of polyhydroxybutyrate (PHB) from *E. coli*. (A) The PhaA, PhaB, and PhaEC enzymes were tagged N-terminally with affibodies $Z_{WT}$, $Z_{HER2}$, and $Z_{IgA}$, respectively. Genes encoding the enzymes were expressed from the IPTG-inducible promoter $P_{A1lacO1}$, and the three-site anti-idiotypic affibody scaffold (anti-$Z_{WT}$−anti-$Z_{HER2}$−anti-$Z_{IgA}$) was expressed from the arabinose-inducible promoter $P_{BAD}$. (B) The heterologous PHB pathway consists of three enzymes and was cloned into *E. coli*. (C) PHB levels 24 h after enzyme and scaffold induction in M9 medium supplemented with glycerol to 2%. PHB quantification was done using Nile Red staining and fluorescence measurements and was normalized by cell density. (left) PHB enzymes were induced at low IPTG concentrations (0.05 mM). Fusion of affibody tags increased the PHB levels significantly (*, $P < 0.05$; n.s., not significant ($P > 0.05$); Student's $t$ test). Induction of the $Z_3$ scaffold also increased the PHB levels, but only at low scaffold induction (60 $\mu$M arabinose). The presence of a nonbinding antibody ($Z_{dummy}$) did not affect the PHB levels. (right) PHB levels when PHB enzymes were induced at high IPTG concentrations (0.5 mM). Reproduced from ref 120. Copyright 2016 American Chemical Society.

hundred nanometers. These were stable at pH 5−9 and up to 50 °C. Attachment of SpyTag−GFP could be done at the same time as self-assembly or after self-assembly. In some cases, there was not a 100% yield of SpyTag fusion(s) attachment to SpyCatcher fusion(s); this has been documented previously for this system and reflects the complexity of optimizing conditions for efficient completion of the reaction.[201]

Encouraged by these results, the same authors aimed to assemble two enzymes to enantioselectively convert (*S*)-2-hexanol to (*R*)-2-aminohexane as proof of concept based on a cascade developed by Mutti *et al.*[202] SpyTags were fused to the broad-specificity $NAD^+$-dependent alcohol dehydrogenase Prelog AA-ADH and a chimeric Ch1-AmDH NADH-dependent amine dehydrogenase engineered for stability.[203−205] N-terminal fusion of the SpyTag slightly improved the activity of the enzymes; C-terminal fusion to AA-ADH severely lowered activity. Overall, SpyTag−Ch1-AmDH had ∼300-fold lower catalytic efficiency ($k_{cat}/K_M$) than SpyTag−AA-ADH, so the loading ratios onto EutM−SpyCatcher were adjusted to partially compensate for this. Different ratios of the fusion enzymes versus the scaffold were also tested (1:1−1:6), and attachment resulted in a dense filmlike material on top of the fibril-like scaffold (in contrast to GFP fusion, which did not change the appearance of the scaffold). As the enzymes are multimers, they may attach to the scaffold in multiple places, and this may account for the change in appearance.[205−207] Overall, the scaffolded system improved the percentage of chemical conversion versus free tagged enzymes (Figure 14B)



DOI: 10.1021/acscatal.9b02413
ACS Catal. 2019, 9, 10812−10869

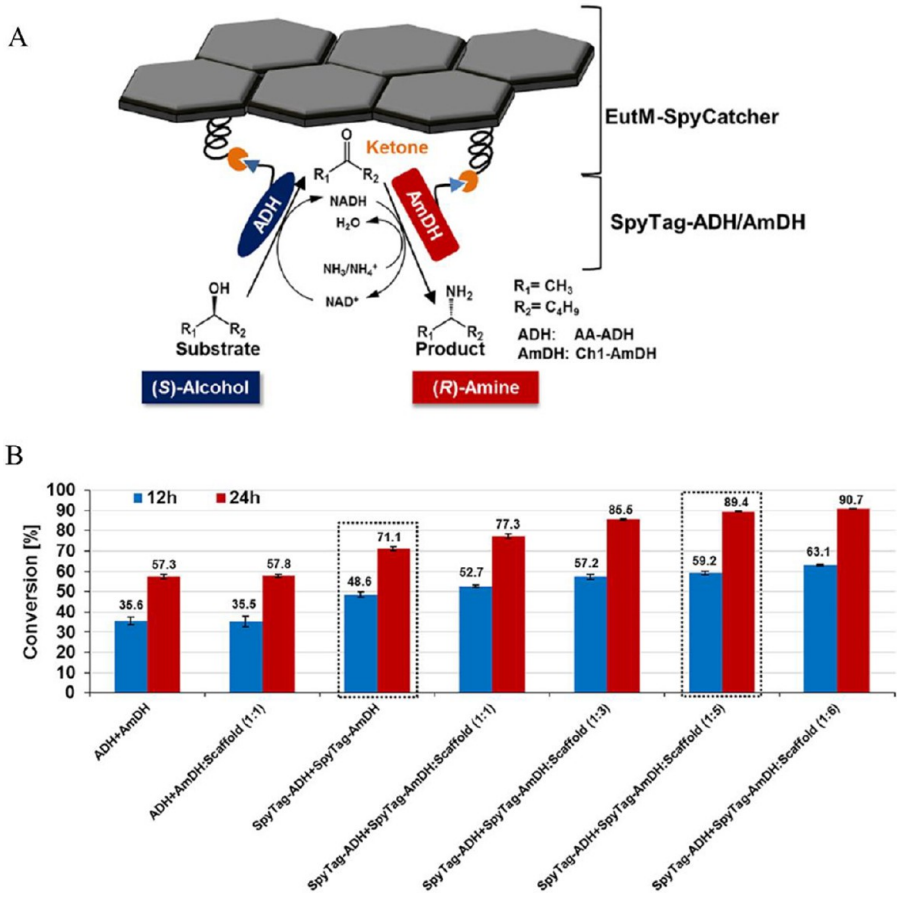


**Figure 14.** Coimmobilization of a dual enzyme cascade for chiral amine synthesis. (A) Schematic of the dual enzyme cascade coimmobilized on EutM (bacterial microcompartment protein)−SpyCatcher protein scaffolds. An $NAD^+$-dependent alcohol dehydrogenase (ADH) oxidizes an alcohol substrate into the corresponding ketone intermediate, which is subsequently reduced by an NADH-dependent amine dehydrogenase (AmDH) into a chiral amine. In this study, a Prelog AA-ADH with broad substrate specificity was combined with an engineered, stable, chimeric Chl1-AmDH for the conversion (*S*)-2-hexanol to (*R*)-2-aminohexane. (B) One-pot amination reaction with free and EutM−SpyCatcher-scaffolded dual-enzyme cascade. Conversion rates of (*S*)-2-hexanol to (*R*)-2-aminohexane by free and scaffolded SpyTag−ADH/AmDH dual-enzyme cascades (controls contain untagged ADH/AmDH) containing increasing molar ratios of EutM−SpyCatcher after 12 and 24 h are shown. Data are averages of three replicate experiments, and error bars are standard errors of the mean. All of the cascade reactions were performed at 30 °C and 190 rpm in a 3 mL reaction volume with ammonium chloride buffer (2 M, pH 8.7) containing 20 mM (*S*)-2-hexanol, 1 mM $NAD^+$, 6 $\mu$M ADH, 150 $\mu$M AmDH, and EutM−SpyCatcher (scaffold) added to obtain differing molar ratios of enzymes to scaffold. Conversion rates are shown as the percentages of alcohol converted to the ketone intermediate and final amine product. Reproduced from ref 123. Copyright 2018 American Chemical Society.

and reached close to the same yield of (*R*)-2-aminohexane in only 24 h as the free enzymes (untagged) did at 48 h (~90%)[202] with low enzyme fusion to EutM ratios (*e.g.*, 1:5, 1:6). This increase in activity could be due to increased stability of the enzymes at these ratios, though at ratios of 1:1 and 1:3 the SpyTag−AA-ADH exhibited lower activity at all time points, perhaps because of problems in quaternary structure. Of note regarding this approach, a toolbox of EutM proteins from diverse microorganisms with different properties such as different architectures was developed, with potential for use in future enzyme immobilization.[208]

*Multienzyme Fusions.* Another method for creating scaffolded multienzyme cascades is to fuse enzymes together using a peptide bridge. An excellent example that specifically addresses substrate channeling was described by Liu *et al.* using the enzymes hexokinase (HK) and glucose-6-phosphate dehydrogenase (G6PDH).[62] The authors sought not only to fuse these two enzymes together with a peptide bridge but also to specifically use a cationic peptide to exploit electrostatic attraction with the dually negatively charged intermediate glucose-6-phosphate. In this approach, electrostatic interactions can facilitate substrate channeling even at longer distances between active sites.[209] This could be considered as using the barrier to (bulk) diffusion as described in the Introduction. The authors used molecular dynamics simulations and found that the best cationic amino acid to use was lysine (vs histidine or arginine) and that it is best used as slightly nonsaturating in the bridge. They additionally found through these simulations that dually negatively charged intermediates are much better than singly negatively charged intermediates, as the dual negative charge allows for coordination with two lysine residues that helps with diffusion along the bridge. A pentalysine bridge was then constructed to fuse the two enzymes together, linking through a convergent synthesis (Figure 15A). The use of neutral linking techniques makes the entire bridge close to the nonsaturated, theoretical optimum lysine density; furthermore, the total bridge was only ~4 nm long, within the expected distance to allow for substrate channeling facilitated by electrostatics.[62,209] A control bridge constructed from the neutral amino acid glycine was also used. It was found that the


DOI: 10.1021/acscatal.9b02413
*ACS Catal.* 2019, 9, 10812−10869

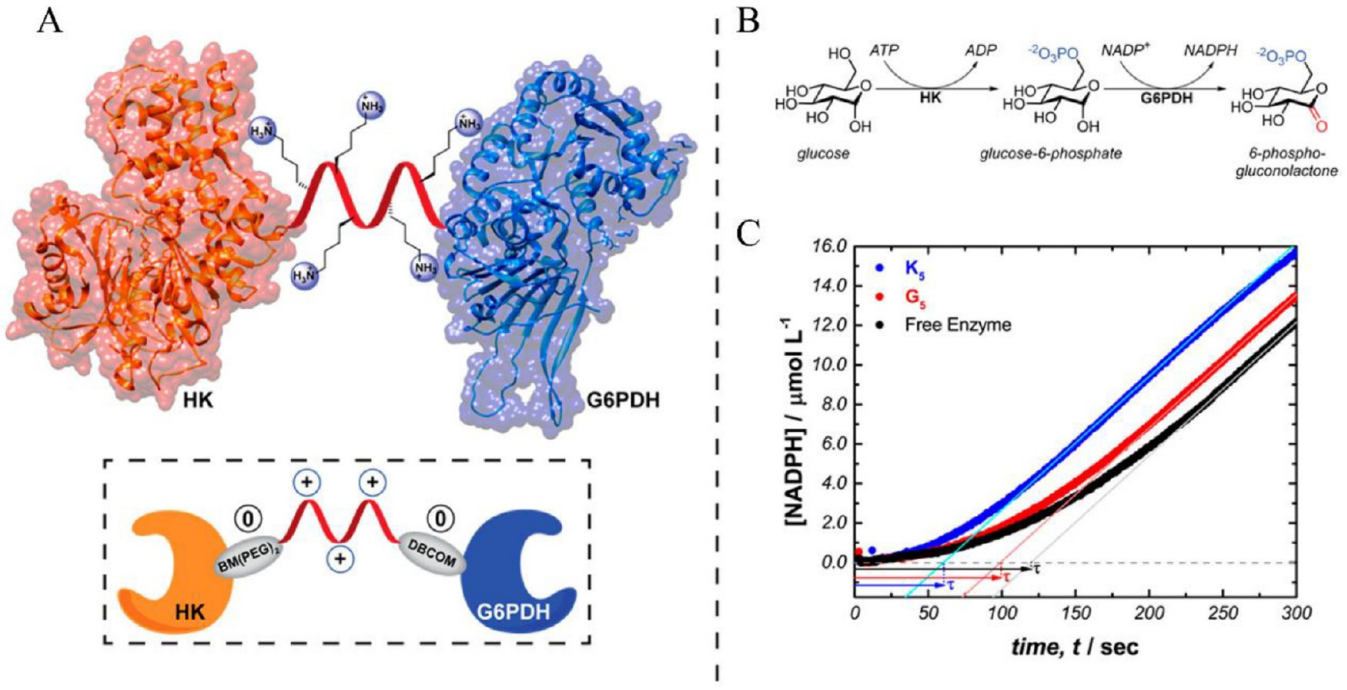


**Figure 15.** Electrostatic bridge for substrate channeling. (A) Illustration of the proposed channeling complex using a poly(lysine) bridge as an electrostatic surface between hexokinase (HK) (PDB entry 3VF6) and glucose-6-phosphate dehydrogenase (G6PDH) (PDB entry 4LGV). (B) Experimental reaction scheme used to study electrostatic channeling of the charged intermediate (glucose-6-phosphate) across a cationic peptide bridge. (C) Sample absorbance plot highlighting the determination of the experimental lag time ($\tau$) for complexes containing a 4 nm cationic bridge ($K_5$), a neutral bridge ($G_5$), or free enzymes. Reproduced from ref 62. Copyright 2017 American Chemical Society.

lag time decreased significantly using only the lysine bridge, indicating substrate channeling (Figure 15B,C). This conclusion was bolstered by the finding that increasing the enzyme concentration to the point where the free enzymes would be close together in space obviated the relative decrease in lag time for the peptide-fused construct. To demonstrate that electrostatics did indeed play a role, the authors went on to show that the decrease in lag time was dependent on the ionic strength, increasing to nearly the free enzyme level at a NaCl concentration of 100 mM. Altogether, this combined theoretical and experimental work demonstrated that this technique is a viable method for producing substrate channeling between enzymes with a dually charged intermediate.

In contrast to using paired binding domains as a scaffold or to bind a scaffold, one can use them to attach enzymes directly to each other. This can be particularly valuable if one or more of the enzymes is dimeric/multimeric, as it can facilitate enzyme ratios beyond 1:1, which can have benefits such as aligning the catalytic activity more closely to the ratio of desired enzyme activities. One example of using binding domains in this way was described by Yang *et al.*,[122] who explored the production of itaconic acid, a building block for various polymers.[122,210−213] The three enzymes used in the cascade to produce itaconic acid were citrate synthase (gltA, GA; predicted dimeric), aconitase (acnA, ACN; monomeric), and *cis*-aconitate decarboxylase (cadA, CAD; dimeric).[214] As shown in Figure 16A,B, GA was produced as a fusion to a C-terminal scaffolding domain encoding the Src homology domains PSD95/DlgA/Zo-1 (PDZ) and the murine SH3 domain. To ensure rigidity and position of the PDZ and SH3 domains, a rigid 5 nm $\alpha$-helical domain was incorporated between GA and the PDZ domain as well as between the PDZ and SH3 domains.[17,215,216] As GA is dimeric, the C-terminal scaffold allows for the assembly of two monomeric ACN−PDZ and a single CAD−SH3 dimer as they bind to their respective binding domains. Of note, the linker $(GGGGS)_2$ was used between the fusions of ACN/CAD and PDZ ligand/SH3 ligand, respectively.[215] All of the additions were fused to the C-termini of the respective enzymes, and the location of the additions did indeed impact the overall efficiency.[17] Therefore, the complex had a final GA:ACN:CAD ratio of 1:2:1. The fused enzymes retained most of their specific activity versus unfused enzymes. This complex self-assembled into 50−120 nm particle-like structures as multiple complexes (likely two to four units of complex). Aggregation did increase the overall efficiency of the system, likely as a result of the increased likelihood that any intermediates that happened to escape the complex would quickly hit another complex (see the Introduction).[12,14,28,56,59,60] Overall, *in vivo* an *E. coli* strain expressing the entire complex produced 3.84-fold more itaconic acid than the control strain expressing free enzymes. After additional metabolic engineering, the production of itaconic acid was 3.06 g/L, and the concentration of byproducts was significantly reduced (Figure 16C).

In another example, Price *et al.* were able to effect a large 1:10 enzyme ratio just by using enzyme fusion.[118] They focused on a multienzyme cascade converting methanol to fructose-6-phosphate to facilitate the use of methanol as a feedstock. This cascade utilizes the decameric methanol dehydrogenase MGA3 (Mdh3), 3-hexulose-6-phosphate synthase (Hps), and 6-phospho-3-hexuloseisomerase (Phi).[217−222] A significant aspect of this reaction is that the first enzyme, methanol dehydrogenase, favors the reverse direction (formaldehyde to methanol); having enough Hps and Phi is one way to irreversibly sequester formaldehyde and drive the reaction forward efficiently.[220] The authors noted that one could do this by expressing 10-fold more Hps than Mdh3 *in vivo* but that this


DOI: 10.1021/acscatal.9b02413
ACS Catal. 2019, 9, 10812−10869

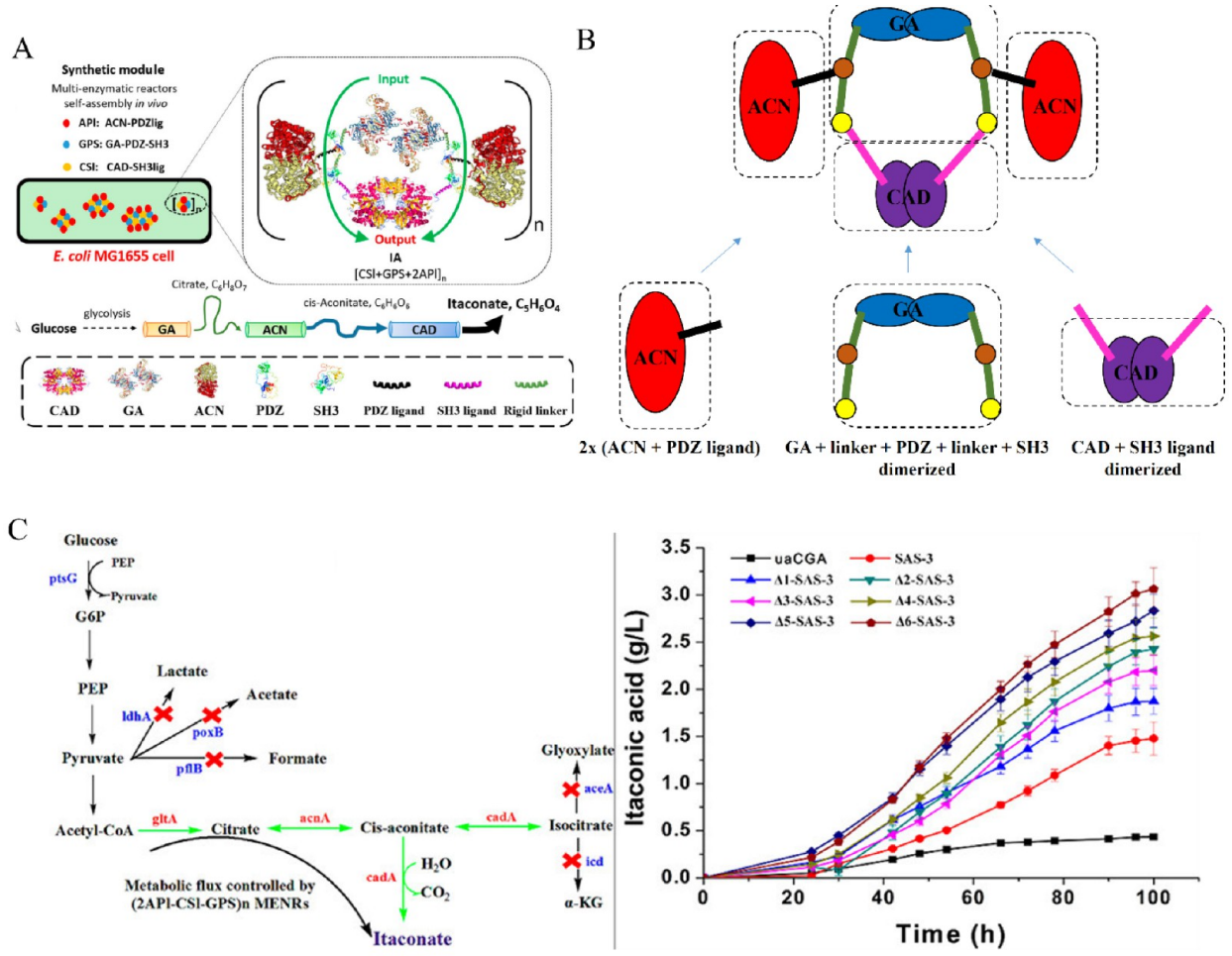


**Figure 16.** Sequential self-assembly of a multienzymatic complex reactor. (A) Strategy for self-assembly of complex reactors of the heterogeneous dimeric citrate synthase (GA), monomeric aconitase (CAN), and dimeric *cis*-aconitate decarboxylate (CAD) using protein−peptide interaction domains and ligands (mouse SH3 and PDZ domains/ligands). The scheme at the right presents the putative self-assembly mechanism for the conversion of citric acid to itaconic acid (IA) in the presence of a sequential catalytic flux (green arrows). (B) Simplified cartoon representation of (A) for illustrative purposes. (C) Illustration of the cooperating metabolic engineering strategy with the sequential self-assembly system to increase the biocatalytic efficiencies. (left) Schematic representation of the metabolic networks integrating the itaconate pathway in *E. coli*. (right) The IA productions were measured in all of the genetically manipulated strains, with the unassembled strain uaCGA employed as the control. Each data point represents the mean ± SD of three measurements. Adapted from ref 122. Copyright 2018 American Chemical Society.

may result in a heavy cellular burden, especially if all of the downstream enzymes also had to be expressed at a high level. Instead, they used Mdh3 as a core for a complex as well as Hps alone and a previously investigated Hps−Phi fusion that had more activity than a 1:1 mixture of Hps and Phi.[223] On the basis of the understanding that multimeric enzymes are typically hard to assemble and can form large and disordered complexes if random cross-linking between enzymes and scaffolds is used,[224] they opted to use interaction domains and take advantage of the self-assembly of multimers.[225] The SH3 domain/ligand pair was used to complex Mdh3 with the Hps−Phi fusion; this pair has $K_D$ = 0.1 $\mu$M.[17] The SH3 ligand (sSH3lig, PPPALPPKRRR) was fused to the decameric Mdh3, and the SH3 domain was fused to Hps alone or the Hps−Phi fusion (Figure 17A). The complex of Mdh3−Hps with free Phi at a 1:1:1 ratio led to 27-fold greater production of fructose-6-phosphate than the free enzymes *in vitro*; using the Hps−Phi fusion at a 1:1 ratio led to 50-fold greater production, which was better than even an Mdh:Hps:Phi ratio of 1:5:5 (Figure 17B). The size of the complex between Mdh and the Hps−Phi fusion was 24 nm, indicating that large multienzyme complexes did not form. To improve the reaction even more, the authors added an NADH sink using lactate dehydrogenase; this resulted in a 97-fold increase overall relative to the free enzymes. This system was also tested *in vivo*, where methanol consumption was approximately 9-fold faster using the complex, though only 2.3-fold faster after 24 h, perhaps because of limitations in resting cell cultures.[118] Overall, this example clearly illustrates the power of enzyme fusions using designer multimeric enzymes.

*Inclusion-Body-Based Scaffolding and the Use of Coiled Coils/Leucine Zippers.* *A priori*, if one wanted to design a simple system to bring two enzymes together, one might start by trying to find short complementary-binding peptides and then fuse them to those enzymes. Coiled coils represent a family of just this type of system: two or more $\alpha$-helices, each with seven amino acid repeats, that twist together in a supercoiled bundle with micromolar to subnanomolar affinities.[226−228] An important subfamily of coiled coils are the leucine zipper peptides, which are ∼40 residues long and combine two to four helices.[227] Extensive research has


DOI: 10.1021/acscatal.9b02413
ACS Catal. 2019, 9, 10812−10869

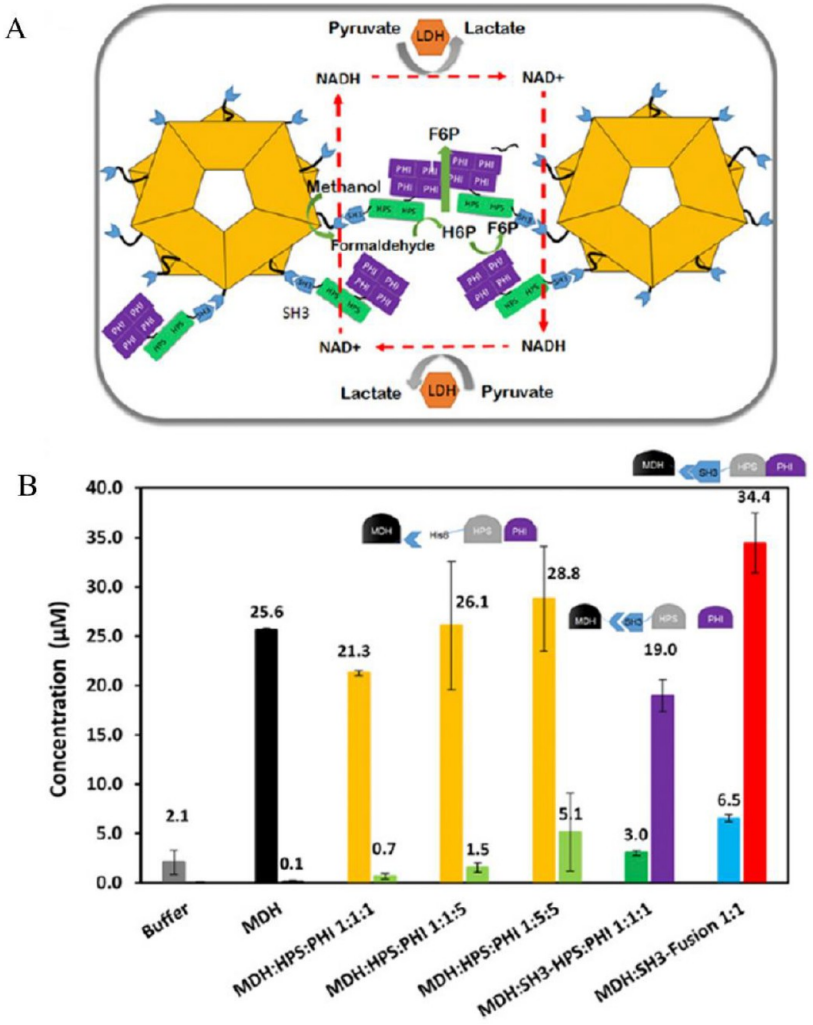


**Figure 17.** Mdh3−Hps−Phi supramolecular enzyme complex. (A) Schematic of the methanol dehydrogenase−3-hexulose-6-phosphate synthase−6-phospho-3-hexuloseisomerase (Mdh3−Hps−Phi) supramolecular enzyme complex and corresponding cascade reactions. Lactate dehydrogenase (LDH) was used as an NADH sink to further minimize formaldehyde reduction. H6P = hexulose-6-phosphate; SH3 = Src homology 3 domain from the adaptor protein CRK; SH3lig = SH3 ligand. (B) Formaldehyde (first bar) and fructose 6-phosphate (F6P) (second bar) formation with and without SH3-tethered enzymes. Purified Mdh−sSH3lig was mixed with either Hps and Phi, SH3−Hps and Phi, or the SH3−Hps−Phi fusion. Formaldehyde was assayed using the Nash reagent. Error bars represent SDs of at least three replicate experiments. Reproduced with permission from ref 118. Copyright 2016 reference authors.

expanded our knowledge of the various coiled-coil domains that are available for further utility.[226,227,229−232]

An exciting application of coiled coils with regard to multienzyme cascades is to use them with inclusion bodies (IBs). IBs are aggregates of proteins found both in prokaryotes and eukaryotes (a.k.a. aggresomes); historically, these aggregates were thought to be only inactive, unfolded proteins, but recent research has shown that, at least in *E. coli*, these aggregates can retain some activity (they are known as CatIBs when catalytically active).[114,233,234] Therefore, a protein scaffold that facilitates IB formation can be fused to one helix of a coiled coil, while the enzymes constituting the reaction cascade can be fused to the complementary helix; upon formation of the IB and mixing, the coiled-coil interaction brings the multienzyme cascade into proximity. Han *et al.* took advantage of this with their system to produce 1-butanol from acetoacetyl-CoA.[113] They used the CBD of *Cellulomonas fimi* exoglucanase to induce IB formation and fused this to one part of a leucine zipper.[113,235,236] The complementary part (to form an antiparallel leucine zipper) was fused to four enzymes of the final cascade: 3-hydroxybutyl-CoA dehydrogenase (Hbd), crotonase (Crt), butyryl-CoA dehydrogenase (Ter), and butylaldehyde dehydrogenase/butanol dehydrogenase (AdhE2), where all but Ter (from *Treponema denticola*) were from *Clostridium acetobutylicum* (Figure 18A).[113,237] The IB−leucine zipper−enzymes construct was tested both *in vitro* and *in vivo* (Figure 18B). *In vitro*, separate cell-free extracts of the tagged enzymes and the IB were prepared, mixed, and washed, resulting in a 7.3−7.9-fold increase in the rate of butanol production versus free enzymes (free enzymes did show lower activity in insoluble fractions). *In vivo*, the rate increase was estimated to be 1.5−2-fold (Figure 18C).

Jäger *et al.* also exploited an IB/coiled-coil system, but in a different way.[114] They fused the tetrameric coiled-coil domain of tetrabrachion from *Staphylotermus marinus* both to induce inclusion body formation and to bind the enzymes together.[114,238,239] They specifically pointed out the following advantages of CatIBs: they are easy to produce in *E. coli*; they can be handled/stored in frozen suspension or lyophilized; often they are more stable long-term; and they are easily


DOI: 10.1021/acscatal.9b02413
*ACS Catal.* 2019, 9, 10812−10869

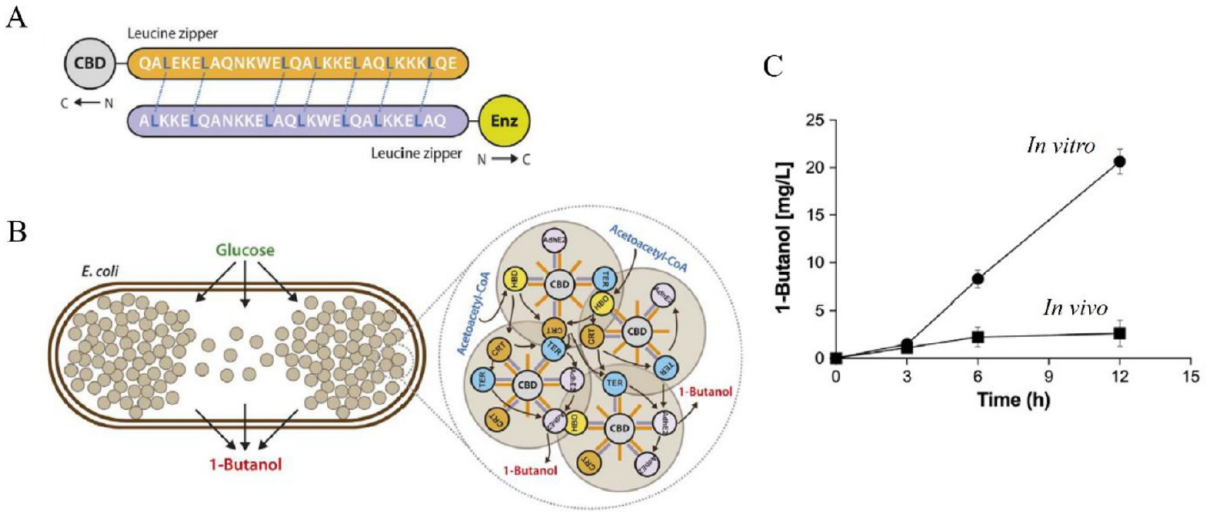


**Figure 18.** CBD inclusion body (IB)-based novel metabolon system for the production of molecules of interest. (A) Peptide−peptide interaction between two antiparallel leucine zipper (LZ) domains of enzymes and CBD IBs. (B) Scheme for colocalization of multiple heterologous enzymes involved in 1-butanol production onto the CBD IBs. Arrows indicate the possible intermediate channeling. Hbd = 3-hydroxybutyryl-CoA dehydrogenase; Crt = crotonase; Ter = butyryl-CoA dehydrogenase; AdhE2 = butylaldehyde/butanol dehydrogenase. *hbd*, *crt*, and *adhE2* genes were from *Clostridium acetobutylicum*, and *ter* was from *Treponema denticola*.[237] (C) Bioconversion profiles of acetoacetyl-CoA to 1-butanol in metabolon-free *E. coli* (■; *in vivo*) and in the CBD-IB-based metabolon (●; *in vitro*). Data represent means ± SD of three replicate cultures. Reproduced with permission from ref 113. Copyright 2016 International Metabolic Engineering Society.

recycled because of their insolubility in aqueous or organic systems.[114,238] They used this system to produce (1*R*,2*R*)-1-phenylpropane-1,2-diol (a precursor for the calcium channel blocking drug diltiazem) from benzaldehyde and acetaldehyde using two enzymes attached to the coiled coil through a flexible linker: benzaldehyde lyase from *Pseudomonas fluorescens* and alcohol dehydrogenase from *Ralstonia* sp.[240−243] They found that >80% of the activity in the cell lysates was in the insoluble fraction, indicating that the enzymes were pulled to inclusion bodies; however, the enzymes retained only ∼1−3.3% of their activity compared with purified enzymes (although the higher yield partially compensated for this). Importantly, though, the inclusion body system showed more stability than free enzymes, with 7- to 15-fold higher residual activity after 4 days of reaction. Furthermore, the inclusion body system worked even though the enzymes required cofactors, were tetrameric (with minimal functional units as dimers/monomers), and had subunit sizes of 60.0 and 26.7 kDa, indicating the flexibility of this approach.[114,242,244,245]

*Protein Crystalline Inclusions by Cip Scaffolds.* In an alternate aggregate-type approach, Wang *et al.* focused on Cip scaffolds.[121] Cip scaffolds are composed of the protein CipA (104 amino acids) or CipB (100 amino acids) from *Photorhabdus luminescens* fused to enzymes of interest.[121,246,247] Cip scaffolds can (1) organize single or multiple proteins into protein crystalline inclusions (PCIs), (2) be used *in vivo* or readily isolated and utilized *in vitro*, and (3) organize multiple enzymes into functional complexes. Wang *et al.* showed that Cip−enzyme fusions could form insoluble PCIs that could be purified within 2 h simply by cell disruption, centrifugation, and washing (90% pure by polyacrylamide gel electrophoresis (PAGE)); these PCIs could be dissolved only in high levels of denaturing solutions (10% w/v SDS or 8 M urea), strongly acidic (pH 3) or alkaline (pH 11) conditions, or partially with 50% v/v glycerol, but not with high concentrations of NaCl or EDTA; this facilitated their easy isolation. Cip−enzyme fusions could also move the enzyme maximum activity to higher temperatures, as the optimum temperature of $\beta$-galactosidase (LacZ, $\beta$-Gal) was moved from 42 °C as His−LacZ to 52 °C as CipB−LacZ. In terms of a multienzyme cascade, the violacein pathway was investigated *in vivo*. This pathway consists of five enzymes (VioA−E) to make the bisindole violacein, which has potential applications in medicine.[248,249] Different combinations of selected enzymes from this pathway fused to a Cip scaffold or left free in solution were tested, including the situation where all of the enzymes were fused to a Cip scaffold and a control in which all of the enzymes were free in solution. Importantly, the combination resulting in the highest yield per $OD_{600}$ and the highest percentage of product over byproduct did not have all of the enzymes fused to a Cip scaffold: only three of the five enzymes were fused, with the remaining two free in solution. This combination resulted in a 2.6-fold increase in yield/$OD_{600}$ and an 8.8-fold increase in rate. The highest overall combination was 3.2- and 22.2-fold, respectively, but this combination had a higher percentage of byproduct. In contrast, having all of the enzymes fused to a Cip scaffold led to a 7.5-fold *decrease* in yield/$OD_{600}$; the authors indicated that this was due to a decrease in the specific activities of the enzymes.[121] Therefore, a critical aspect of this approach is that different combinations should be tested to see which results in the best improvement.

**Cross-Linked Enzyme Aggregates.** The previous two examples highlighted IBs/PCIs initiated and maintained by peptides (CBDs, coiled coils, and Cip scaffolds). Similarly, enzymes can be precipitated but then maintained as aggregates through synthetic chemistry, affording cross-linked enzyme aggregates (CLEAs). Enzymes are aggregated using a precipitant such as ammonium sulfate, poly(ethylene glycol) (PEG), or *tert*-butyl alcohol in such a way as to maintain (partial) catalytic activity and then cross-linked using a chemical such as glutaraldehyde, which cross-links the amines of lysine residues.[250−252] There are several properties that can affect the efficiency of this method. First, enzymes can be precipitated alone or with an additive, such as bovine serum


DOI: 10.1021/acscatal.9b02413
*ACS Catal.* 2019, 9, 10812−10869

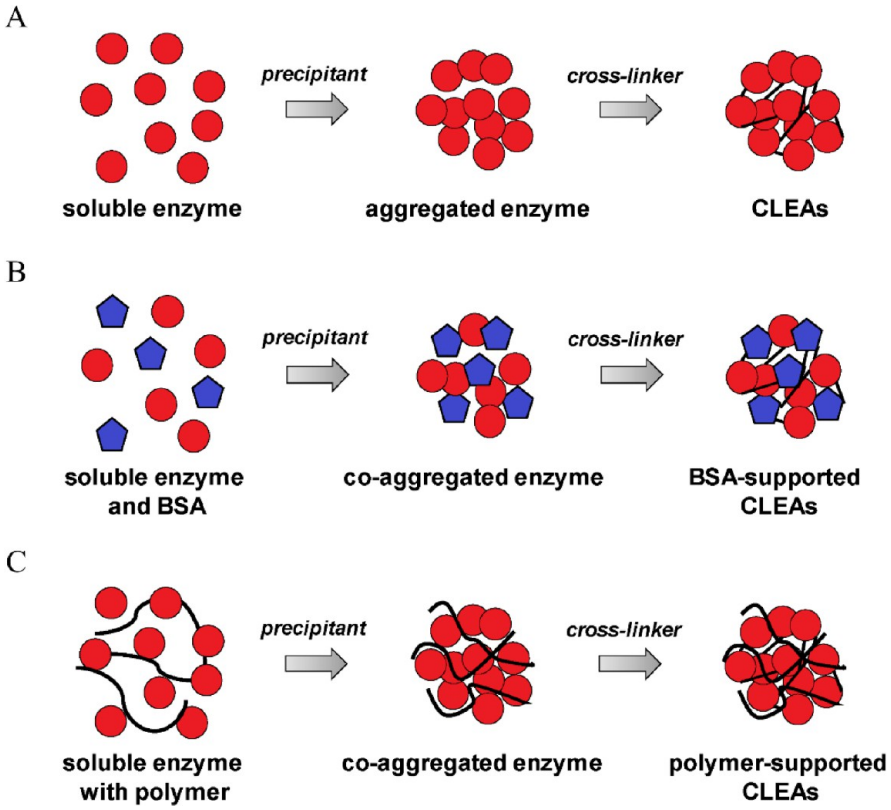


**Figure 19.** Methods of preparing cross-linked enzyme aggregates (CLEAs). (A) General cross-linking method. (B) Another protein like bovine serum albumin (BSA) can be added for the protein-supported CLEA cross-linking method. Combined CLEAs (combi-CLEAs) are prepared by similar processes. (C) Ionic polymers can be used to support CLEAs. Adapted from ref 250 under a Creative Commons license (https://creativecommons.org/licenses/by/4.0/).

albumin (BSA) or polymers (Figure 19A,B).[250] BSA can improve the CLEA yield when dealing with low enzyme concentrations or enzymes that are particularly susceptible to inactivation by glutaraldehyde.[253] Polycationic polymers such as polyethylenimine (PEI) can also improve CLEA cross-linking when enzymes have low amounts of lysines available for cross-linking (Figure 19C).[254−256] Second, the choice of precipitant can affect the activity[252] as well as the choice of cross-linker, particularly if the cross-linker reacts with side-chain functional groups on key catalytic residues.[257] Instead of glutaraldehyde, ethylene glycol bis(succinimidyl succinate) (EG-$(NHS)_2$) has been used as a milder cross-linker. Third, the sizes of most reported CLEAs are less than 10 $\mu$m, which may not be optimal for a given application.[258] To modulate the size, CLEAs can be cross-linked into materials such as mesoporous silica or alginate[127,251,259,260] or onto magnetic NPs, which can also facilitate their reuse.[261] Finally, a form of molecular imprinting can be used by adding in a molecule to help keep the enzyme in an open conformation during preparation.[262,263] CLEAs can also be prepared immobilized in a polytetrafluoroethylene tube reactor using laminar flow.[250,264,265] While many CLEAs have been constructed from individual enzymes, they have also been constructed from multiple enzymes as part of a cascade (combi-CLEAs).[250] Advantages of CLEAs include ease of preparation, potential increased stability, reusability, and the ability to pack enzymes densely, which may help facilitate aggregation-based substrate channeling.[12,14,28,56,59,60,73,126−128] Disadvantages include potential lower activity, particularly for non-site-specific cross-linking, and difficulty in producing homogeneous CLEAs with regard to size and enzyme ratio.[73]

One prime example of the use of a combi-CLEA where the protection of an intermediate (*i.e.*, substrate channeling) was specifically investigated was reported by Nguyen and Yang.[73] They used the GOx and HRP bienzyme cascade with the goal of producing a colorimetric glucose assay. Key to this reaction is the unstable intermediate $H_2O_2$; the authors investigated whether this was protected (*i.e.*, substrate channeling) by adding catalase, which competes with HRP for $H_2O_2$.[73] In order to circumvent problems of heterogeneous shapes and sizes of combi-CLEAs and consequential inconsistent efficiencies due to batch production, the authors used a millifluidic reactor. Coaxial flows of (1) phosphate-buffered GOx and HRP and (2) acetonitrile containing glutaraldehyde were used, and the outflow was collected in phosphate buffer to quench the cross-linking reaction.[73,266,267] This process led to doughnut-shaped combi-CLEAs with an average size of around 250 nm.[268] Two parameters were optimized in their combi-CLEA production: the GOx:HRP ratio and the glutaraldehyde concentration. The optimum GOx:HRP ratio was found to be 150 by weight, which on the basis of the specific enzyme activities of the free enzymes was equivalent to a ratio of 1.1, suggesting that the two enzymes retained similar percentages of their activity as part of the combi-CLEA. The concentration of glutaraldehyde was optimized for efficient cross-linking while minimizing activity loss. At a concentration of 0.5 mM, the yield was 100% (no enzyme in filtrate solution), and the activity remained high at 96.5%, perhaps as a result of the short time of the reaction (15.6


DOI: 10.1021/acscatal.9b02413
*ACS Catal.* 2019, 9, 10812−10869

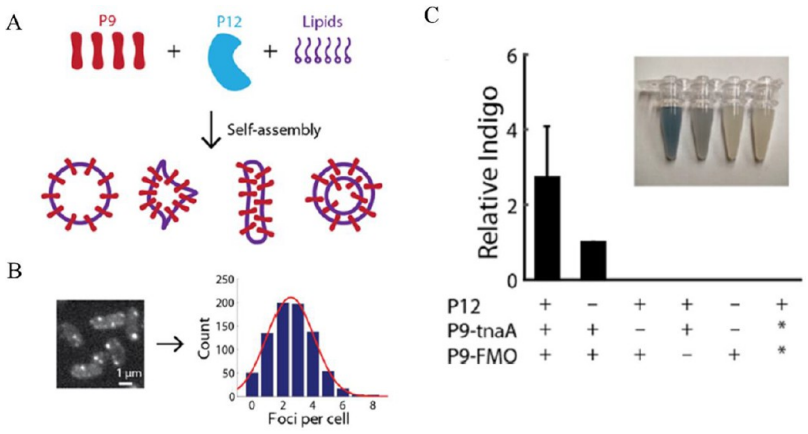


**Figure 20.** Synthetic lipid-containing scaffolds (SLSs). (A) SLSs were designed to self-assemble from the $\phi$6 phage structural protein P9 in the presence of the required assembly factor P12. (B) The mean number of foci per cell was 2.5 ($N$ = 797 cells). (C) Indigo production values for strains expressing P9−$His_6$−TnaA and P9−FLAG−FMO fusions in the presence or absence of P12. Data are normalized such that production values for strains without P12 are equal to 1. Error bars indicate one standard deviation based on $N$ = 4 experiments. Asterisks indicate mutant forms of P9 that do not contain the transmembrane domain (P9ΔTM). Indigo production in the rightmost four samples was insufficient to allow for quantitation. TnaA and FMO are two enzymes involved in indigo synthesis. Reproduced from ref 125. Copyright 2016 American Chemical Society.

s) and the doughnut shape. Below 0.5 mM glutaraldehyde, the yield decreased; above 0.5 mM, the activity decreased.

After the production was optimized, the performance of the GOx−HRP combi-CLEA was tested. Formation of the combi-CLEA protected $H_2O_2$ from catalase, as the reaction rate fell only from 10.2 to 8.3 $\mu$M/min (*i.e.*, by 18.7%) in the presence of 6.3 milliunits/mL catalase, whereas the rate decreased from ~10.6 to 0.6 $\mu$M/min in the presence of 6.3 milliunits/mL catalase when free GOx and HRP were used. With regard to the reaction rates at various glucose concentrations with a fixed colorimetric substrate concentration, the catalytic efficiency of the combi-CLEA ($k_{cat}/K_M$) was 1.47-fold higher, mostly as a result of a decreased $K_M$. It was concluded that this was due to fast transfer of $H_2O_2$ from GOx to HRP as well as decreased buildup of $H_2O_2$, limiting its product inhibition of GOx.[73,269−271] Finally, the authors demonstrated that the detection of glucose by the combi-CLEA was linear to 11.1 mM. Importantly, the combi-CLEAs were then immobilized on a nylon membrane, which could not be done in the same fashion with free enzymes. With this system, not only was the linear range extended (likely because of a lower reaction rate), but the immobilized combi-CLEAs could be used multiple times, with the correlation coefficient dropping only to 0.99 and 0.94 in the second and third cycles. Overall, this report demonstrated the moderate ease of this scaffolding approach (although it requires a millifluidic apparatus for consistency) and the potential for accessing and exploiting substrate channeling.

**Lipids.** In addition to naturally derived protein and peptide scaffolds, scaffolds exploiting naturally derived lipids have also been reported. The recent development of lipid-based scaffolds has opened a new way to assemble multienzyme cascades with unique capabilities such as a large size, tolerance to hydrophobicity, and the ability to use membrane proteins.[125] In fact, these scaffolds may provide special advantages for processes that involve hydrophobic intermediates such as fatty acids, steroids, or biofuels. They may also be challenged by limitations where hydrophobicity or large size is not desired.

*Intracellular Lipid/Protein-Based Scaffolds.* Myhrvold *et al.* recently designed and built synthetic lipid-containing scaffolds (SLSs) in *E. coli* facilitated by two proteins derived from the bacteriophage $\phi$6.[125] This bacteriophage is uncommon in that it uses an envelope of lipids and membrane proteins to encapsulate a proteinaceous nucleocapsid.[272,273] This system was based on expressing in *E. coli* two bacteriophage proteins required for forming lipid/protein particles: P9 (a major membrane protein) and P12 (a nonstructural protein) (see Figure 20A,B).[274,275] It was found that proteins/enzymes could be fused to the C-terminus of P9 for localization to the lipid scaffold, but fusion to the N-terminus was less successful. Fusion of fluorescent proteins showed that (1) on average 2.5 foci were found per cell, (2) the foci were likely transiently associated with the membrane and/or were not in the nucleoid, and (3) the foci were likely greater than 20 nm in diameter. Additional experiments showed that the SLSs were likely discrete but amorphous and did not cause a growth burden to cells. Importantly, isoforms of P9 can colocalize on the SLSs, as shown by both colocalization experiments with two P9−fluorescent protein fusions as well as with a P9−fluorescent protein fusion and a P9−$His_6$ fusion. The latter could be isolated with affinity purification, indicating that at least some of the C-terminus of P9 faced out toward the cytosol. To demonstrate the ability of their system to be used for multienzyme reactions, the authors fused two enzymes for indigo production, TnaA and FMO, to the C-termini of two P9s. One reason for this choice was that an intermediate of the reaction, indole, is a diffusible signaling molecule, so any decrease in diffusion away from the enzymes (*i.e.*, increase in substrate channeling) should improve indigo production. In fact, strains expressing both P9s plus P12 produced 2−3-fold more indigo than control strains that did not express P12 (Figure 20C). Western blots confirmed that this was not due to a change in P9−TnaA or P9−FMO levels. It is worth noting that while the authors did show that some of the C-terminus of P9 was displayed toward the cytosol, this does not exclude the possibility that some of the enzymes were displayed inside the lipid particle and that the system benefited from encapsulation as well.

*Lipid Droplets.* In a different approach, Lin *et al.* developed a system based on naturally occurring lipid droplets (LDs) in yeast.[124] The authors targeted ester production, as esters can be useful as solvents or for flavor and fragrance materials and are


DOI: 10.1021/acscatal.9b02413
ACS Catal. 2019, 9, 10812−10869

naturally produced in low levels in yeast. In *S. cerevisiae*, pyruvate is converted into acetaldehyde, which can then be converted into acetate by aldehyde dehydrogenase (Ald6). In turn, acetate is converted into acetyl-CoA by Acs1 and finally condensed with an alcohol (*e.g.*, ethanol) to form an ester (*e.g.*, ethyl acetate) by the membrane-bound, LD-associated (in stationary phase) alcohol-*O*-acetyltransferase (Atf1) (see Figure 21A).[276,277] In yeast, Ald6 and Acs1 are separated

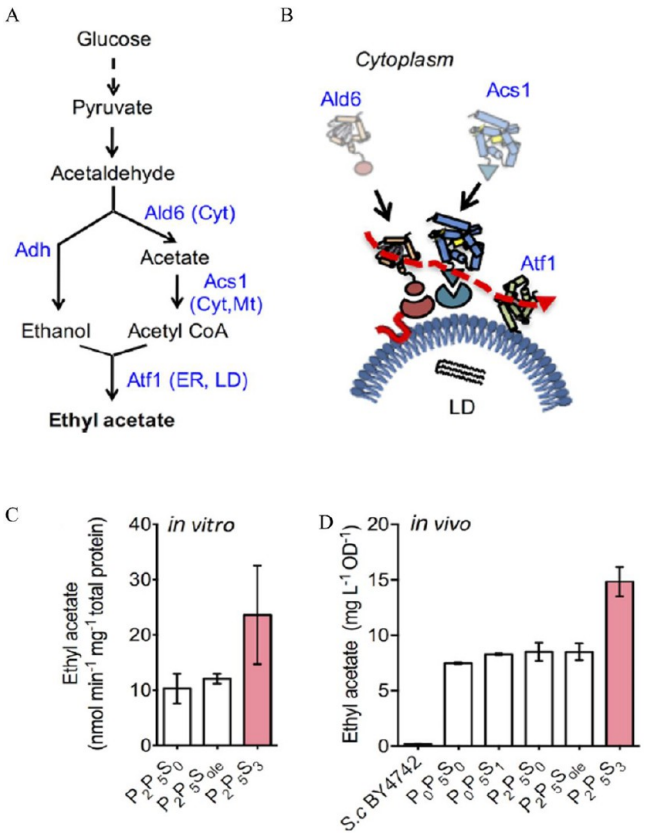


**Figure 21.** Ethyl acetate biosynthesis in *S. cerevisiae*. (A) Ethyl acetate biosynthesis in *S. cerevisiae* and the subcellular localization of aldehyde dehydrogenase (Ald6), acetyl-CoA synthetase (Acs1), and alcohol-*O*-acetyltransferase (Atf1). Abbreviations: Cyt = cytosol; Mt = mitochondria; ER = endoplasmic reticulum; LD = lipid droplet. (B) Schematic diagram of the scaffolding strategy colocalizing Ald6 and Acs1 with Atf1 on LDs *via* a membrane-bound protein scaffold. (C) Rates of ethyl acetate production from *in vitro* assays of lysates containing $P_2P_5S_3$, $P_2P_5S_{ole}$, and $P_2P_5S_0$. The data are shown as mean ± standard deviation ($n = 3$). Activity is reported in units of nmol $min^{-1}$ (mg of total lysate protein)$^{-1}$. (D) Specific productivities of ethyl acetate from 24 h fermentations with strains expressing the pathway without a scaffold ($P_0P_5S_0$), with scaffold ($P_0P_5S_1$), with optimized scaffold ($P_2P_5S_3$), without the optimized scaffold ($P_2P_5S_0$), and with an oleosin-only scaffold ($P_2P_5S_{ole}$). The titers were quantified by GC-FID. Reproduced from ref 124. Copyright 2017 American Chemical Society.

from Atf1, as they are found in the cytosol (and mitochondria as well for Acs1).[278−280] The authors hypothesized that assembling Ald6 and Acs1 in close proximity with Atf1 on LDs would increase the production of esters. Screening for LD-targeting proteins, it was shown that oleosin (Ole) from *Zea mays*[281] fused to cyan fluorescent protein localized with LDs under both aerobic and anaerobic growth conditions. Ald6 and Acs1 were then fused to Ole and expressed, but the reaction activity in whole-cell lysates did not increase over background. The authors speculated that this could be due to enzyme orientation, especially since Acs1 is cationic around the active site and may interact with the anionic phosphate groups of the LD.[282] To address this issue, the system was split, so that the LD-targeting Ole protein was fused to two cohesin domains (see above for discussion of cohesin−dockerin interaction domains), and the Ald6 and Acs1 enzymes were separately fused to dockerin domains. Specifically, the two pairs were $D_1$−$C_1$ from *Clostridium perfringens*[283] and $D_2$−$C_2$ from *C. thermocellum*,[284] leading to the fusions Ole−$C_1$−$C_2$, Ald6−$D_1$, and Acs1−$D_2$ (Figure 21B). Further, fusions also contained a tag for Western blot identification. Each fusion had modest activity increases above the cell lysate background, but the $D_1$/$D_2$−enzyme fusions were less active than cytosolically targeted expressed enzymes, perhaps because of lower expression levels.

Importantly, the authors investigated the distance between enzymes assembled on an LD to determine whether they were separated by less than 5 nm, as this has been noted to be important for substrate channeling.[285] Using fluorescence resonance energy transfer (FRET) studies, they determined that the distance between Adl6 and Acs1 and the distance between Ole−$C_1$−$C_2$ and Atf1 were less than an average of 4.5 nm, indicating the possibility for substrate channeling. Additional tests of their system were performed starting with the use of Atf1 integrated into the genome at a high-expression integration site, with the other fusions expressed in a single-copy expression vector.[286] Using cell lysates from the stationary phase, there was a 1.9-fold improvement for the assembled system versus natively expressed Ald6 and Acs1 (and integrated Atf1) and a 1.7-fold improvement for the assembled system versus overexpressed but unassembled Ald6−$D_1$ and Acs1−$D_2$ (see Figure 21C). Beside the fact that the distances between enzymes were less than 5 nm, substrate channeling was also indicated as helping the reaction, as there are native reactions that compete for acetate, CoA-SH, and acetyl-CoA intermediates, though additional experiments would be necessary to conclude that substrate channeling helped.[276] Acs1 was indicated as having the limiting activity for the cascade, so the system was then optimized by adding a second copy of Acs1 with varying promoter strength, changing the ratio on the LDs by varying the number of $C_2$ domains between one and three, and varying the promoter strength of the scaffold. The final *in vivo* optimized version showed 2.5-fold increased ethyl acetate production versus the *in vivo* control version (also used previously *in vitro*). A retransformed version produced ethyl acetate at 14.8 mg $L^{-1}$ $OD^{-1}$, which was 1.7-fold higher than with the scaffoldless controls (Figure 21D). However, the unoptimized version was only very modestly better than the scaffoldless control, showing some difference between the *in vitro* and *in vivo* results. An interesting aspect of this system is that LDs may partition compounds to their inner core versus the cytosol, as has been seen with carotenoids;[287] this may help in the case of toxic compounds but hurt if the product is lost. As ethyl acetate is particularly volatile, significant loss of product was not expected.

**The Special Case of DNA Scaffolds.** In the previous parts of this section on biotic scaffolds, we have focused on cellular display, naturally derived proteins and peptides, CLEAs, and lipids. We now focus on the special case of DNA scaffolds, which offer unique structural and functional differences compared with the above platform materials. This section describes the use of DNA as a template to arrange multiple


DOI: 10.1021/acscatal.9b02413
ACS Catal. 2019, 9, 10812−10869

**Table 3. Overview of Representative DNA-Templated Multienzyme Cascades[88,a]**

| enzymes | year | scaffold name | enzyme attachment chemistry | decrease in activity caused by conjugation | assembly yield | highest-fold enhancement observed (enzyme separation distance)[b] | notes | ref |
|---|---|---|---|---|---|---|---|---|
| GOx and HRP | 2008 | single DNA helix | sSMCC | NE | NE | 3 (8 nm) | attached on the surface of microtiter plates | 72 |
| GOx and HRP | 2012 | DNA origami rectangle | NHS ester (amine) + SPDP | 25% | 45% (10 nm); 95% (45 nm) | 3.4 (10 nm) | excess enzymes not removed, mathematical correction applied | 36 |
| GOx and HRP | 2013 | DNA tweezers | heterobifunctional cross-linker | NE | 100% | 1.9 (6 nm) | – | 78 |
| GOx and HRP | 2015 | DNA-origami-based nanoreactor | streptavidin–biotin | NE | NE | 25 (30 nm) | – | 79 |
| GOx and HRP | 2018 | flexible DNA triangular prism | sSMCC | NE | 77.5% | 2.1 (7 nm) | attached to streptavidin-coated microbeads | 80 |
| GOx and HRP | 2018 | DNA origami rectangle | copper-catalyzed azide–alkyne Huisgen cycloaddition (click chemistry) | 64% (HRP pair) | 31% (GOx); 68% (HRP) | 2.1 (10 nm) on a DNA rectangle; 10 (10 nm) on a DNA rectangle on silica | attached to the surface of activated silica particles; kinetics determined through chemiluminescence | 81 |
| G6PDH, MDH, and LDH | 2014 | DX tile and DNA-scaffolded 4 × 4 tile | NHS ester (amine) + SPDP | 60–80% (G6PDH); 20–55% (MDH) | 80% | 277 (14 nm) | – | 100 |
| G6PDH, MDH, and LDH | 2016 | rectangular DNA origami | SPDP for LDH; HaloTag for MDH and G6PDH | NE | >80% | 5.3 (25 nm) for G6PDH/LDH; 2.4 (20 nm) for G6PDH/MDH | first demonstration of directional control of substrate channeling | 296 |
| MDH, OAD, and LDH | 2016 | three-pointed-star DNA | SPDP for OAD and LDH; HaloTag for MDH | NE | 80% | 2.5 for a linear template; 4.2 for a star template | – | 297 |
| HRP, GOx, MDH, G6PDH, LDH, and $\beta$-Gal | 2016 | DNA nanocage | SPDP | 15% (HRP pair) | 64–98% | 8 (5 nm) | – | 64 |
| G6PDH and LDH | 2018 | 2D DNA origami enzyme network | HaloTag for G6PDH; NHS ester (lysine-thiol) for LDH | NE | 90% | ~305[c] | – | 298 |
| NFOR and Luc | 2002 | single DNA helix | streptavidin–biotin | NE | NE | 2.7 (8 nm) | first DNA multienzyme cascade; attached on the surface of microtiter plates | 299 |
| XR and XDH | 2016 | DNA origami with three rectangular cavities | protein fusion: DNA binding proteins zinc finger protein (zif268) and the basic leucine-zipper protein (GCN4) | 83% increase (XR); 50% increase (XDH) | 95% ZS-XR (cavity I); 78% G-XDH (cavity II) | 4.4 (10 nm) | – | 300 |

[a]Abbreviations: SPDP = succinimidyl 3-(2-pyridyldithio)propionate; sSMCC = sulfosuccinimidyl 4-(*N*-maleimidomethyl)cyclohexane-1-carboxylate; NHS = *N*-hydroxysuccinimide; NE = not evaluated; GOx = glucose oxidase; HRP = horseradish peroxidase; G6PDH = glucose-6-phosphate dehydrogenase; MDH = malate dehydrogenase; LDH = lactate dehydrogenase; OAD = oxaloacetate decarboxylase; $\beta$-Gal = $\beta$-galactosidase; XR = xylose reductase; XDH = xylitol dehydrogenase; NFOR = oxidoreductase; Luc = luciferase. [b]Interenzyme distances and turnover rates were estimated using the reported data when not specifically listed or given in the corresponding papers. When multiple configurations of the same DNA template were investigated, only the most substantial reported turnover rate is listed. [c]10% greater than DX tile.[100]



DOI: 10.1021/acscatal.9b02413
ACS Catal. 2019, 9, 10812–10869

enzymes from coupled reactions or pathways in specific geometries. Because of the unique aspects of this scaffolding material, a brief introduction to the field of structural DNA nanotechnology, how enzymes are attached to DNA, and the unique advantages and disadvantages of DNA-based enzyme cascades are briefly discussed, as they are directly relevant for both motivation and understanding of the results. An overall summary of the enzyme systems discussed in this section is shown in Table 3 along with key information such as the DNA scaffold name/type, the enzyme attachment chemistry used, the percentage decrease in enzyme activity caused by DNA conjugation, the assembly yield of the cascade, and the highest observed enhancement in coupled activity. This table was supplemented with information from a recent and noteworthy review by Rajendran *et al.*[88] We also note that several other excellent reviews on this same subject are available.[12,288−290]

*Structural DNA Nanotechnology.* Over the past decade, DNA nanotechnology has rapidly developed to the point that nearly any three-dimensional shape can be formed in a bottom-up self-assembled manner.[291] The predetermined geometry is created when sets of complementary DNA oligomers are combined, allowing them to hybridize to each other at specific locations and thus form a defined nanoscale shape. In the current context, the formed DNA-based geometry is then used as a template for the arrangement of active enzymes. Designing, folding, and characterizing self-assembled DNA structures for technological uses has now developed into its own fully formed research area. This field, pioneered by Seeman in the 1980s, is composed of two subfields, structural DNA nanotechnology and dynamic DNA nanotechnology.[292] Its use for arranging enzymes near one another is not new, as Seeman's original purpose was to use DNA as a structural material to align and crystallize proteins that would not crystallize using conventional means for subsequent structural determination using X-ray crystallography. To date, large-scale, high-yield protein crystals have yet to be realized in this manner, but it has been shown repeatedly that DNA can be used to arrange proteins with nanometer resolution and in specific geometries.[36,293,294] In the early 2000s, it was shown that larger structures could be created in high yield by the use of a relatively long scaffold strand and relatively impure staple strands.[295]

DNA origami, described by Paul Rothemund in his seminal 2006 paper, exploits the now commonly used single-stranded (ss) M13mph18 phage DNA (7249 bp) as a universal template that can be assembled into almost any structure design by the addition of staple strands derived from open-source software.[301] Douglas *et al.* later extended DNA self-assembly into three-dimensional shapes, greatly extending the utility of the method.[302] A major enabler in this field is the fact that the synthetic ssDNA oligonucleotides used as the staples are commercially available in high yield at low cost. Advances in structural DNA nanotechnology have been well-summarized in two excellent reviews by Lin *et al.*[303] and Pinheiro *et al.*[67]

The typical DNA enzyme cascade utilizes a DNA template on which enzymes are arranged. Leveraging DNA's specific Watson−Crick base-pair hybridization allows researchers to design and fold three-dimensional templates to which proteins can be further attached in site-specific locations. DNA is well-suited as a template because specific geometries can be created relatively easily utilizing open-source design and modeling software such as CaDNAno,[302] Nanoengineer-1 by Nanorex,[304] vHelix,[305] DNA Origami Sequence Design Algorithm for User-defined Structures (DAEDALUS),[306] and CanDo.[307]

Using DNA as a structural scaffold material for these purposes offers several advantages and some liabilities. One of the greatest benefits is the ability to form designer nanoscaffolds of nearly any three-dimensional shape.[291] The second advantage is the attachment specificity or addressability offered by the technique. Typically, the proteins are DNA-conjugated and then attached to the DNA scaffold in a precise manner. Site-specific attachment directly results from the complementary Watson−Crick base-pairing between the ssDNA tether strand extending from the scaffold and the ssDNA strand extending from the conjugated protein. Another inherent benefit is the ease with which a container can be formed around the enzymes, and this stands out in particular because it offers a direct method for investigating enzymes in confined spaces of desired shape and even porosity.[64] Although still not fully understood, the molecular structure of DNA itself may potentially act to increase the turnover rate of attached enzymes. It has been postulated that the negative charge of the DNA backbone acts to lower the pH near the surface of the structure relative to the bulk pH, and this can optimize the enzyme activity.[49]

Utilizing DNA-scaffolded enzyme systems also presents several significant liabilities. In many cases, the procedure results in decreased enzymatic activity compared with the native counterparts. Average decreases in activity in the 15−50% range are typically seen,[36,80,100] with up to an 83% activity loss observed in extreme cases.[300] The complex protein attachment chemistries are difficult to scale, and thus, production of enzyme-conjugated DNA scaffolds in high yields in the large amounts needed for industrial scales has yet to be realized.[308] There has been some recent work to scale the yield of GOx and HRP by attaching them to the surface of activated silica particles (*vide infra*).[81] However, much more work would be required in order to scale up and improve the long-term stability of a majority of the cascades discussed herein.

*Attaching Enzymes to DNA.* The previously mentioned considerations regarding how an enzyme is associated with its scaffold are particularly important here. There are many methods for conjugating DNA to proteins based primarily on utilization of covalent or non-covalent chemistries. The interested reader is directed to reviews by Niemeyer,[309] Saccà and Niemeyer,[289] and Yang *et al.*[310] for a more complete accounting of protein-to-DNA attachment strategies. In terms of non-covalent attachment strategies, the most widely used non-covalent protein−DNA coupling strategy is based on the ubiquitous biotin−streptavidin chemistry. The method is quite versatile since a relatively large number of proteins can be expressed as an avidin fusion.[79] Niemeyer *et al.* implemented this interaction as a "smart glue" to join supramolecules with biotinylated oligonucleotides.[311,312] Another popular non-covalent coupling strategy is that of metal affinity coordination between $Ni^{2+}$-chelated nitrilotriacetic acid (NTA) groups and polyhistidine motifs, most often $His_6$ introduced at the termini of proteins for initial purification.[299,309,313] However, this method suffers from dissociation constants that occur above the relatively low (nM) concentrations utilized for many DNA-based enzyme cascades. Such low concentrations are typically required in order to observe substrate channeling.

In general, covalent attachment strategies provide more benefit since the DNA enzyme cascade can be diluted to subnanomolar concentrations without the worry of enzyme dissociation as in the case of many non-covalent attachment strategies.[98] Covalent attachment strategies are thus more



DOI: 10.1021/acscatal.9b02413
*ACS Catal.* 2019, 9, 10812−10869

commonly utilized, and they further offer more control and specificity despite the more complex procedures and the requirement for elaborate purification to remove components that were added in excess to help drive the conjugation reactions to completion. Some methods require the enzymes first to be modified with the addition of unnatural amino acids and bio-orthogonal chemical tags such as azides.[312,314] Chemistries involving the use of "SnapTag"[315] and/or "HaloTag"[316] have also been described. One of the best references on this subject, published by Fu *et al.*, systematically explains the techniques for preparing and characterizing DNA enzyme cascades and discusses their advantages and disadvantages at length.[293] An alternative and elegant chemistry is the DNA-templated protein conjugation (DTPC) method developed by Gothelf's group, which is typically accomplished in two steps (see Figure 22 for a stepwise overview of the process).[317,318]

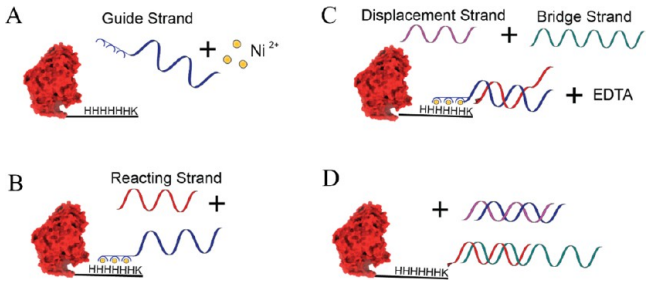


**Figure 22.** DNA-templated protein conjugation. (A) The $His_6$-tagged protein (H) with lysine (K) placed adjacent to the $His_6$ tag is combined with a tris(NTA)-modified DNA guide strand in the presence of $Ni^{2+}$. (B) A reacting DNA strand that has been modified with an aldehyde is added. The reacting strand binds to the guide strand, thus colocating the aldehyde in close proximity to the lysine, and then a covalent bond is formed through reductive amination. (C) Displacement and bridge strands (cyan) are then added to displace the guide strand. (D) The final product of the reaction is a DNA-labeled protein with a bridge strand that can be hybridized to attachment tethers on the DNA scaffold.[317] Adding two lysine residues at the termini can improve the yield of DNA-modified protein.

Many different enzyme cascades have been assembled using DNA structures. We first focus on the GOx−HRP cascade, as this common cascade has been used with multiple different architectures, before addressing examples from some other multienzyme cascades.

*DNA-Based Glucose Oxidase−Horseradish Peroxidase Systems.* Given its popularity, the GOx−HRP coupled system has been extensively prototyped within DNA architectures, and the caveats about this discussed in the Introduction have direct relevance to the following examples. Herein we highlight how this system has been investigated using (1) single ssDNA "1D" architectures, (2) 2D tiles, (3) 3D nanotubes and prisms, and (4) DNA scaffolds attached to silica particles. In 2008, Müller and Niemeyer[72] set out to investigate proximity effects in multienzyme systems using a relatively simple system composed of a single ssDNA backbone with commercially obtained GOx and HRP attached. The kinetics was investigated using an Amplex Red assay, as shown in Figure 23A. The four DNA enzyme configurations investigated (called complexes) are shown in Figure 23B. Complexes 1 and 2 consisted of single GOx−HRP pairs, but the enzyme order was reversed between them. Complexes 3 and 4 consisted of GOx or HRP pairs only and were used as controls. The enzymes were DNA-conjugated using sulfosuccinimidyl 4-(*N*-maleimidomethyl)cyclohexane-1-carboxylate (sSMCC) by cross-linking target enzyme lysine residues and commercially available thiolated DNA. A significant amount of free DNA-conjugated enzymes were still present in solution because of the dissociation/association equilibrium, so kinetic investigations were conducted by binding the ssDNA backbone of each complex on the surface of a streptavidin-coated microplate, where bound biotinylated ssDNA strands acted as "carrier strands", and then washing away unbound material. In the kinetic investigations, the amount of carrier stands was varied from 30 to 500 fmol while the concentration of DNA-conjugated enzymes was kept constant; Figure 23C shows representative results. At low carrier concentrations, a 1.8-fold increased turnover rate was observed in configurations 1 and 2 relative to the controls. As the carrier concentration was increased, the turnover rate decreased to 1-fold. It was hypothesized that at low carrier concentrations the separation between individual complexes increased, which eliminated cross-diffusion between adjacent complexes, thus promoting enzyme channeling. Additionally, adding a $T_6$ spacer to extend the distance between the enzymes and the microbead surface lowered the number of unbound enzymes and resulted in a 3.0-fold increase in overall turnover rate (Figure 23D). Kinetic investigations utilizing catalase as a $H_2O_2$ scavenger were conducted to confirm the presence of channeling, but this caused a significant decrease in the turnover rate of both complex 1 and complex 2, indicating that diffusional transport was still present in the investigated cascade.

To investigate the kinetics of the GOx−HRP system with regard to the distance between enzymes in a more 2D layout, Fu *et al.* investigated coupled GOx and HRP kinetics on a DNA origami tile.[36] In this configuration, the kinetics of four different enzyme spacings of 10, 20, 45, and 65 nm on the DNA origami tile were evaluated (Figure 24A,B). Critically, the activity of the coupled pathway was found to be dramatically decreased when the enzyme separation was increased from 10 to 20 nm (Figure 24C). The activity then only decreased by another ∼10% up to the final spacing of 65 nm. A Brownian diffusion model accounted for the rapid decrease in activity when the distance was increased but could not explain the strong enhancement observed when the enzymes were close. The nonparticipating protein *β*-Gal was placed between the enzymes as a way to test whether dimensionally restricted diffusion was present in the system. Since $H_2O_2$ is known to have some affinity for protein surfaces, it could facilitate dimensionally limited diffusion, resulting in decreased diffusion times of the substrate. Indeed, an activity increase of ∼42% was observed with *β*-Gal placed between GOx and HRP at longer enzyme separations. This led the authors to suggest that the formation of a hydration layer around the protein was responsible for the increase in activity. Similar to the previous example, the enzyme cascade was not purified (to remove the 3-fold excess of enzymes added to promote attachment) before the kinetic investigations, and this was taken into account by a correction to the analyses.

Using a scaffold resembling DNA tweezers and called a DNA machine, Xin *et al.* constructed a scaffolded GOx−HRP enzyme cascade.[78] The cascade consisted of two parallel double crossover (DX) arms with GOx and HRP attached at the ends, as shown in Figure 24D. Formation and assembly ratios of DNA-conjugated protein to DNA were also evaluated, and it was found that a GOx:HRP:DNA machine ratio of 1.5:3:1


DOI: 10.1021/acscatal.9b02413
*ACS Catal.* 2019, 9, 10812−10869

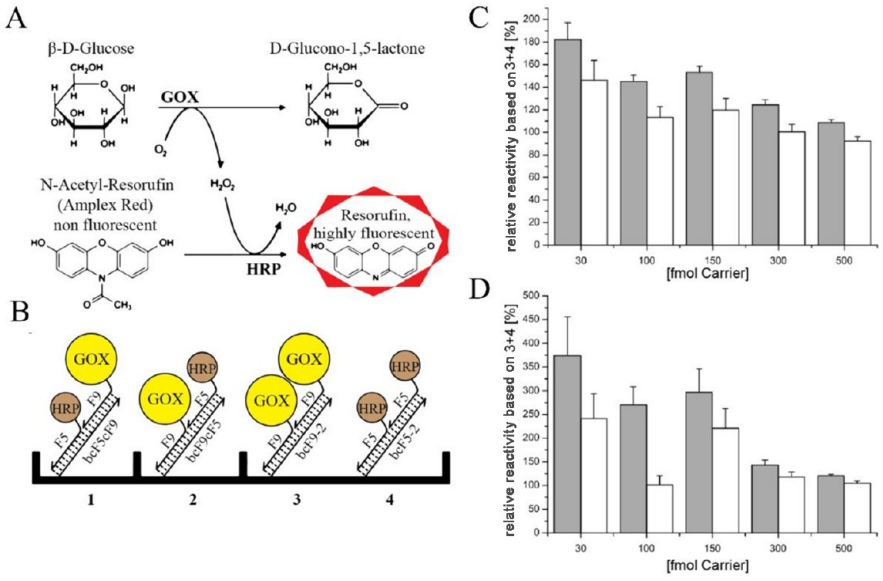


**Figure 23.** ssDNA-scaffolded GOx–HRP system. (A) Molecular components and reaction of the Amplex Red GOx and HRP kinetic assay. Glucose is oxidized by GOx, which forms $H_2O_2$ as a byproduct. In the second step, HRP reduces $H_2O_2$ to $H_2O$. The highly fluorescent resorufin product is formed when Amplex Red is oxidized by $H_2O_2$. (B) The four enzyme configurations/complexes investigated. (C) Bar plot showing how the turnover rate generally decreased for complex 1 (gray bars) and complex 2 (white bars) as the carrier stand concentration was increased. A 1.8-fold increased turnover rate was observed at the lowest concentration. (D) Bar plot similar to that shown in (C) for modified versions of complex 1 (gray bars) and complex 2 (white bars) in which $T_6$ spacer was inserted between the enzymes and the DNA scaffold. This modification resulted in more heterodimeric complexes (complexes consisting of GOx and HRP), which further increased the turnover rate. A 3.0-fold increase was observed. Reproduced with permission from ref 72. Copyright 2008 Elsevier Inc.

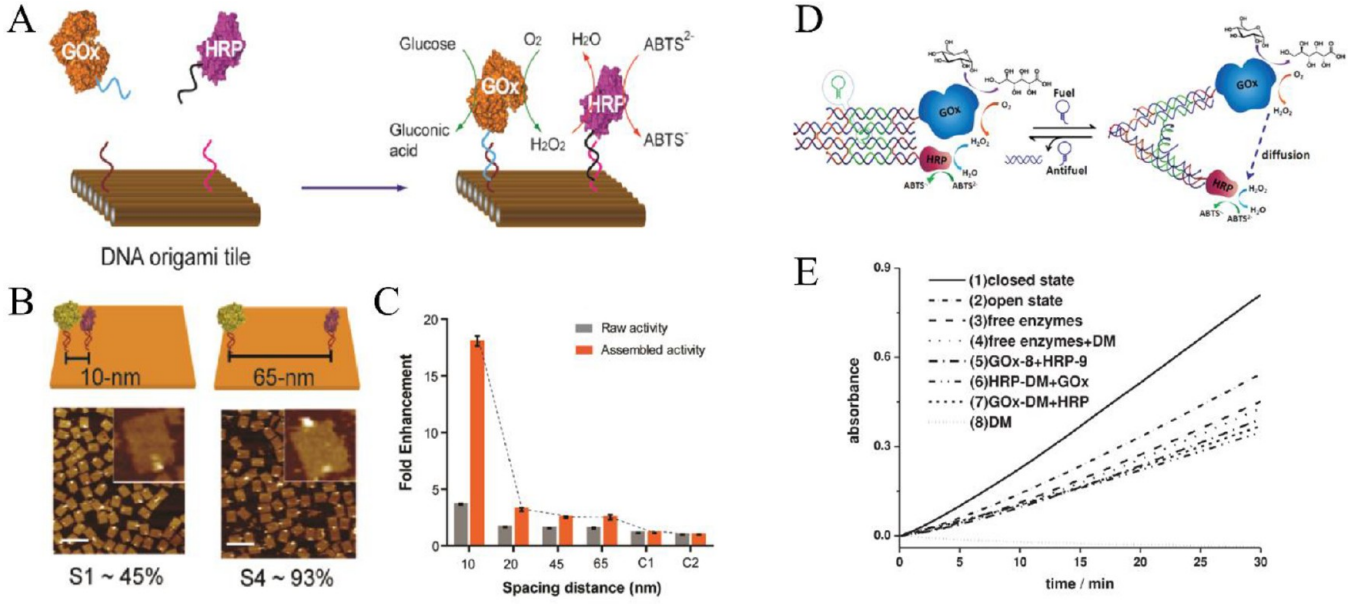


**Figure 24.** Cascaded GOx–HRP DNA origami tile system. (A) Schematic of the GOx–HRP DNA origami tile enzyme cascade. (B) Schematics showing enzyme separations of 10 and 65 nm. Corresponding AFM images are shown below the schematics. (C) Plot of the enzymatic enhancement vs the enzyme spacing. A dramatic decrease in the turnover rate was observed when the spacing was increased from 10 to 20 nm. (D) Schematic of the DNA tweezers GOx–HRP enzyme cascade and accompanying GOx–HRP pathway. The cascade was capable of being cycled between two states (open and closed) with the addition of a fuel or antifuel DNA strand, respectively. (E) Plot of increasing absorbance vs time showing that the cascade's initial rate is the highest when the system is in its closed configuration with the enzymes close to one another, allowing for channeling as opposed to diffusion. Reproduced with permission from (A–C) ref 36 and (D, E) ref 78. Copyright 2012 American Chemical Society and 2013 Wiley-VCH Verlag GmbH & Co. KgaA, Weinheim, respectively.

resulted in the highest assembly efficiency. A 1.9-fold enhancement in coupled activity was observed when the DNA tweezers were in their closed state versus freely diffusing enzymes, as depicted in Figure 24E. The modest improvement was attributed to the decreased distance between the enzymes from the estimated closed state separation of 6 nm.

In terms of DNA-based 3D architecture, soon thereafter Linko *et al.* created a more sophisticated DNA-origami-based



DOI: 10.1021/acscatal.9b02413
*ACS Catal.* 2019, 9, 10812–10869

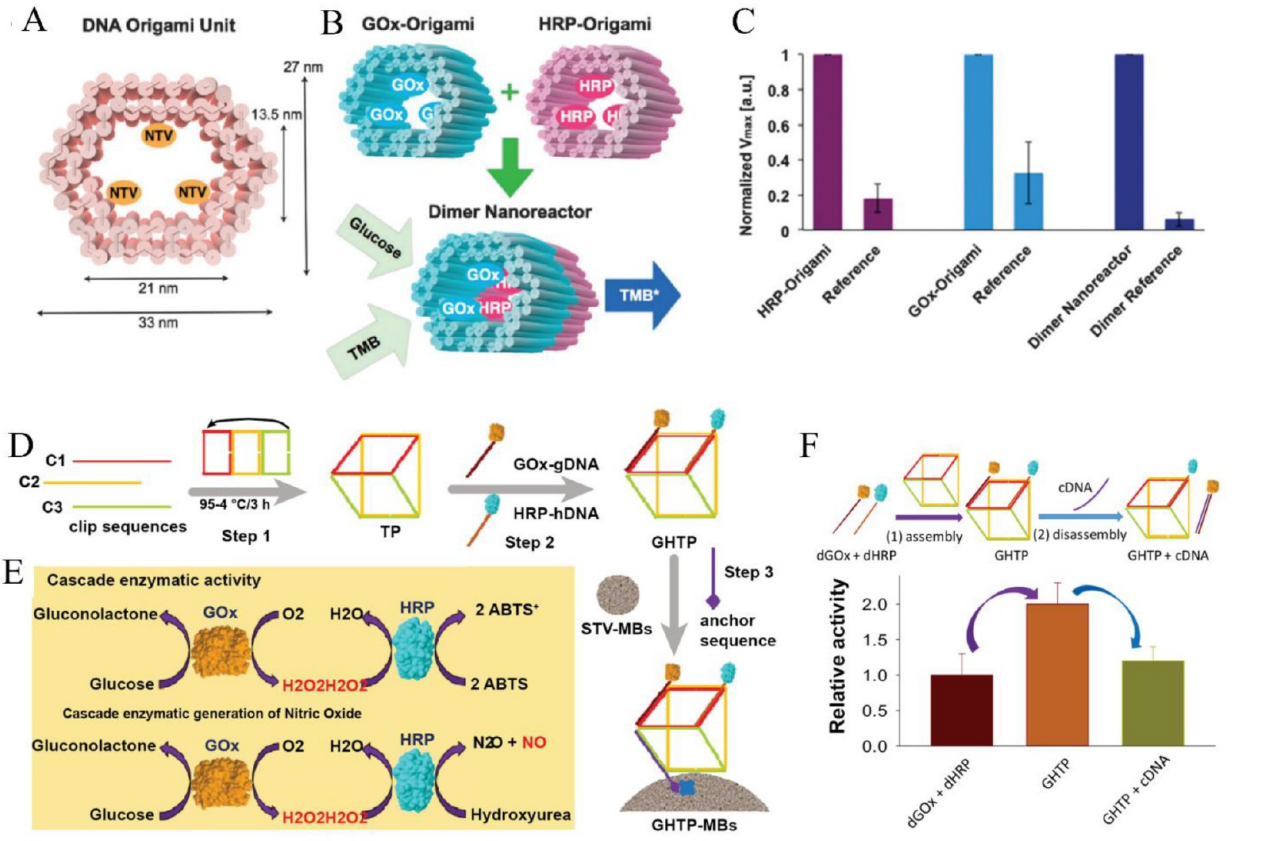


**Figure 25.** DNA-origami-based nanoreactor. (A) Schematic of the DNA-origami-based nanoreactor highlighting the dimensions and location of the neutravidin (NTV) binding locations. (B) Schematic depicting the formation of the dimer nanoreactor assembled from two DNA origamis, one with three GOx enzymes and one with three HRP enzymes, which were attached inside a tubular DNA origami dimer. (C) Plot of the normalized initial rate $V_{max}$ vs three nanoreactor configurations: HRP only, GOx only, and the dimer with both GOx and HRP. Initial rates for reference controls are shown to the right the corresponding bars. Reproduced from ref 79. Published by the Royal Society of Chemistry. (D) Diagram highlighting the formation of the DNA triangle prism enzyme cascade along with the enzyme attachment locations and subsequent immobilization on the microbead. (E) The cascade reaction pathway and colorimetric assay scheme used for kinetic characterization. (F) Plot of the enzyme cascade relative activities for the three different states shown above the respective bars. The highest activity was observed when both GOx and HRP were attached to the DNA scaffold. Reproduced with permission from ref 80. Copyright 2018 Wiley-VCH Verlag GmbH & Co. KgaA, Weinheim.

nanoreactor composed of GOx and HRP attached inside a tubular DNA origami dimer (Figure 25A).[79] The enzymes were connected inside the DNA origami nanotube *via* streptavidin–biotin interactions, and the HRP activity was detected using TMB as a reporter. Approximately 5- and 3-fold increases in the kinetics of the individual uncoupled HRP and GOx, respectively, were observed as a result of a localized DNA effect. Combining the two DNA origami in an end-to-end configuration (Figure 25B) resulted in an ~12-fold increase in the coupled kinetics (Figure 25C). Overall, the enhanced reaction rates here were attributed to the compartmentalization the DNA origami structure provided. In 2018, Zhou *et al.* investigated GOx–HRP attached on a relatively flexible DNA triangle prism that was connected to streptavidin-coated microbeads as a possible alternative route for the biomimetic generation of nitric oxide, as shown schematically in Figure 25D,E.[80] The coassembled yield of the enzymes on the DNA scaffold was estimated to be 77.5% as determined by PAGE and dynamic light scattering (DLS). A 2.1-fold enhancement relative to free enzyme was observed using a $H_2O_2$–ABTS colorimetric assay, with the enzyme cascade consisting of GOx–HRP bound to the DNA prism having the highest turnover rate (Figure 25F).

In 2018, Vogele *et al.* took an additional step toward realizing a more advanced application by placing a DNA-scaffolded GOx–HRP enzyme system on the surface of activated silica particles and assaying the activity using luminol-based chemiluminescence (Figure 26A).[81] A twist-corrected DNA origami rectangle was prepared where the DNA-conjugated GOx and HRP enzymes were attached in an array pattern with interenzyme distances of ~10 nm. Copper-assisted azide–alkyne Huisgen cycloaddition (*i.e.*, click chemistry) was used to attach the DNA to the enzymes, and their DNA-conjugated activity was found to decrease by 64% compared with the free native protein. The attachment yields were determined to be 31 and 68% for GOx and HRP, respectively. A plot of the normalized chemiluminescence observed for each of the enzyme colocalization strategies investigated is shown in Figure 26B. Enhancements of 2.1- and then 10-fold were observed when the enzymes were attached to the DNA origami rectangle and then placed on the surface of the silica particles, respectively. The investigators concluded that the cascade in its present form is not stable for long-term continuous operating conditions as a result of mechanical interactions between the particles and the accumulation of products. However, the work does suggest a pathway for potential upscaling of future DNA-based enzyme cascades.



DOI: 10.1021/acscatal.9b02413
*ACS Catal.* 2019, 9, 10812–10869

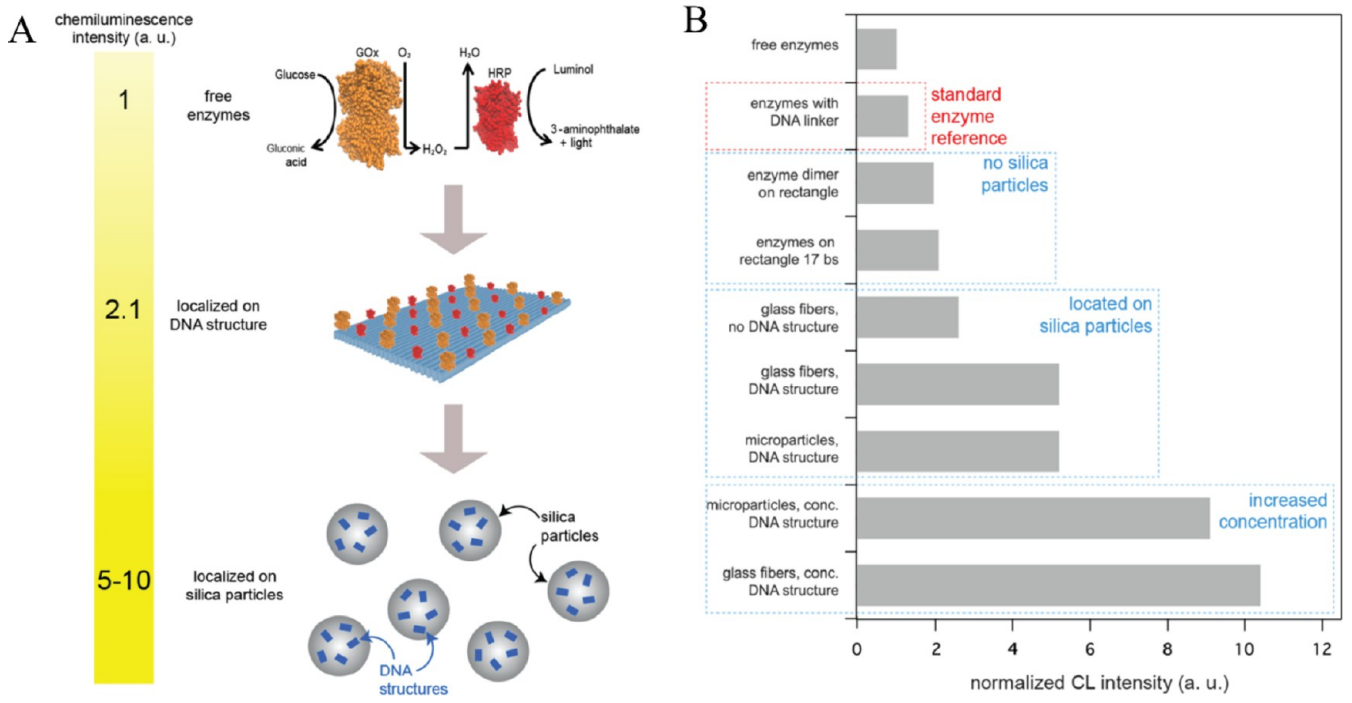


**Figure 26.** DNA-scaffolded GOx and HRP on activated silica particles. (A) Diagram highlighting the experimental approach for attaching DNA-scaffolded GOx and HRP on activated silica particles. (B) Plot of the normalized fold enhancement determined *via* chemiluminescence (CL) assay. Enhancements of 2.1- and 10-fold were observed when the enzymes were attached to the DNA origami rectangle and then placed on the surface of the silica particle, respectively. Reproduced from ref 81. Copyright 2018 American Chemical Society.

*Other DNA-Scaffolded Multienzyme Cascades.* Given the exquisite control over location on DNA scaffolds, powerful mechanisms can be investigated. In 2014, Fu *et al.* designed, evaluated, and optimized a DNA DX tile-based swinging-arm DNA enzyme cascade utilizing glucose-6-phosphate dehydrogenase (G6PDH) and malic dehydrogenase (MDH).[100] The arm itself displayed the key NADH cofactor for enzyme catalysis, and the effect of this on the overall activity was the prime research question investigated (Figure 27A). The enzymes were DNA-functionalized using homobifunctional NHS linker chemistry and purified using fast-protein liquid chromatography (FPLC) to select the fraction containing enzymes with only single DNA tethers. A phenazine methosulfate-catalyzed resazurin fluorescence assay was used to determine how the distance between the enzyme and the swinging arm affected the turnover rate. Swinging-arm−enzyme separation distances of 7, 14, and 21 nm were kinetically evaluated, and the 7 nm distance was found to be the most efficient, demonstrating a remarkable ∼90-fold higher rate than the same cascade lacking the arm. The structure was then extended by forming a cross with either G6PDH or MDH enzymes at the center surrounded by up to four swinging arms, termed a 4 × 4 tile (Figure 27B). The activity of the enzymes at the center of the 4 × 4 tile was observed to increase nearly linearly in the case of G6PDH. However, only a 2-fold increase in the MDH turnover rate was observed when it was surrounded by four swinging arms, indicating that MDH was approaching saturation. The catalytic efficiency could be even further improved by increasing the number of MDHs and swinging arms. Indeed, an astonishing 277-fold turnover enhancement was observed when an MDH:NADH swinging arm:G6PDH ratio of 4:4:1 was utilized (Figure 27C). Finally, the channeling efficiency was evaluated by adding the scavenging enzyme lactate dehydrogenase (LDH) to compete for NADH. As the percentage of the swinging arm structure increased, the MDH activity also increased, indicating that the swinging arm was effective at channeling NADH from the first G6PDH enzyme to the final MDH enzyme. Yang *et al.* extended this swinging arm concept by creating a network of G6PDH and LDH on a 100 nm square-lattice-like DNA origami template, as shown in Figure 27D.[298] Here the enzyme attachments were accomplished using either ssDNA−HaloTag or SPDP chemistry. The largest cascade investigated consisted of a total of eight pairs of G6PDH and LDH with 24 $NAD^+$ swinging arms on a 6 × 6 DNA origami lattice. Surprisingly, only an ∼10% increase in turnover was observed relative to the previously designed (DX) 4 × 4 tile-based swinging-arm configuration functionalized with a much lower number of G6PDH/LDH (Figure 27E).[100,298] No explanation for this modest increase was provided, but it is not beyond speculation that this may have to do with the enzyme attachment yield and the complexity of highly localized coupled enzymatic processes that are further dependent upon cofactors.

Again, because of the localization control DNA offers, in 2016 Ke *et al.* were able to demonstrate the first directional regulation of a three-enzyme G6PDH, MDH, and LDH pathway assembled on a DNA origami rectangle, as shown in Figure 28A.[296] Enzyme conjugations were achieved using SPDP chemistry for LDH and enzymatic HaloTag chemistry for MDH and G6PDH. Agarose gel and AFM evaluation found assembly yields of >80% and 36−66%, respectively, with the incongruity presumably due to AFM tip interactions with loosely held surface DNA assemblies. Control over the direction of substrate channeling between the two-enzyme pathways (G6PDH−MDH and G6PDH−LDH) was elicited by changing the position of the $NAD^+$ cofactor swinging arm *via* a DNA-toehold-mediated strand displacement driven by addition of the appropriate complementary DNA strand. Switch


DOI: 10.1021/acscatal.9b02413
ACS Catal. 2019, 9, 10812−10869

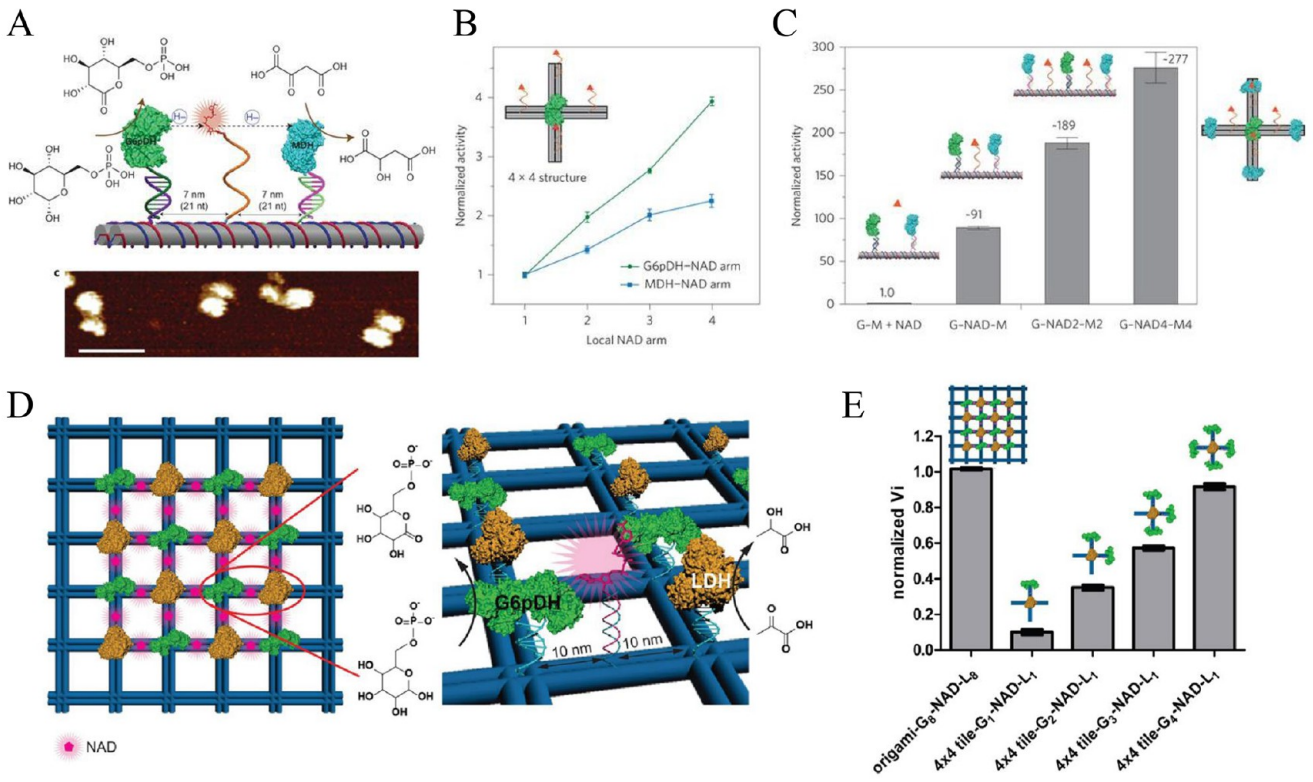


**Figure 27.** Swinging-arm DNA enzyme cascade. (A) Schematic of the DNA double-crossover (DX) tile-based swinging-arm DNA enzyme cascade and accompanying pathway. (B) Plot of normalized cascade activity vs the number of swinging arms present. As the number of swinging arms is increased from 1 to 4, the activity of the cascade increases. (C) Bar plot of the normalized cascade activity for the four configurations investigated. The tallest bar corresponds to the cross configuration with a total of four swinging arms. (D) Cartoon of the fully assembled G6pDH and LDH square enzyme cascade array consisting of a remarkable eight pairs of G6pDH and LDH with 24 $NAD^+$ swinging arms. (E) Plot comparing the catalytic turnover rate of the full 6 × 6 array to that of the previously investigated 4 × 4 tile cascades with increasing numbers of G6pDH enzymes attached. Reproduced with permission from (A–C) ref 100 and (D, E) ref 298. Copyright 2014 Springer Nature and 2018 Wiley-VCH Verlag GmbH & Co. KGaA, Weinheim, respectively.

1 activated the G6PDH–MDH pathway, whereas switch 2 activated the G6PDH–LDH pathway and reduced the G6PDH–MDH pathway. Optimization focused on the length of the poly(T) spacer that attached the $NAD^+$ to the swinging arm and the interenzyme spacings (Figure 28B–E). These data revealed that 25 and 20 nm resulted in the highest turnover for G6pDH–MDH and G6PDH–LDH, respectively. Similarly, Liu *et al.* created a three-pointed-star DNA-scaffolded enzyme cascade utilizing MDH, oxaloacetate decarboxylase (OAD), and LDH to understand how substrate coupling modulates the favored direction of a reaction pathway (Figure 28F).[297] Here an MDH fusion was DNA-conjugated using a commercially available HaloTag succinimidyl ester, whereas OAD and LDH enzymes were conjugated to thiol-modified DNA by SPDP chemistry. Enzyme attachment to each point of the star resulted in distances between any two enzymes of approximately 12 nm. The assembly yield was evaluated using PAGE and size-exclusion chromatography and found to be >80%. Evaluation of the MDH/OAD and OAD/LDH enzyme pairs demonstrated 1.7- and 10-fold increased turnover rates, respectively. Further distance-dependent activity experiments on the MDH/OAD pair linearly attached with varying spacings of 7, 14, 21, and 28 nm revealed activity variations of <20%, a finding that is significantly lower than in previously reported investigations.[36] The effect of the enzyme geometric arrangement on the turnover rate is summarized in Figure 28G. The three-pointed-star configuration resulted in the highest turnover rate, with a 4.5-fold enhancement relative to freely diffusing enzymes. The key finding was that the overall activity of the three-enzyme configuration was more dependent on geometric placement than interenzyme spacing.

In contrast to most of the above planar configurations, Zhao *et al.* created an elaborate DNA origami nanocage by combining two half-cages into a hollow rectangular box, as shown in Figure 29A.[64] The two honeycomb DNA origami lattice half-cages were initially folded and purified, and then the DNA-conjugated enzymes were attached in the center void of each half before the halves were joined together. Enzymes were DNA-conjugated using SPDP chemistry by cross-linking thiol-modified oligonucleotide with a lysine residue on the protein surface. Six different enzymes (HRP, MDH, G6PDH, LDH, GOx, and *β*-Gal) were all successfully conjugated and encapsulated within full DNA nanocages in yields ranging from 64 to 98%. TEM images of the assembled cascades are shown in Figure 29B,C. The closed cage had 42 small nanopores approximately 2.5 nm in diameter as a direct result of the honeycomb lattice. Individual and selected coupled enzyme activities were tested, and the activity of a full closed cage loaded with GOx and HRP (estimated interenzyme distance of ∼5 nm) was found to be ∼8-fold higher than that of a control without encapsulation (Figure 29D). Two explanations for the increased turnover rate were posited: a proximity effect that promoted substrate


DOI: 10.1021/acscatal.9b02413
*ACS Catal.* 2019, 9, 10812–10869

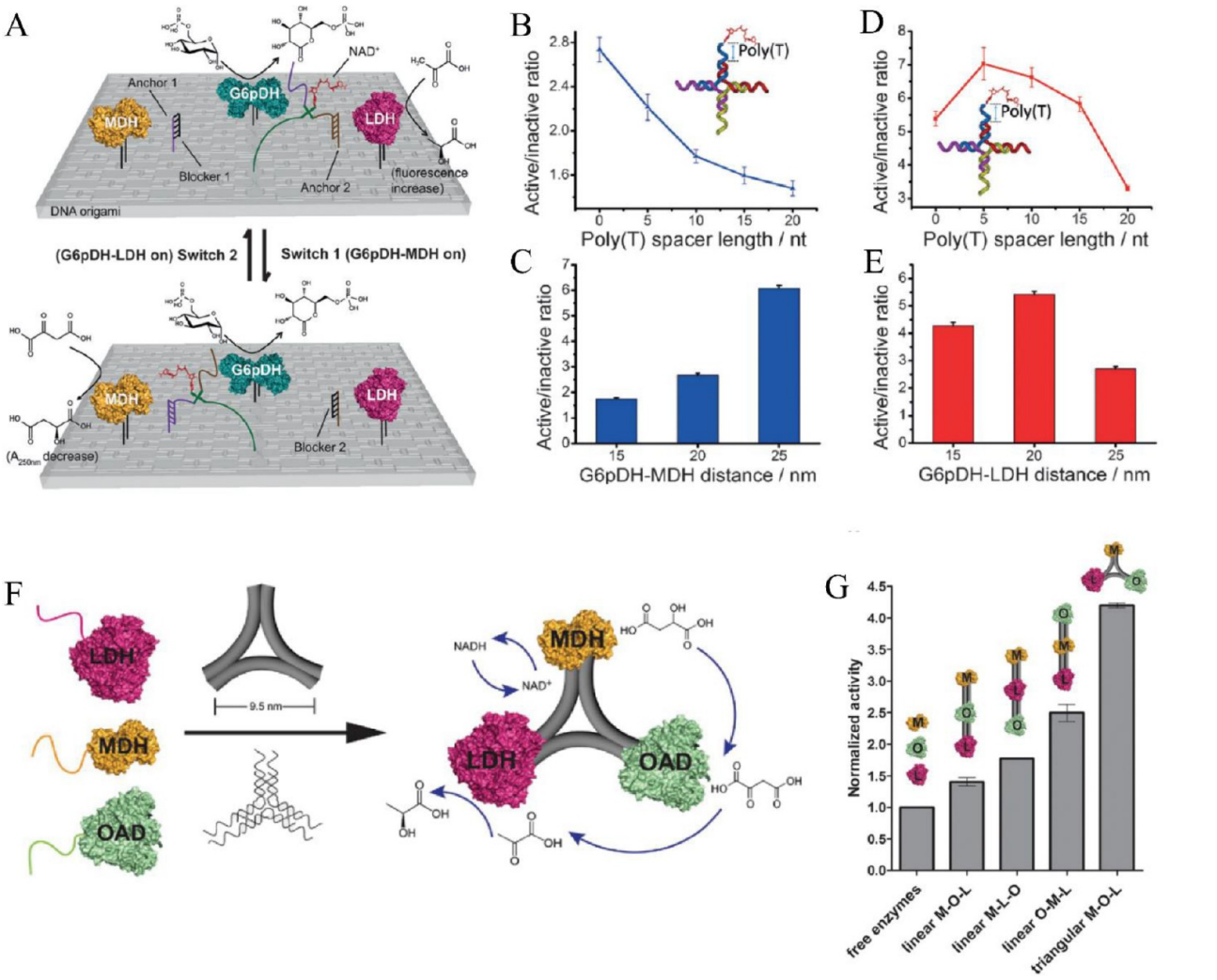


**Figure 28.** Three-enzyme DNA origami pathways. (A) Schematic of the three-enzyme pathway assembled on a DNA origami rectangle. The enzyme cascade was capable of switching between two pathways (G6pDH−MDH and G6pDH−LDH) by changing the positions of a $NAD^+$ swinging arm and a blocker DNA strand. (B, D) Plots showing how changing the length of a poly(T) spacer attaching the $NAD^+$ to the substrate swinging arm affected the turnover rate for the (B) G6pDH−MDH and (D) G6pDH−LDH pathways. (C, E) Bar plots showing how the activity varied as a function of different interenzyme distances for the (C) G6pDH−MDH and (E) G6pDH−LDH pathways. The optimal distances were found to be 25 and 20 nm for G6pDH−MDH and G6pDH−LDH pairs, respectively. (F) Schematic of the OAD−LDH−MDH enzyme cascade highlighting the component parts and reaction pathway direction. (G) Plot showing the enzyme cascade's normalized activity vs the control and the four configurations investigated. The star configuration resulted in a 4.2-fold increase in the pathway's turnover rate. Reproduced with permission from (A−E) ref 296 and (F, G) ref 297. Copyright 2016 Wiley-VCH Verlag GmbH & Co. KGaA, Weinheim.

transfer and contributions from high charge density arising from the DNA's negatively charged phosphates surrounding the enzymes. Another interesting finding was that an ∼4-fold enhancement in the turnover rate was observed when a sample was prepared that consisted of an equimolar mixture of separate nanocages, each encapsulating only single enzymes. This suggests that the putative DNA charge density effect is stronger than the proximity effect.

An artificial D-xylose metabolic pathway composed of the enzymes xylose (XR) reductase and xylitol dehydrogenase (XDH) displayed on a DNA origami rectangle was reported by Ngo *et al.* (Figure 29E).[300] In the pathway's first step, XR converts xylose into xylitol by consuming the cofactor NADH. In the second step, XDH transforms xylitol into xylulose. The enzymes were attached inside three rectangular cavities designed into the DNA rectangle, as shown in Figure 29F. Enzyme attachment was unique in this case, as it was accomplished using sequence-specific DNA-binding proteins. XR was fused to the zinc finger protein (zif268), whereas XDH attachment was achieved using a Gly-Gly-Ser linkage to the basic leucine zipper protein (GCN4) to give G-XDH. Interenzyme distances of 10, 54, and 98 nm were evaluated for assembly yield and kinetic performance since each cavity contained four binding sites for four ZS-XR enzymes and eight G-XDH enzymes (four homodimers). The attachment probability was determined from AFM image counts and revealed that the coassembly yields for the three different distances were 75%, 71%, and 81%, respectively. The coupled enzyme activity was monitored by following the oxidation of NADH spectrophotometrically at 340 nm. The cascaded reaction efficiency was found to be highly dependent on the interenzyme distance, with the highest flux observed when the enzymes were placed at a distance of 10 nm (Figure 29G). This last example also serves to highlight the strong potential of


DOI: 10.1021/acscatal.9b02413
*ACS Catal.* 2019, 9, 10812−10869

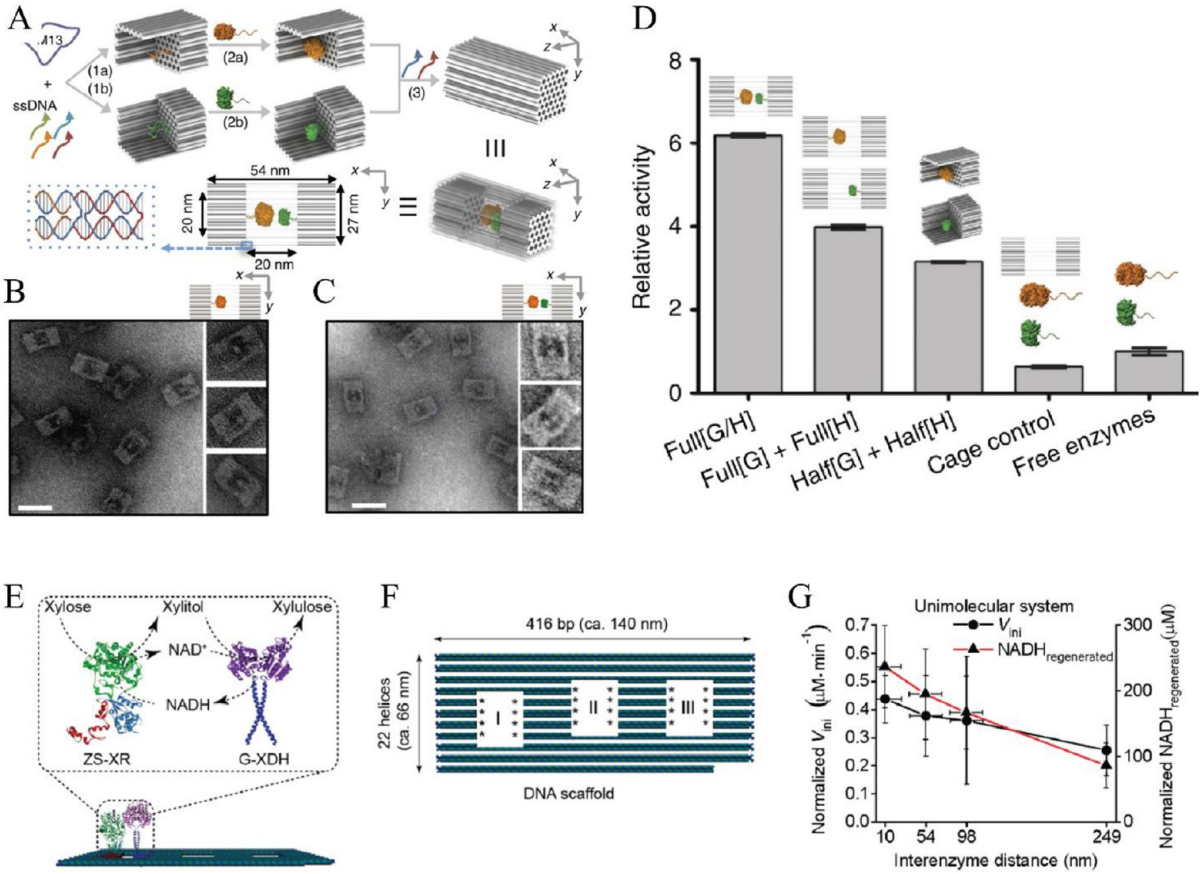


**Figure 29.** DNA origami nanocage and xylose pathway. (A) Schematic depicting the assembly of the DNA origami nanocage from two halves. Enzymes are first attached to each DNA origami half, and then the two halves are coassembled to form a DNA shell around the two enzymes. (B, C) TEM images of the assembled nanocages. The enzymes are clearly visible. (D) Bar plot of the relative activities of the five DNA origami nanocage configurations investigated. The greatest increase (~6-fold) was observed when HRP and GOx were enclosed with in the nanocage. (E) Schematic of the artificial D-xylose metabolic pathway composed of xylose reductase (XR) and xylitol dehydrogenase (XDH) assembled on a DNA origami rectangle. (F) Top view of the cascade highlighting the available sequence-specific DNA-binding protein attachment points. (G) Plot of normalized initial rate vs interenzyme distance for the four separations investigated. The highest initial rate was observed at the shortest interenzyme distance (10 nm). Reproduced from (A–D) ref 64 and (E–G) ref 300. Copyright 2016 Springer Nature and American Chemical Society, respectively.

using DNA-binding proteins (in the form of enzyme fusions) as an alternative and powerful way to assemble such hybrid structures.[319]

DNA offers not only precise localization but also the possibility of dynamic control. In 2018, Chen *et al.* used a toehold strand displacement strategy to dynamically control the rate of degradation of cellulose.[320] The endoglucanse CelA and the cellulose-binding module (CBM) were attached to DNA using elastic-like-polypeptide (ELP)–HaloTag fusions, where the ELP was used for purification. DNA was modified with cyclohexane to covalently link to the HaloTag. The two DNA strands connected to CelA and CBM were bound to a third strand, keeping CelA and CBM in close proximity and facilitating 1.5-fold higher cellulase activity than the free proteins. Addition of a "NOT" strand disrupts the DNA complex through a toehold domain on the DNA attached to CBM and decreases the overall cellulase activity. While this example was not a multienzyme cascade (as CBM is a binding protein and not an enzyme), as the authors noted, this example along with known aptamer switches for toehold displacement that are metabolite-sensitive portends the ability to dynamically control multienzyme cascades in the future.

## ■ ABIOTIC SCAFFOLDS

As mentioned, researchers have shown that enzyme activity and stability can be improved under variable reaction conditions, both ideal and nonideal, when the enzymes are immobilized on solid supports. In many instances, the scaffold material itself is selected to facilitate enzyme recovery and reuse, further enabling enzyme utility in large-scale catalytic applications.[26,321,322] Like the enzymes immobilized on them, abiotic or synthetic scaffolds are highly diverse and often tailored to the specific enzyme reaction or biocatalytic process. The hydrophobicity/hydrophilicity, surface charge, presence/absence of reactive functional groups, and other physicochemical properties allow for the use of specific enzyme immobilization strategies that directly affect downstream applications. While enzyme immobilization can result in some loss of activity, careful selection of these strategies and the scaffold material can lead to improvements in a variety of enzyme properties, as discussed by Rodrigues *et al.*[269] Though outside our direct purview, reviews written by Sheldon and van Pelt discuss some of the immobilization strategies routinely employed and their benefit to the assembly of enzyme/abiotic scaffold catalysts.[321,323]

Classically, abiotic materials for enzyme immobilization were classified simply as those derived from metal oxides, minerals,


DOI: 10.1021/acscatal.9b02413
ACS Catal. 2019, 9, 10812–10869

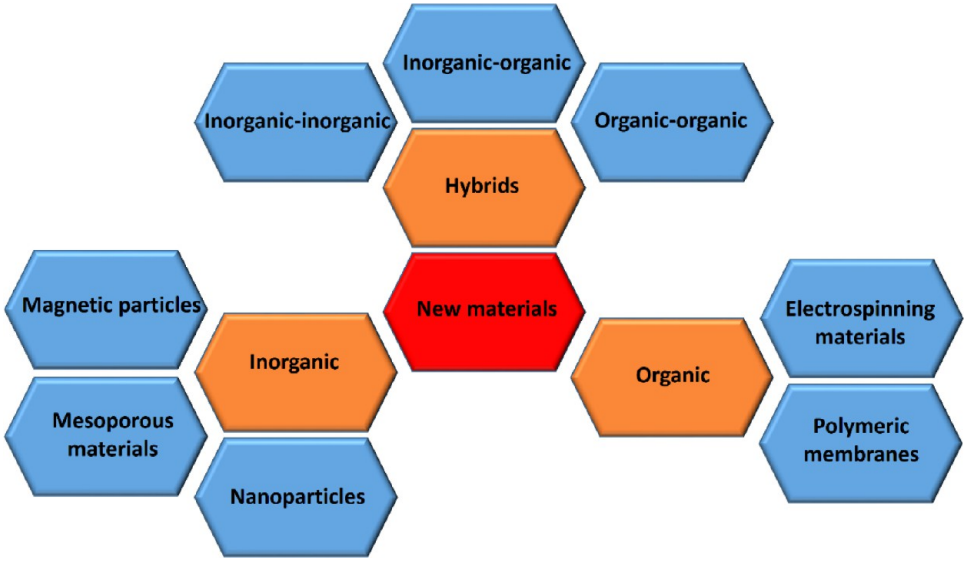


**Figure 30.** Abiotic materials for enzyme assembly. Major classes or families of materials being investigated for enzyme assembly with direct relevance to multienzyme cascades are shown. Reproduced from ref 322 under a Creative Commons license (https://creativecommons.org/licenses/by/4.0/).

or carbon materials.[322] More recently, many different materials have emerged that demonstrate improved thermal, chemical, and even mechanical properties, significantly improving the effectiveness and applicability of enzyme catalysts. Figure 30 presents an overview of the different material types currently being investigated for these purposes.[322] NPs of varied composition,[324,325] carbon nanotubes,[326−328] and graphene sheets,[329,330] have demonstrated success as substrates for surface immobilization of enzymes to enable enzymatic processes and are just a few examples of the abiotic scaffolds currently being employed by both industry and academic researchers. In this section, we highlight selected abiotic scaffolds that have documented success with multienzyme cascades, describing both their advantages and limitations as they apply to enzyme enhancement. Beyond these examples, additional enzyme systems utilizing abiotic scaffolds have been very effectively summarized by Zdarta *et al.*[322]

**Nanoparticles.** By definition, a nanoparticle is a material that exists in the 1−100 nm size range and exhibits properties that are dissimilar from those of larger particles or bulk accumulations of the same material. Often this can translate into materials with unexpected optical and diffusional properties, among others. Abiotic NPs typically comprise an inorganic particle surrounded by an interfacial "capping" layer that is composed of organic molecules that serve as passivating agents and provide colloidal stability.[331] In many instances, this capping layer contributes to the overall behavior and properties of the NP itself. This surface layer can often be tailored to experimental or application needs in order to facilitate enzyme immobilization and performance.[332] Inorganic NPs are differentiated and quite distinct from more biotic nanoparticulate materials such as liposomes and organic dendrimers, which are more commonly utilized in drug delivery.

*Magnetic Nanoparticles.* Magnetic NPs have found use in numerous biotechnology and medical applications. Though most magnetic NPs are iron oxides, magnetic properties can be improved through the addition of metal dopants such as Zn, Mn, Co, and Ni.[333] Once synthesized, magnetic NPs are usually capped with a wide range of passivating layers that can be chosen on the basis of the application, reaction conditions, and immobilization strategy.[333−336] As with other NP scaffolds, they possess a high surface-to-volume ratio, which makes them ideal for enzyme immobilization and the assembly of multicomponent enzyme catalysts.[337] Additionally, magnetic NPs are relatively inexpensive to manufacture, very stable, and biotolerant under a range of physiological conditions.[333] In combination, the inherent magnetic and other properties of iron oxide NPs have allowed the development of biomedical separation processes, protein purification methods, and biosensor platforms, as described in several recent reviews.[337−341] One potential limitation is that some enzymes have reduced activity when immobilized on magnetic NPs, perhaps because of the formation of aggregates.[342] Below we highlight three recent examples of the use of magnetic NPs based on application.

Carbon dioxide accumulation in the environment and its capture and sequestration are ever-growing topics in scientific and societal discussions. Plants and other autotrophic organisms employ enzyme cascades to produce sugars and other metabolic components from $CO_2$, but carbohydrates such as glucose are not the only products that can be enzymatically synthesized from this precursor. Using an engineered non-natural enzyme pathway, Marques Netto *et al.* were able to produce methanol from $CO_2$ using four enzymes immobilized on magnetic NPs;[343] this is the converse of the pathway utilized by Liu *et al.* (Figure 11A), which also employed most of the same enzymes.[116] The conversion process required four enzymes: alcohol dehydrogenase (ADH) from *S. cerevisiae*, formaldehyde dehydrogenase (FALDH) from *P. putida*, formate dehydrogenase (FDH) from *Candida boidinii*, and glutamate dehydrogenase (GluDH) from bovine liver cells. The authors determined empirically that each enzyme required a magnetic NP of different size and composition, which was validated through independent interrogation of each component of the complete enzymatic process. When combined, the stepwise synthetic reactions yielded a 2.3% increase in methanol production per NADH molecule. In pressurized batch reactions containing all four enzymes and a separate NADH regeneration component, the reaction was markedly improved, with a 64-fold increase in methanol yield. Although


DOI: 10.1021/acscatal.9b02413
*ACS Catal.* 2019, 9, 10812−10869

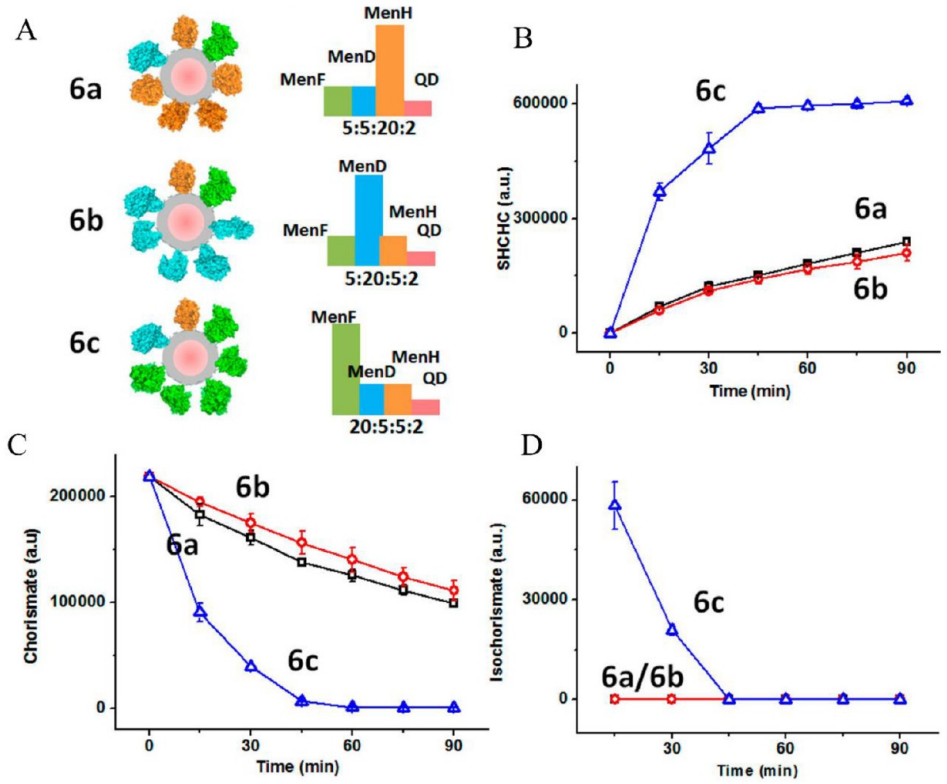


**Figure 31.** Menaquinol synthesis by multienzyme−QD assemblies. (A) Schematic illustration of three multienzyme−QD assemblies with excess MenH (**6a**), MenD (**6b**), and MenF (**6c**), respectively. The composition of the enzymes in the assemblies drastically affected the catalytic efficacy and intermediate flow. (B) Product (SHCHC) generation catalyzed by the three assemblies. (C) Substrate (chorismate) consumption catalyzed by the three assemblies. (D) Intermediate (isochorismate) accumulation catalyzed by the three assemblies. The total amounts of the enzymes and QDs, volumes of the reaction solutions, and the initial concentrations of chorismate were all the same in **6a**, **6b**, and **6c**. Reproduced from ref 354. Copyright 2014 American Chemical Society.

the authors speculated about the material and NP size effects on each enzyme, the reasons that different NP materials were required still remain unknown, suggesting that there is much to be learned about bioconjugation effects.

Throughout the literature, the assembly of enzyme cascades on abiotic scaffolds is described with the goal of improving commercial applications. As an example, Dong *et al.* showed that an enzyme cascade assembled on magnetic NPs enabled a relatively low-cost method of producing a precursor necessary for *in vitro* glycosylation.[344] Glycosylation of proteins and other biomolecules is often important to their cellular function.[345,346] Therapeutic biomolecules are therefore often glycosylated during formulation to ensure accurate function within the body. In cells, glycosylation of proteins is facilitated by glycosyltransferases that utilize a sugar-modified uridine nucleotide as a substrate. While these modified nucleotides can be synthesized through chemical means, enzymatic processes are desired because of favorable reaction conditions and the regioselectivity of enzyme reactions.[347,348] However, enzyme systems are often burdened with the high cost of precursors, as shown by the cascade designed by Jiang *et al.* that relied on a glucose-1-phosphate substrate.[348] In contrast, the mechanism described by Dong *et al.* targeted low-cost substrates, specifically maltodextrin, uracil triphosphate, and free phosphate. To facilitate the synthesis of uridine diphosphoglucose (UDP-Glc), the authors employed three enzymes assembled on amino-functionalized magnetic NPs: maltodextrin phosphorylase, glucose-1-phosphate thymidyltransferase, and inorganic pyrophosphatase. The authors observed a 30% loss of activity following immobilization, but when interrogated individually, the enzymes showed specific activities similar to those of the free enzymes. In all cases, the enzymes showed higher $K_M$ and $V_{max}$ values for the immobilized enzymes for at least one substrate. With this system, the authors were able to achieve a moderate yield (50%) of the UDP-Glc precursor using low-cost starting materials and an enzyme catalyst that could easily be recovered and reused a number of times.

Magnetic particles have been shown to be viable not only as abiotic scaffolds for enzyme assembly but also as mediators of reaction mixing, a critical parameter for the design of large-scale reactions, through alternating magnetic fields. In a demonstration of this capability, Yang *et al.* immobilized glucoamylase and $\alpha$-amylase on ferric oxide powders in chitosan beads.[349] The goal was to implement an enzymatic system that was amenable to manipulation using magnetic fields that would eliminate the need for secondary pumps or mixers in biosensor or bioanalytical tool development. In this study, both enzymes maintained their catalytic activities and were successfully able to reduce the starch substrate to its monomer components over the course of the experiment. As enzyme kinetics was not their focus, the enhancement of starch conversion was not monitored.

*Semiconductor Quantum Dots.* Semiconductor quantum dots (QDs) are small nanocrystals formed from the nucleation and crystallization of elements such as cadmium and selenium


DOI: 10.1021/acscatal.9b02413
*ACS Catal.* 2019, 9, 10812−10869

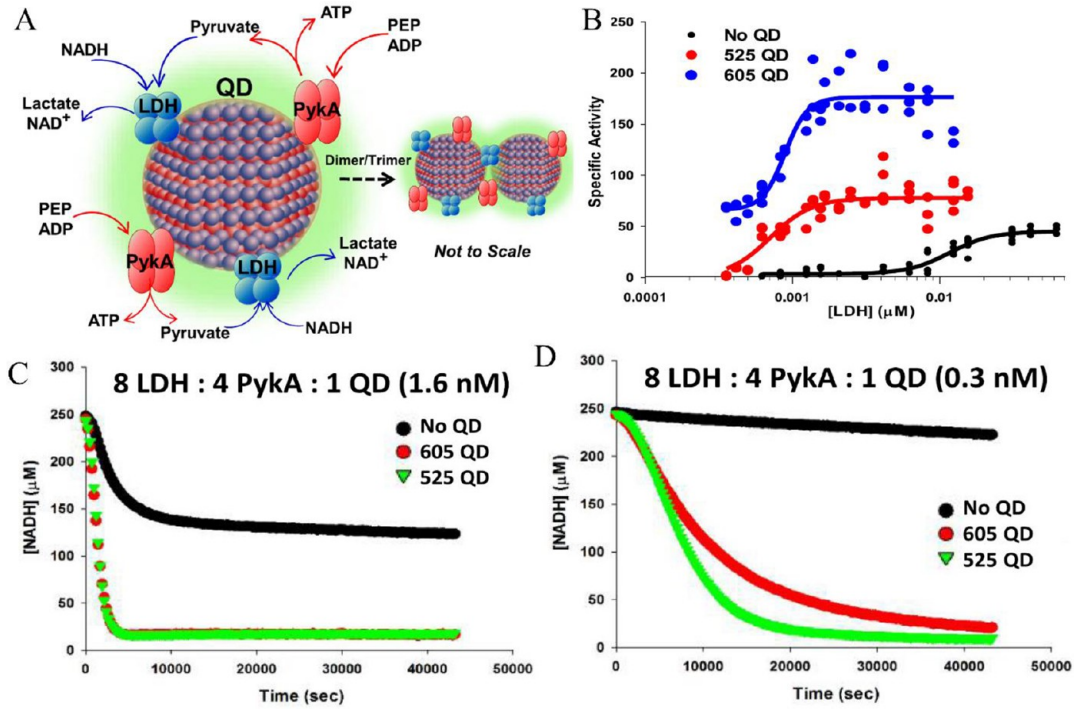


**Figure 32.** Substrate channeling and enzyme stabilization on QD scaffolds. (A) Schematic of the coupled PykA−LDH enzyme system colocalized on a QD surface. The propensity of the enzymes to form cross-linked QD dimers and, to a lesser extent, trimers *via* the enzymes' tetrameric polyhistidine tags is also schematically indicated. The schematic is not to scale. (B) Specific activity of LDH ($\mu$M of NADH consumed $s^{-1}$ ($\mu$M LDH)$^{-1}$) determined at various enzyme concentrations in the absence (black) or presence of 605 QDs (blue) or 525 QDs (red). (C, D) Concentration of NADH in a combined PykA−LDH reaction monitored with enzymes assembled on 605 (red) or 525 QDs (green) or QD-free (black). The reactions were monitored at (C) a high concentration of 8 LDH (12.8 nM)/4 PykA (6.4 nM)/1 QD (1.6 nM) and (D) a 5-fold lower concentration of 8 LDH (2.4 nM)/4 PykA (1.2 nM)/1 QD (0.3 nM). Enzyme-only contained the equivalent amount of free enzyme. Reproduced from ref 61. Copyright 2018 American Chemical Society.

that are commonly employed as semiconductor materials.[350] They have come to prominence in biological applications for both their unique optical properties and the ease of surface modification or capping, which allows them to be employed in a wide array of biological assays.[350,351] Beyond imaging assays and biosensors, QDs also serve as reliable scaffolds for the immobilization of enzymes and other biomolecules. While the chemical diversity of the QD cap can readily be tailored to experimental needs, the most direct route of oriented protein immobilization utilizes the $His_6$ purification epitope that is typically added to the C- or N-terminus of the recombinantly produced enzyme.[91,99,352,353] Here the imidazole side chains bind to $Zn^{2+}$ on the shell of CdSe/ZnS core/shell QDs by metal affinity coordination. This method of high-affinity enzyme immobilization offers not only a mechanism of oriented immobilization but also control over the relative ratio of enzyme per QD and eliminates the need for chemical conjugation methods, which often detrimentally affect the enzyme activity. QDs can be beneficial as a scaffold because of the ease of modifying the number of enzymes immobilized, for example, using the $His_6$ method of immobilization. Assembly of enzymes on NPs is meant to facilitate the reassembly of functional multiprotein complexes such as those seen within cells. Often, the positional assembly (*i.e.*, the distance between enzymes) is important to ensure efficient catalytic activity from the enzyme system or cascade.

Menaquinones are redox-active compounds found within the membranes of bacteria and other organisms. In *E. coli*, the menaquinol-8 biosynthetic pathway utilizes products of both the chorismate biosynthesis I pathway and the *trans,trans*-farnesyl disphosphate biosynthesis pathway as starting substrates for two convergent enzyme pathways. The first three enzymes of the chorismate arm, MenF, MenD, and MenH, have all been produced recombinantly and function normally as part of *in vitro* assays. To investigate the distance between enzymes and its effect on their catalytic activity, Kang *et al.* exploited the same $His_6$-driven metal ion affinity immobilization to assemble each of these enzymes in varying ratios to 3.5 nm (565 nm emission maxima) CdSe/ZnS core/shell QDs.[354] In their initial trials, where the enzyme was immobilized at an enzyme:QD ratio of 5:1, the authors observed a reaction rate less than or equal to that with the free enzymes in solution. However, through iterative modification of both the enzyme:QD and enzyme:enzyme ratios on QDs, the authors observed an increased rate in production formation (Figure 31). While the enzyme:enzyme ratio likely contributed to reducing the bottleneck of rate-limiting steps in the catalytic process, the authors theorized that the increase in the enzyme:QD ratio is directly correlated to a reduction in the interenzyme spacing, thereby aiding in intraparticle substrate flow. Though the authors stopped short of comparing the assembled systems to free-enzyme or alternate biosynthetic approaches, their thorough examination of the intraenzyme spacing and substrate channeling reflect the critical components needed for understanding the enhancement observed when enzymes and enzyme cascades are assembled on NPs. Moreover, since each enzyme has a different intrinsic catalytic rate, numerical simulations of


DOI: 10.1021/acscatal.9b02413
*ACS Catal.* 2019, 9, 10812−10869

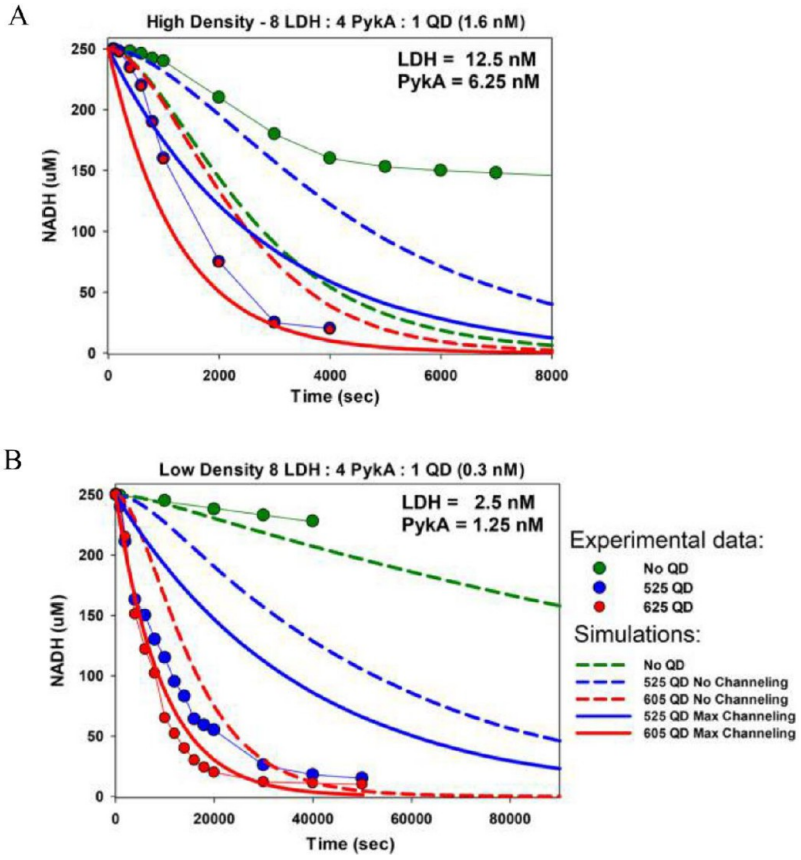


**Figure 33.** Simulation of channeling of a pyruvate intermediate between QD-immobilized PykA and LDH. Experimental data for (A) high density and (B) low density enzyme formats are compared with predictions of a kinetic model of the PykA−LDH cascade. The experimental data are denoted as points connected by thin lines of the same color, and the simulation results are given by thicker solid or dashed lines. Reproduced from ref 61. Copyright 2018 American Chemical Society.

each system's kinetic profile can be quite useful to determine the optimal ratio of each enzyme to use within a given cascade.

In addition to activity, immobilization of enzymes on abiotic scaffolds such as QDs is often associated with stabilizing enzyme function, although this characterization is often used quite ambiguously with little interpretation as to its actual meaning. Important to this discussion, *in vivo* many enzymes are active not as simple monomers but as multimeric proteins or multiprotein complexes. In a study of the kinetic parameters of pyruvate kinase (PykA) and lactate dehydrogenase (LDH) assembled on QDs, Vranish *et al.* observed an interesting variability in the activity of these enzymes assembled on QDs that was affected by both the concentration of the enzyme itself and the location of the $His_6$ epitope tag that was used for NP immobilization.[61] In preliminary studies, the authors observed that the tetrameric PykA showed reduced kinetic activity when immobilized on QDs at low enzyme concentrations, which is contrary to the author's previous studies with other enzymes.[63,355−357] However, when higher enzyme:QD ratios were used, the enzyme activity reached levels comparable to those of free enzyme in solution. In contrast, the LDH enzyme showed significant enhancement of activity, nearly 50-fold, when immobilized on similarly sized QDs using the same metal affinity tag for assembly. Like PykA, LDH is a tetramer, although it dissociates to the monomer form at low concentrations.[358] On the basis of modeling of the protein structure and the positioning of the $His_6$ tag, the authors hypothesized that the epitope tag in this instance actually serves to stabilize the multimeric structure, contributing to the significant increase in enzyme activity. In conjunction with these studies, the authors examined bienzyme assembly on particles at varying enzyme:QD ratios to further improve the catalytic activity (Figure 32). To better understand the mechanisms at play, the authors performed a number of simulations in which the surface diffusion of the pyruvate intermediate was varied to predict the maximum reaction velocity attainable through substrate channeling (Figure 33). Comparison of the experimental data with the model-predicted activities at low and high enzyme concentrations supported the authors' hypothesis that at the optimized enzyme ratios the observed improvements in catalytic activity are the product of both improved enzyme stability and substrate channeling between the QD-immobilized enzymes. Interestingly, a large number of other enzymes have shown some type of enhanced activity when assembled on both QDs and similarly sized gold nanoparticles (AuNPs), including alkaline phosphatase, phosphotriesterase and many of its engineered structural variants, luciferase, $\beta$-Gal, and acetylcholine esterase, among others.[77,355−357,359−372] This phenomenon seems to arise from the unique environment around NPs, which appears to alleviate certain rate-limiting steps along with the aforementioned improvement in stability. It also certainly bodes well for their utility in any type of NP-scaffolded cascade. Moreover, this enhancement was shown for HRP attachment to QDs and was even maintained when HRP was functionally coupled to GOx in solution.[63]



DOI: 10.1021/acscatal.9b02413
*ACS Catal.* 2019, 9, 10812−10869

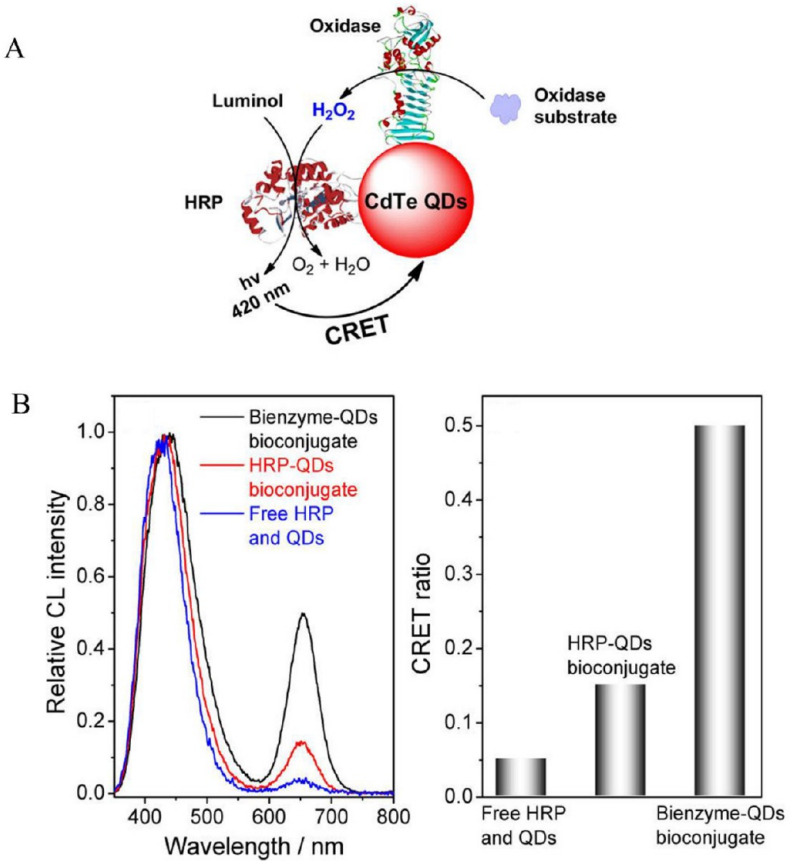


**Figure 34.** Bienzyme system to enhance sensor activity. (A) Schematic principle of CRET from luminol to CdTe QDs with a bienzyme−QDs bioconjugate. (B) Comparison of the CRET performances of the GOx−HRP−CdTe QDs bioconjugate, the HRP−CdTe QDs bioconjugate, and a mixture of free HRP and CdTe QDs: (left) CRET spectra and (right) CRET ratios reflecting the efficiency of energy transfer. Reproduced from ref 375. Copyright 2016 American Chemical Society.

The inherent optical properties of QDs are often paired with chemical or biological sensors in the development of sensors or bioanalytical tools and devices. When used in conjunction with a reporter such as HRP that can utilize chemiluminescent substrates, QD-based reporters typically have advantages over conventional FRET-based sensors, as no light source is required for activation and there is little activation of the energy donor. Despite these advantages, chemiluminescent substrates such as luminol are enzymatically cleaved to form $H_2O_2$ as a product that can oxidize QDs and reduce the activity. Referencing the observations of Limoges *et al.*, who described improved enzyme activity when confined within nanometric range,[374] Xu *et al.*[375] successfully demonstrated improved chemiluminescence resonance energy transfer (CRET)[373] efficiencies in their QD-based sensor when an oxidase enzyme was added to control the formation of $H_2O_2$. Here the authors used carbodiimide chemistry to attach HRP and one of three oxidase enzymes—GOx, cholesterol oxidase (ChOx), or benzylamine oxidase (BeOx)—to a QD to demonstrate a proof-of-concept CRET-based sensor for serum biomolecules (Figure 34A). The authors validated the initial design using glucose oxidase showing that compared with free HRP or QD-conjugated HRP, the bienzyme system possessing the immobilized oxidase enzyme showed a much greater CRET efficiency (Figure 34B). In subsequent serum analysis experiments, the QD-based sensors showed detection limits comparable to or better than those of hospital-performed blood assays.

*Gold Nanoparticles.* AuNPs are highly adaptable to a range of biological and medical applications because of their optical properties, biotolerance, and amenability to a range of chemical and biological strategies for surface immobilization.[376−378] One such strategy that is directly conducive to subsequent protein or enzyme immobilization is surface functionalization with a $Ni^{2+}$-NTA group. As discussed in the preceding section, inclusion of a small $His_6$ tag in recombinantly produced enzymes allows for both immobilization and orientation on NP surfaces that possess divalent metal ions such as $Ni^{2+}$ or $Zn^{2+}$. Other typical AuNP chemical immobilization or bioconjugation strategies are based on cysteine thiol affinity to gold surfaces or the ubiquitous biotin−avidin chemistry.[92] In addition to surface modification, the years of invested research have established well-defined protocols for the synthesis of AuNPs of various shapes and sizes.[379] In conjunction, these properties make AuNPs ideal not only for both downstream medical and commercial applications but also for studying the behavior of enzymes and other biomolecules on NP surfaces.

While the material composition of NPs often contributes to some of their unique properties and reported biological enhancements, the size and shape are also important to some of these behaviors. To explore the effect of NP size on enzyme activity, Lata *et al.* performed a series of experiments examining the kinetic properties of three enzymes—glucose-6-phosphate isomerase (GPI), glyceraldehyde-3-phosphate dehydrogenase (GAPDH), and pyruvate kinase (PykA)—immobilized at high


DOI: 10.1021/acscatal.9b02413
*ACS Catal.* 2019, 9, 10812−10869

and low concentrations on AuNPs of four sizes (5, 10, 20, and 50 nm).[380] Here the enzymes were chosen on the basis of classification (an isomerase, an oxidoreductase, and a transferase, respectively) and not for their ability to shuttle or channel intermediates between enzymes. Of consequence, the authors reported little to no improvement in activity when the enzyme was immobilized as a monolayer (less than 100% surface coverage) to any of the four particles, in contrast to previous reports by other groups who routinely observed reductions in $K_M$ or increases in $k_{cat}/K_M$. Interestingly, the group observed increasing catalytic activity as the NP size and enzyme concentration increased. On the basis of quantitation of the immobilized proteins, the authors speculated that multilayer enzyme structures likely formed. This is a somewhat counterintuitive finding, as it would be expected that multilayer structures may nullify access to some of the enzymes. Geometrically, increasing NP size correlates to decreasing surface curvature, which here was hypothesized to encourage multilayer assembly. While the authors were not able to accurately calculate how much enzyme was active on the saturated NPs, the observed improvements in total activity per particle were consistent among the enzymes.

*Silica Nanoparticles.* The synthesis of silica NPs is a highly controlled process that allows researchers to tune the size, porosity, crystallinity, and shape of the particles.[381,382] Their biocompatibility and amenability to surface modification have allowed researchers to readily implement them in the development of therapeutics for drug delivery, diagnostics, and tools for imaging.[383] For enzyme assembly, silica NPs in their various forms and compositions offer an alternative set of chemical properties that can be utilized to ensure function. In their attempts to construct a 10-enzyme sequential reaction, Mukai *et al.* found that 500 nm magnetic silica NP scaffolds significantly reduced the activities of some enzymes.[342] The authors therefore adopted NTA-modified silica-based NPs as an alternative scaffold. In these studies, the genes encoding 10 enzymes involved in glucose metabolism were isolated from mammalian sperm and recombinantly produced as $His_6$-tagged proteins in mammalian cell cultures. The enzymes were divided into three distinct clusters, each possessing at least one tractable cofactor that allowed the enzyme activity to be assessed. When examined independently, each of the three NP/enzyme assemblies showed a higher rate of product formation than free enzyme controls. Additionally, when supernatant from each reaction was removed and sequentially added to the next enzyme cluster, the NP-assembled enzyme systems showed elevated levels of lactate production from each nanomole of glucose consumed compared with control reactions. The authors proposed that this enhancement is likely attributable to the diffusion of intermediates within the hydration shell of adjacent enzymes or substrate channeling, although the free enzyme system still produced substantially more lactate per microgram of enzyme. It should also be noted that the 0.5 $\mu$m-sized silica particles utilized in this study are technically microparticles and do not meet the strict definition of NPs; this also points out a potential issue, as the size of this type of scaffold may have a strong influence on access to channeling, and further investigation is certainly warranted.

**Metal–Organic Frameworks.** Metal–organic frameworks (MOFs) are materials constructed by linking metal-containing units *via* organic linkers to create crystalline frameworks with defined porosity.[384] The flexibility in the selection of both the metal-containing unit and the linkers has enabled the formation of thousands of MOF materials that have widely varying properties and applications, including storage of fuels, enabling catalytic conversions, serving as drug carriers, and many more.[87,384,385] Similar to NPs, exposed functional groups and surface features can be tailored for specific biomolecule immobilization strategies, including passive absorbance through hydrogen bonding and van der Waals interactions, *via* salt bridges, or through covalent modification.[386] MOFs also provide an elevated level of control in enzyme and biomolecule packaging, as the synthesis reactions can be optimized to control the pore size, shape, volume, and surface area, which can directly correlate to the enzyme loading.[384,387,388] Such control over the physical properties of MOFs has allowed researchers to develop several effective strategies for loading of enzymes into MOF structures (Figure 35).[386] For the development of enzyme catalysts, encapsulation within MOFs has been shown to improve biomolecule stability under harsh thermal, mechanical, and chemical conditions similar to other scaffold platforms.[389] These stability improvements are often the product of physical inhibition of denaturation or aggregation that can occur under environmental stress. The combined properties of MOFs have contributed to an ever-growing interest in these materials as abiotic scaffolds for enhancing enzyme viability as a tool for commercial applications.

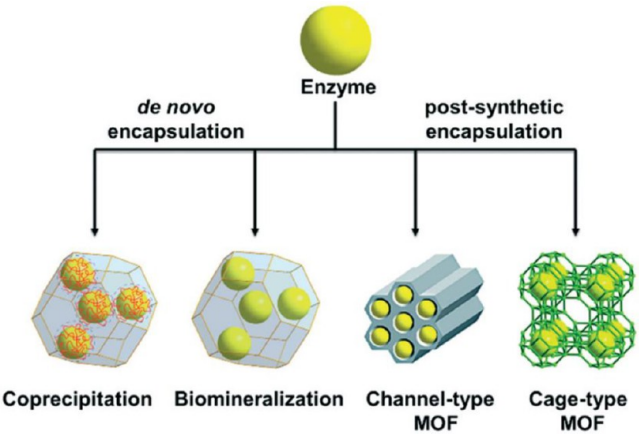


**Figure 35.** Methods of enzyme encapsulation within MOFs. The schematic highlights how enzymes can be encapsulated by coprecipitation or biomineralization as well as postsynthetically in the channels or cages of MOFs. Reproduced with permission from ref 386. Copyright 2017 Royal Society of Chemistry.

Despite their numerous advantages, MOF–enzyme systems often show reduced enzyme activity relative to the free enzymes due to inhibition of substrate diffusion through the crystalline lattice. The diversity of available metals and ligands, however, allows for exquisite control over the pore size and structure of MOFs, which can allow these limitations to be overcome. As an example, Li *et al.* demonstrated that the activity of an organophosphorous acid anhydrolase enzyme could be improved beyond that of the free enzyme through the use of a *csq-net* zirconium MOF that featured a large mesoporous aperture.[390] Similarly, Lyu *et al.* employed a coprecipitation method of capture to anchor cytochrome *c* to the surface of a zeolite imidazole framework and observed a 10-fold increase in catalytic activity.[391] While there are numerous examples of single-enzyme improvements in MOFs, there are minimal references to multienzyme systems or cascades. Recently, Chen


DOI: 10.1021/acscatal.9b02413
*ACS Catal.* 2019, 9, 10812–10869

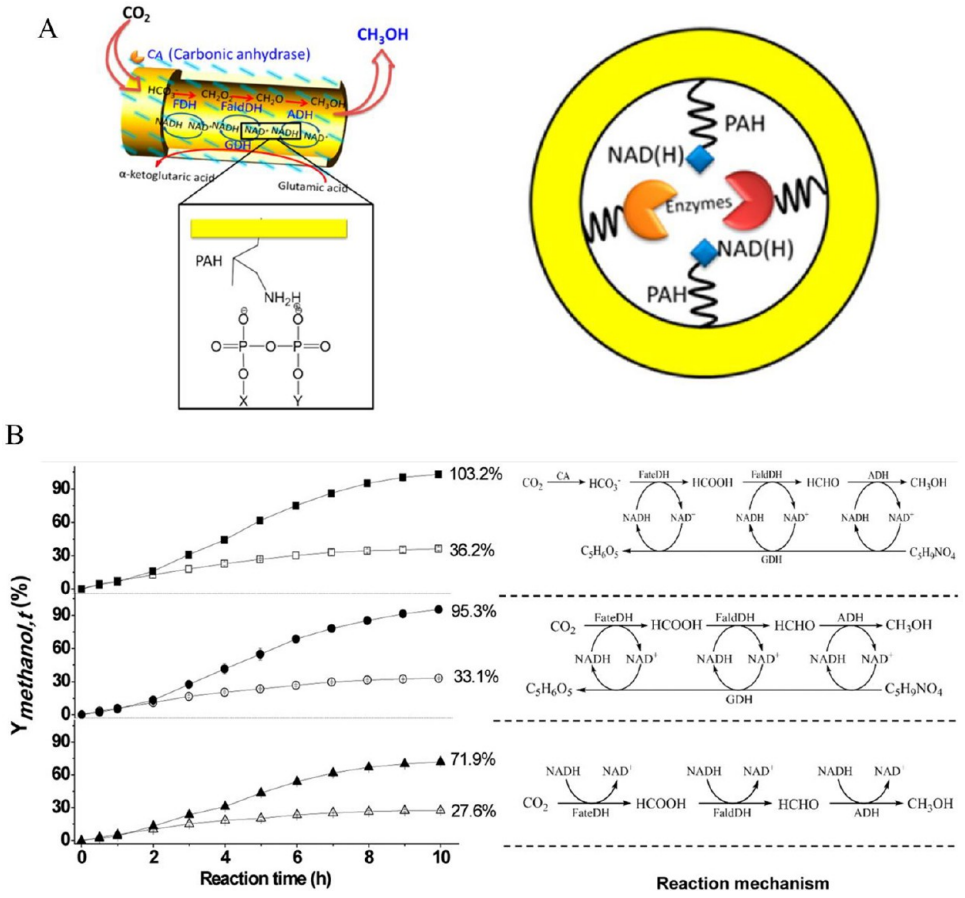


**Figure 36.** Polymer nanotubes for reduction of $CO_2$ to methanol. (A) Electrospun polyurethane fibers were doped with poly(allylamine hydrochloride) (PAH) to enable passive immobilization of enzymes and NADH cofactor. Enzymatic conversion of $CO_2$ to methanol occurred through a three-step reduction facilitated by formate dehydrogenase, formaldehyde dehydrogenase, and alcohol dehydrogenase, each utilizing NADH as the cofactor. (B) Regeneration of the NADH cofactor was vital to the efficiency of the entire pathway and was improved when local concentrations were increased through a cofactor regeneration system. (left) Plots of methanol yield as a function of reaction time for methanol synthesis from $CO_2$ by using multiple enzymes (△, ▲) without cofactor regeneration, (○, ●) with coupled GDH for cofactor regeneration, and (□, ■) with both GDH for cofactor regeneration and CA for accelerating hydration of $CO_2$. (right) Reaction mechanisms corresponding to these multienzyme systems. Open symbols represent results for the free multienzyme systems, and solid symbols present results for the hollow-nanofiber-supported multienzyme systems. Reproduced from ref 394. Copyright 2015 American Chemical Society.

*et al.* demonstrated MOF-associated enhancement of two distinct enzyme systems.[87] In their initial trials, the authors encapsulated the ubiquitous GOx−HRP pair within a zeolitic imidazole framework and measured the coupled enzyme activity *via* the oxidation of Amplex Red to its resorufin fluorescent product by HRP. The nanoreactor system exhibited a 7.5-fold increase in catalytic activity compared with free enzyme controls. Expanding upon this success, the system was modified to include *β*-Gal as the initiator enzyme to degrade lactose to the glucose substrate for GOx. The three-enzyme system again showed rate enhancement with a calculated 5.3-fold improvement over control reactions. In both of these studies, the authors confirmed colocalization of enzymes *via* fluorescence microscopy. The authors hypothesized that similar to other scaffolded enzyme systems, the MOFs enable catalytic rate enhancement through an increase in the local concentrations of substrates/products and the enzymes.

**Polymeric Structures.** Abiotic scaffolds are highly diverse in their structure and composition. Polymeric structures are a general classification of repeating subunit scaffolds that do not readily fall into the other more distinct groups previously described. Polymers have an inherent advantage of a well-defined structure that allows for precise control over the chemical handles or functional groups they display and that can be targeted for enzyme immobilization as described by Katyal *et al.*[392] This allows for well-controlled positioning of enzymes in these structures. As reviewed by Schmidt-Dannert and Lopez-Gallego[393] and by Chen *et al.*,[6] polymeric scaffolds and other similar structures provide a pathway to the realization of commercial biosynthesis, as these systems have been shown to improve enzyme activity, stability, and reusability while employing a scaffold that can be easily and cost-effectively manufactured.

In addition to the complexities of assembling enzymatic systems for *in vitro* catalysis, regeneration of cofactors and other necessary components can severely limit reaction efficiency. The pathway previously described by Liu *et al.*[116] (Figure 11A) reduces the greenhouse gas $CO_2$ to methanol through an enzymatic cascade comprising formate dehydrogenase (FDH), formaldehyde dehydrogenase (FALDH), and alcohol dehydrogenase (ADH). Each of these requires an NADH cofactor for the enzymatic reduction of its substrate. As direct capture of NADH molecules by the solid support does not increase catalysis, Ji *et al.* focused upon passive immobilization of the


DOI: 10.1021/acscatal.9b02413
*ACS Catal.* 2019, 9, 10812−10869

cofactor through electrostatic interactions.[394] Here the authors electrospun polyurethane nanofibers doped with a water-soluble cationic polyelectrolyte, poly(allylamine hydrochloride). Electrostatic interactions with the negatively charged NADH ensured localization within the lumen of the fiber along with glutamate dehydrogenase to allow for its regeneration (Figure 36). While the authors did not directly monitor the enzyme kinetics for each individual enzyme in the cascade, they did report that through the addition of the cofactor regeneration system to the cascade, a 2.85-fold increase in methanol production was observed. Additionally, the authors indicated that this improvement was observed only when the NADH regeneration system was colocalized within the lumen of the fiber and could not be reproduced with exogenous addition of NADH. As with other shuttling mechanisms, the elevated local concentration of the cofactor likely leads to the improvement in reaction efficiency.

As with any immobilization strategy, careful selection of the chemistries used for immobilization is critical to ensure activity. Zore *et al.* examined different approaches for enzyme assembly to a poly(acrylic acid) abiotic scaffold to form multienzyme polymer conjugates (MECs).[395] In both of the strategies employed for MEC assembly, carbodiimide chemistry was used to form the abiotic scaffold. The authors tested both parallel and sequential addition of enzymes and polymer, assaying the specific activities of individual enzymes in the MEC to assess the impact of the immobilization strategy on each. Interestingly, the effect on enzyme activity was inconsistent for different enzymes. While this study did not directly address substrate channeling, it does highlight the need to carefully select the protocols used for formation of multicomponent enzyme assemblies to ensure that the activities of each individual component are retained.

**Other Abiotic Scaffolds.** *Carbon Nanotubes.* Single-walled carbon nanotubes (SWNTs) and multiwalled carbon nanotubes (MWNTs) rose to prominence as nanomaterials with remarkable electronic and tensile properties.[396] For biological applications, carbon nanotubes offer a platform for biomolecule assembly, as many such molecules readily adsorb on these structures passively or through common chemical cross-linking methods such as carbodiimide chemistry.[326,328] Additionally, unlike many other NP systems, the intrinsic length of carbon nanotubes enables purification and recovery from reactions using filtration rather than high-speed centrifugation.[327] Finally, carbon nanotubes also have inducible ionic charges that can alter the enzyme activity under some conditions, be integrated into sensor platforms, or used to induce secondary processes.[328] To date, SWNTs and MWNTs have been used in a variety of enzyme-based applications and shown significant potential for subsequent studies in cascade enzyme reactions. Though not an examination of shuttling, Zhang *et al.* paired tyrosinase and $\beta$-Gal in a carbon-nanotube-based biosensor.[397] This paired enzyme system was able to achieve pg/mL levels of detection and outperformed single-enzyme sensors by 44−80% in experimental studies. In addition to biosensor development, the unique conductive properties of carbon nanotubes offer great potential for fuel cell design. Exploiting the glycolytic enzymes invertase and glucose dehydrogenase, researchers from Auburn University described a stacked carbon nanotube fuel cell.[398] They used sucrose as a starting substrate and harnessed the free electrons from the oxidation of NADH to $NAD^+$ by glucose dehydrogenase. The enhancements to enzyme catalysis and its translation into these applications to power generation and biosensor improvements provide a foundation for the use of SWNTs and MWNTs in increasingly complex enzyme systems.

*Hydrogels.* Hydrogels are cross-linked polymer structures that are able to swell and retain a large amount of water or biological fluid.[399] Hydrogel materials can be assembled from a variety of monomers, allowing them to be developed for use as food additives, as tools for tissue engineering, for encapsulation of biomaterials, and so on.[399,400] As has been discussed throughout this section and others, immobilization strategies such as carbodiimide chemistry or random attachment strategies can have a detrimental impact on enzyme activity. In contrast, hydrogels utilize a passive encapsulation strategy in which aqueous solutions containing biomolecules and reaction buffers are sequestered within the hydrogel itself. Hydrogel encapsulation has been shown for a number of single enzymes as well as systems of increasing complexity. In a recent publication, Wu *et al.* assembled an enzyme cascade including superoxide dismutase and chloroperoxidase with the intention of forming reactive oxygen species to mimic the cellular lysosome.[401] Here a magnetic NP served as a core structure onto which the enzymes were assembled within a hydrogel shell. These materials were able to induce a cytotoxic effect in tumor cell lines. While hydrogel materials are able to encapsulate buffers and solutions favorable to enzyme activity, they are not without their limitations. In a comprehensive study of four enzymes independently encapsulated with hydrogel materials, Schmieg *et al.* showed that in many instances the unique environment within these materials can diminish the relative enzyme activity as a result of diffusional limitations.[402] As with many abiotic scaffolds, the unique properties of hydrogels make them viable candidates and one of many scaffolds for future studies of multicomponent enzyme systems.

## OUTLOOK AND PERSPECTIVE

In this review, we have strived to guide the reader through a background on the benefits of artificial multienzyme scaffolds, the underlying mechanisms of those benefits (especially substrate channeling), the chemistries involved in conjugating enzymes to different scaffolding (nano)materials, and importantly, the biotic and abiotic scaffolds themselves. We have provided illustrative examples of advancements in scaffolds mostly within the last ∼5 years, which emphasizes the rapid and continuing expansion of this field. From these examples it is also clear that many of the systems can access and benefit from channeling phenomena, but what is not transparent is how much of the full potential benefits from channeling have been achieved in a given system, and much remains to be accomplished here as the systems themselves mature and the methods for analyzing them become more sophisticated.[403]

Key to the growth of this research field will be continued and sustained development of at least three directly correlated areas. First is that of the scaffolding materials themselves. These must provide for control over relative size, shape, availability for controlled bioconjugation, and of course the many other physicochemical characteristics that can aid in the final application; the latter can include, for example, biocompatibility, amenability to chemical modification, colloidal stability, and solubility. In terms of designer control over just the scaffold architectures that can be achieved along with control over 3D placement of different enzymes on those structures, it appears that DNA nanotechnology has the most to offer. This comes at the cost of requiring very specialized knowledge to design and


DOI: 10.1021/acscatal.9b02413
*ACS Catal.* 2019, 9, 10812−10869

assemble the structures along with chemically modifying the enzymes (site-specifically) to display the requisite complementary DNA for attachment. How these structures will accommodate enzymes that are dimeric or multimeric is not readily apparent, as these enzymes may display multiple DNA linkages on each monomer. It is also hard to anticipate what new material may be tested as an enzyme scaffold next, but likely candidates include many of the new macromolecular protein cages, compartments, and vaultlike subcellular structures that are continuously being discovered and described, as these provide the most biocompatibility and can be sourced from cellular production rather than chemical synthesis.[404] A second key area that still needs much development is that of bioconjugation for site-specific attachment of the enzymes to any given scaffold material. This includes both improving upon current methods and discovering new, broadly applicable means to immobilize enzymes on biotic and abiotic scaffolds. Rather than relying on a chemical reaction between chemoselective bio-orthogonal groups introduced onto the enzymes and the scaffolds, the cohesin−dockerin family of binding interactions along with systems such as SpyTag−SpyCatcher appear to have much to offer in this regard, as each participant can be coexpressed as a fusion with the enzyme and the cognate protein scaffold of choice, respectively. The need here is to develop further unique binding pairs that retain or display very high binding/interaction affinities to allow for sequential placement of a large number of enzymes with varying stoichiometry as desired. Lastly, far more diverse enzymes (especially beyond GOx−HRP) need to be incorporated in these systems to provide a sufficient body of work that can help provide enough background and viable examples for others who wish to venture into this area. Perhaps what could help most in this regard is some type of industrial adoption of prototypical systems, as these will demonstrate and verify the use of robust and rigorous approaches that others can adopt.

In a general sense, much of the work to date on enzyme scaffolding has focused on single-enzyme systems. While this certainly will continue to be, and should continue to be, an area of focus, we hope the examples highlighted in this review foreshadow to some extent the broad potential application space for scaffolded multienzyme cascades. The biggest beneficiary of the development of these materials will be synthetic biology in the form of true cell-free minimalist systems. There is also no reason why such scaffolded multienzyme systems cannot incorporate both bacterial and more complex eukaryotic enzymes to help expand the available chemical and biosynthetic space. Similarly, there is strong potential for arranging enzymes to achieve particularly challenging conversions involving the preference of an isomer and the like. What is also not appreciated is that many enzymatic pathways can function in a bidirectional manner, as exemplified by the glycolytic enzymes, which can function catabolically in converting glucose to lactate and also in the reverse direction as part of gluconeogenesis. This could allow systems to work in either direction as needed and as driven thermodynamically in a manner analogous to the $CO_2$ to methanol and converse examples mentioned above.[116,118,343] Attaching the enzymes to magnetically susceptible scaffolds in a manner similar to that of Yang *et al.*,[349] who immobilized glucoamylase and $\alpha$-amylase on ferric oxide powders in chitosan beads, is also quite intriguing. This approach could potentially allow the enzymes to overcome some diffusion limitations or better exploit channeling phenomena by removing back-inhibiting products in the right configuration. Lastly, these systems do not have to be used solely for synthetic purposes and may be amenable to application as "smart" sensors utilizing enzyme logic for diagnostics.[405,406]

In order to improve upon current scaffolding systems and design novel systems, continued examination of the underlying mechanisms for the benefits of these systems will be crucial. This will require harnessing theoretical platforms as well as accessible analytical methods to monitor improvements in multienzyme activity and stability plus the geometry of the entire scaffolded system (for details, see Substrate Channeling). Accumulation of well-analyzed examples of successful (and unsuccessful) scaffolding systems for disparate multienzyme cascades will build a foundation for future designs. What are the priorities when designing a *de novo* scaffold for a given enzyme cascade: Minimizing the distance between enzyme pairs? Maximizing pH tuning of different scaffold regions to match enzyme preference? Facilitating "superclustering"/aggregation of scaffolds at an ideal size? Maintaining enzyme stability at low concentrations? Recovering enzymes for reuse? Dynamic control of enzymes in the cascade? Ensuring the correct enzyme:scaffold ratios? Ensuring sequentiality if needed? To some degree, all this will depend on the given cascade, but are there any general design rules that can be illuminated? The more accessible techniques are to interrogate different systems theoretically and analytically, the more laboratories will be able to acquire the data needed to address these aspects. One probable marker by which to measure successful development will be if such systems are adopted commercially for sensing or industrially for biosynthesis. In accomplishing this they will in essence have crossed the so-called "Valley of Death" and successfully transitioned from an interesting research area to a viable technology.

## AUTHOR INFORMATION


### Corresponding Authors

*E-mail: Gregory.ellis@nrl.navy.mil.
*E-mail: Igor.medintz@nrl.navy.mil.

### ORCID

Scott A. Walper: 0000-0002-9436-3456
Igor L. Medintz: 0000-0002-8902-4687


### Notes

The authors declare no competing financial interest.

## ACKNOWLEDGMENTS

The authors acknowledge support from ONR, NRL, the NRL Nanoscience Institute, and the National Institute of Food and Agriculture, U.S. Department of Agriculture, under Award 11901762. W.P.K. acknowledges a National Research Council postdoctoral fellowship at NRL. G.A.E. acknowledges additional support in part by the Assistant Secretary of Defense for Research and Engineering (ASD(R&E)) through the Applied Research for the Advancement of S&T Priorities Synthetic Biology for Military Environments Program.

## ABBREVIATIONS: GENERAL

2D/3D = two-dimensional/three-dimensional
ABTS = 2,2′-azinobis(3-ethylbenzothiazoline-6-sulfonic acid)
AuNP = gold nanoparticle
$c$ = concentration at a radial distance



DOI: 10.1021/acscatal.9b02413
*ACS Catal.* 2019, 9, 10812−10869

C = molar concentration
CaaHc = copper-assisted azide−alkyne Huisgen cycloaddition (*i.e.*, click chemistry)
CatIB = catalytic inclusion body
CBD = cellulose-binding domain
CBM = carbohydrate-binding module
CLEA = cross-linked enzyme aggregate
CMC = carboxymethyl cellulose
Combi-CLEA = cross-linked enzyme aggregate composed of different enzymes
CRET = chemiluminescence resonance energy transfer
$d$, $d_{e-e}$ = distance between enzymes
$D$ = diffusion coefficient
DLS = dynamic light scattering
DNA = deoxyribonucleic acid
DTPC = DNA-templated protein conjugation
DX = double crossover (DNA tile)
DYSD; DYSD CD = direct yeast surface display; specifically codisplay
EDTA = ethylenediaminetetraacetic acid
EG-$(NHS)_2$ = ethylene glycol bis(succinimidyl succinate)
$E_n$ = enzyme $n$
FACS = fluorescence-activated cell sorting
$f_{direct}$ = fraction of the intermediate directly channeled
FPLC = fast-protein liquid chromatography
GPI = glycosylphosphatidylinositol
His = histidine
I = intermediate
IB = inclusion body
INP = ice nucleation protein
$k$ = turnover frequency
$k_{2,scaf}/k_{2,free}$ = ratio of the benefit of the scaffold
$k_{cat}$ = turnover number
$K_D$ = dissociation constant
$K_M$ = Michaelis constant
LD = lipid droplet
MEC = multienzyme polymer conjugate
MWNT = multiwalled carbon nanotube
MOF = metal−organic framework
$NAD^+$ = nicotinamide adenine dinucleotide, oxidized
NADH = nicotinamide adenine dinucleotide, reduced
NE = not evaluated
NHS = *N*-hydroxysuccinimide
NP = nanoparticle
NRPS = nonribosomal peptide synthetase
NTA; Ni-NTA = nitrilotriacetic acid; $Ni^{2+}$-nitriloacetic acid
$OD_{600}$ = optical density at 600 nm
OMV = outer membrane vesicle
P = product
PAGE = polyacrylamide gel electrophoresis
PASC = phosphoric acid-swollen cellulose
PCI = protein crystalline inclusion
PEG = poly(ethylene glycol)
PHB = polyhydroxybutyrate
PKS = polyketide synthase
QD = quantum dot
$r$ = radial distance
$R$ = rate of off-target reaction
RNA = ribonucleic acid
S = substrate
SD = standard deviation
SDS = sodium dodecyl sulfate
SEDC = single enzyme display consortium
SLS = synthetic lipid-containing scaffold
SPDP = succinimidyl 3-(2-pyridyldithio)propionate
ssDNA = single-stranded DNA
sSMCC = sulfosuccinimidyl 4-(*N*-maleimidomethyl)-cyclohexane-1-carboxylate
$(SSSSG)_4$ = $(serine)_4$-glycine linker
SWNT = single-walled carbon nanotube
$t$ = time
$\tau$ = time between reaction events $(=1/k)$
$\tau_{ch}$ = channeling time
TMB = 3,3′,5,5′-tetramethylbenzidine
tRNA = transfer ribonucleic acid
TX-TL = transcription−translation cell-free system
UDP-Glc = uridine diphosphoglucose
$v$ = velocity
$V$ = volume
$V_{max}$ = maximum velocity (per Michaelis−Menten enzyme kinetics)

## ABBREVIATIONS: PROTEINS AND ENZYMES

AA-ADH = broad-specificity $NAD^+$-dependent alcohol dehydrogenase Prelog
acnA, ACN = aconitase
Acs1 = enzyme that converts acetate into acetyl-CoA from *S. cerevisiae*
ADH = alcohol dehydrogenase [from *B. stearothermophilus* in some references in the text]
AdhE2 = butylaldehyde dehydrogenase/butanol dehydrogenase from *C. acetobutylicum*
AGA1, AGA2; Aga1p, Aga2p = *S. cerevisiae* $\alpha$-agglutinin (subunits)
tAga1p = N-terminus of Aga1p that binds Aga2p
Ald6 = aldehyde dehydrogenase from *S. cerevisiae*
Atf1 = alcohol-*O*-acetyltransferase from *S. cerevisiae*
AtoB = acetoacetyl-CoA thiolase from *E. coli*
$\beta$-Gal = $\beta$-galactosidase
BGL = $\beta$-glucosidase
BSA = bovine serum albumin
cadA, CAD = *cis*-aconitate decarboxylase
CBH = cellobiohydrolase
Cel5A = endoglucanase from *C. cellulolyticum*
Cel9E = exoglucanase from *C. cellulolyticum*
Ch1-AmDH = chimeric NADH-dependent amine dehydrogenase engineered for stability
CohI1, CohI-2, CohI-3 = type I cohesins
Crt = crotonase from *C. acetobutylicum*
*Ct*-aCelA = *C. thermophilum* endonuclease fused with Aga2p
$D_1$-$C_1$, $D_2$-$C_2$ = dockerin−cohesin domains from *C. perfringens* and *C. thermocellum*, respectively
DocII = C-terminal type II dockerin
EG = endoglucanase
ER/K = a 5 nm rigid $\alpha$-helical linker
Eut; EutM = ethanolamine utilization; Eut protein of *S. enterica*
FALDH = formaldehyde dehydrogenase [from *P. putida* in some references in the text]
FDH = formate dehydrogenase [from *S. cerevisiae* in some references in the text]
FMO = enzyme for indigo production
G6PDH = glucose-6-phosphate dehydrogenase
GADPH = glyceraldehyde-3-phosphate dehydrogenase
GBD = GTPase binding domain from the actin polymerization switch N-WASP


DOI: 10.1021/acscatal.9b02413
*ACS Catal.* 2019, 9, 10812−10869

GFP = green fluorescent protein
GPI = glucose-6-phosphate isomerase
gltA, GA = citrate synthase
GluDH = glutamate dehydrogenase from bovine liver cells
GOx = glucose oxidase
Hbd = 3-hydroxybutyl-CoA dehydrogenase (Hbd) from *C. acetobutylicum*
HK = hexokinase
HMGS = hydroxyl-methylglutaryl-CoA synthase from *S. cerevisiae*
HMGR = hydroxyl-methylglutaryl-CoA reductase from *S. cerevisiae*
Hps = 3-hexulose-6-phosphate synthase
Hps:Phi = fusion of 3-hexulose-6-phosphate synthase with 6-phospho-3-hexulose isomerase
HRP = horseradish peroxidase
LacZ = a $\beta$-galactosidase
LDH = lactate dehydrogenase
Luc = luciferase
MDH = malic dehydrogenase
MGA Mdh 3 = methanol dehydrogenase
NFOR = oxidoreductase
OAD = oxaloacetate decarboxylase
Ole = oleosin from *Z. mays*
P9 and P12 = bacteriophage proteins required for forming lipid/protein particles: a major membrane protein and a nonstructural protein, respectively
PgsA = anchor protein
PgsBCA = poly-$\gamma$-glutamate synthetase complex from *B. subtilis*
PDZ (domain) = PSD95/DlgA/Zo-1 (domain) from the adaptor protein syntrophin
Phi = 6-phospho-3-hexuloseisomerase
PykA = pyruvate kinase
Sed1 = Sed1 anchoring domain
*Sf*-aBGL1 = *S. fibuligera* $\beta$-glucosidase fused onto Aga2p
SH3 = Src homology 3 domain from the adaptor protein CRK
SH3 ligand = ligand for Src homology 3 domain, PPPALPPKRRR
SP = signal peptide
*Te-a*CBH1 = *T. emersonii* exoglucanase fused with Aga2p
Ter = butyryl-CoA dehydrogenase from *T. denticola*
TnaA = enzyme for indigo production
VioA–E = five enzymes in the violacein biosynthetic pathway
XDH = xylitol dehydrogenase
XR = xylose reductase
$Z_{Taq}$:anti-$Z_{Taq}$, $Z_{IgA}$:anti-$Z_{IgA}$, $Z_{HER2}$:anti-$Z_{HER2}$, and $Z_{WT}$:anti-$Z_{WT}$ = affibody pairs

## REFERENCES


(1) Bornscheuer, U. T.; Huisman, G. W.; Kazlauskas, R. J.; Lutz, S.; Moore, J. C.; Robins, K. Engineering the Third Wave of Biocatalysis. *Nature* **2012**, *485*, 185–194.
(2) Faber, K. *Biotransformations in Organic Chemistry*; Springer: Berlin, 2011.
(3) Richter, M.; Schulenburg, C.; Jankowska, D.; Heck, T.; Faccio, G. Novel Materials through Nature's Catalysts. *Mater. Mater. Today* **2015**, *18*, 459–467.
(4) Schmid, A.; Dordick, J. S.; Hauer, B.; Kiener, A.; Wubbolts, M.; Witholt, B. Industrial Biocatalysis Today and Tomorrow. *Nature* **2001**, *409*, 258–268.
(5) Walper, S. A.; Lasarte Aragonés, G.; Sapsford, K. E.; Brown, C. W., 3rd; Rowland, C. E.; Breger, J. C.; Medintz, I. L. Detecting Biothreat Agents: From Current Diagnostics to Developing Sensor Technologies. *ACS Sens* **2018**, *3*, 1894–2024.
(6) Chen, R.; Chen, Q.; Kim, H.; Siu, K. H.; Sun, Q.; Tsai, S. L.; Chen, W. Biomolecular Scaffolds for Enhanced Signaling and Catalytic Efficiency. *Curr. Opin. Biotechnol.* **2014**, *28*, 59–68.
(7) Ricca, E.; Brucher, B.; Schrittwieser, J. H. Multi-Enzymatic Cascade Reactions: Overview and Perspectives. *Adv. Synth. Catal.* **2011**, *353*, 2239–2262.
(8) Schoffelen, S.; van Hest, J. C. Chemical Approaches for the Construction of Multi-Enzyme Reaction Systems. *Curr. Opin. Struct. Biol.* **2013**, *23*, 613–621.
(9) Abernathy, M. H.; He, L.; Tang, Y. J. Channeling in Native Microbial Pathways: Implications and Challenges for Metabolic Engineering. *Biotechnol. Adv.* **2017**, *35*, 805–814.
(10) Bulutoglu, B.; Garcia, K. E.; Wu, F.; Minteer, S. D.; Banta, S. Direct Evidence for Metabolon Formation and Substrate Channeling in Recombinant TCA Cycle Enzymes. *ACS Chem. Biol.* **2016**, *11*, 2847–2853.
(11) Kuchler, A.; Yoshimoto, M.; Luginbuhl, S.; Mavelli, F.; Walde, P. Enzymatic Reactions in Confined Environments. *Nat. Nanotechnol.* **2016**, *11*, 409–420.
(12) Rabe, K. S.; Muller, J.; Skoupi, M.; Niemeyer, C. M. Cascades in Compartments: En Route to Machine-Assisted Biotechnology. *Angew. Chem., Int. Ed.* **2017**, *56*, 13574–13589.
(13) Srere, P. A. The Metabolon. *Trends Biochem. Sci.* **1985**, *10*, 109–110.
(14) Sweetlove, L. J.; Fernie, A. R. The Role of Dynamic Enzyme Assemblies and Substrate Channelling in Metabolic Regulation. *Nat. Commun.* **2018**, *9*, 2136.
(15) Vance, S.; Tkachenko, O.; Thomas, B.; Bassuni, M.; Hong, H.; Nietlispach, D.; Broadhurst, W. Sticky Swinging Arm Dynamics: Studies of an Acyl Carrier Protein Domain from the Mycolactone Polyketide Synthase. *Biochem. J.* **2016**, *473*, 1097–1110.
(16) Chen, X.; Gao, C.; Guo, L.; Hu, G.; Luo, Q.; Liu, J.; Nielsen, J.; Chen, J.; Liu, L. DCEO Biotechnology: Tools to Design, Construct, Evaluate, and Optimize the Metabolic Pathway for Biosynthesis of Chemicals. *Chem. Rev.* **2018**, *118*, 4–72.
(17) Dueber, J. E.; Wu, G. C.; Malmirchegini, G. R.; Moon, T. S.; Petzold, C. J.; Ullal, A. V.; Prather, K. L.; Keasling, J. D. Synthetic Protein Scaffolds Provide Modular Control over Metabolic Flux. *Nat. Biotechnol.* **2009**, *27*, 753–759.
(18) Kizer, L.; Pitera, D. J.; Pfleger, B. F.; Keasling, J. D. Application of Functional Genomics to Pathway Optimization for Increased Isoprenoid Production. *Appl. Environ. Microbiol.* **2008**, *74*, 3229–3241.
(19) Ro, D. K.; Paradise, E. M.; Ouellet, M.; Fisher, K. J.; Newman, K. L.; Ndungu, J. M.; Ho, K. A.; Eachus, R. A.; Ham, T. S.; Kirby, J.; Chang, M. C.; Withers, S. T.; Shiba, Y.; Sarpong, R.; Keasling, J. D. Production of the Antimalarial Drug Precursor Artemisinic Acid in Engineered Yeast. *Nature* **2006**, *440*, 940–943.
(20) Kwon, Y. C.; Jewett, M. C. High-Throughput Preparation Methods of Crude Extract for Robust Cell-Free Protein Synthesis. *Sci. Rep.* **2015**, *5*, 8663.
(21) Shimizu, Y.; Inoue, A.; Tomari, Y.; Suzuki, T.; Yokogawa, T.; Nishikawa, K.; Ueda, T. Cell-Free Translation Reconstituted with Purified Components. *Nat. Biotechnol.* **2001**, *19*, 751–755.
(22) Opgenorth, P. H.; Korman, T. P.; Bowie, J. U. A Synthetic Biochemistry Molecular Purge Valve Module That Maintains Redox Balance. *Nat. Commun.* **2014**, *5*, 4113–4120.
(23) Dudley, Q. M.; Karim, A. S.; Jewett, M. C. Cell-Free Metabolic Engineering: Biomanufacturing Beyond the Cell. *Biotechnol. J.* **2015**, *10*, 69–82.
(24) Hwang, E. T.; Lee, S. Multienzymatic Cascade Reactions Via Enzyme Complex by Immobilization. *ACS Catal.* **2019**, *9*, 4402–4425.
(25) Sperl, J. M.; Sieber, V. Multienzyme Cascade Reactions—Status and Recent Advances. *ACS Catal.* **2018**, *8*, 2385–2396.



DOI: 10.1021/acscatal.9b02413
*ACS Catal.* 2019, 9, 10812–10869

(26) Zhang, Y.; Ge, J.; Liu, Z. Enhanced Activity of Immobilized or Chemically Modified Enzymes. *ACS Catal.* **2015**, *5*, 4503−4513.
(27) Berg, H. C. *Random Walks in Biology*; Princeton University Press: Princeton, NJ, 1983.
(28) Idan, O.; Hess, H. Origins of Activity Enhancement in Enzyme Cascades on Scaffolds. *ACS Nano* **2013**, *7*, 8658−8665.
(29) Idan, O.; Hess, H. Engineering Enzymatic Cascades on Nanoscale Scaffolds. *Curr. Opin. Biotechnol.* **2013**, *24*, 606−11.
(30) Ovádi, J. Physiological Significance of Metabolic Channeling. *J. Theor. Biol.* **1991**, *152*, 1−22.
(31) Spivey, H. O.; Ovádi, J. Substrate Channeling. *Methods* **1999**, *19*, 306−321.
(32) Wheeldon, I.; Minteer, S. D.; Banta, S.; Barton, S. C.; Atanassov, P.; Sigman, M. Substrate Channelling as an Approach to Cascade Reactions. *Nat. Chem.* **2016**, *8*, 299−309.
(33) Conrado, R. J.; Varner, J. D.; DeLisa, M. P. Engineering the Spatial Organization of Metabolic Enzymes: Mimicking Nature's Synergy. *Curr. Opin. Biotechnol.* **2008**, *19*, 492−499.
(34) Dunn, M. F.; Aguilar, V.; Brzović, P.; Drewe, W. F., Jr.; Houben, K. F.; Leja, C. A.; Roy, M. The Tryptophan Synthase Bienzyme Complex Transfers Indole between the $\alpha$- and B-Sites Via a 25−30 Å Long Tunnel. *Biochemistry* **1990**, *29*, 8598−8607.
(35) Hyde, C. C.; Ahmed, S. A.; Padlan, E. A.; Miles, E. W.; Davies, D. R. Three-Dimensional Structure of the Tryptophan Synthase $\alpha 2\beta 2$ Multienzyme Complex from *Salmonella typhimurium*. *J. Biol. Chem.* **1988**, *263*, 17857−17871.
(36) Fu, J.; Liu, M.; Liu, Y.; Woodbury, N. W.; Yan, H. Interenzyme Substrate Diffusion for an Enzyme Cascade Organized on Spatially Addressable DNA Nanostructures. *J. Am. Chem. Soc.* **2012**, *134*, 5516−5519.
(37) Sweetlove, L. J.; Fernie, A. R. The Spatial Organization of Metabolism within the Plant Cell. *Annu. Rev. Plant Biol.* **2013**, *64*, 723−746.
(38) Schumb, W. C.; Satterfield, C. N.; Wentworth, R. L. *Hydrogen Peroxide*; Reinhold Publishing Corporation: New York, 1955.
(39) Bar-Even, A.; Noor, E.; Savir, Y.; Liebermeister, W.; Davidi, D.; Tawfik, D. S.; Milo, R. The Moderately Efficient Enzyme: Evolutionary and Physicochemical Trends Shaping Enzyme Parameters. *Biochemistry* **2011**, *50*, 4402−4410.
(40) Zhang, Y.; Hess, H. Toward Rational Design of High-Efficiency Enzyme Cascades. *ACS Catal.* **2017**, *7*, 6018−6027.
(41) Erickson, H. P. Size and Shape of Protein Molecules at the Nanometer Level Determined by Sedimentation, Gel Filtration, and Electron Microscopy. *Biol. Proced. Online* **2009**, *11*, 32−51.
(42) Laberge, M.; Huang, Q.; Schweitzer-Stenner, R.; Fidy, J. The Endogenous Calcium Ions of Horseradish Peroxidase C Are Required to Maintain the Functional Nonplanarity of the Heme. *Biophys. J.* **2003**, *84*, 2542−2552.
(43) Kim, Y. E.; Hipp, M. S.; Bracher, A.; Hayer-Hartl, M.; Hartl, F. U. Molecular Chaperone Functions in Protein Folding and Proteostasis. *Annu. Rev. Biochem.* **2013**, *82*, 323−355.
(44) Bionumbers. https://bionumbers.hms.harvard.edu/search.aspx (accessed Aug 24, 2018).
(45) Maier, T.; Schmidt, A.; Güell, M.; Kühner, S.; Gavin, A.-C.; Aebersold, R.; Serrano, L. Quantification of mRNA and Protein and Integration with Protein Turnover in a Bacterium. *Mol. Syst. Biol.* **2011**, *7*, 511.
(46) Milo, R.; Jorgensen, P.; Moran, U.; Weber, G.; Springer, M. Bionumbers–the Database of Key Numbers in Molecular and Cell Biology. *Nucleic Acids Res.* **2010**, *38*, D750−D753.
(47) Jia, B.; Jeon, C. O. High-Throughput Recombinant Protein Expression in *Escherichia coli*: Current Status and Future Perspectives. *Open Biol.* **2016**, *6*, 160196.
(48) Idan, O.; Hess, H. Diffusive Transport Phenomena in Artificial Enzyme Cascades on Scaffolds. *Nat. Nanotechnol.* **2012**, *7*, 769−770.
(49) Zhang, Y.; Tsitkov, S.; Hess, H. Proximity Does Not Contribute to Activity Enhancement in the Glucose Oxidase−Horseradish Peroxidase Cascade. *Nat. Commun.* **2016**, *7*, 13982.
(50) Kubitschek, H. E.; Friske, J. A. Determination of Bacterial Cell Volume with the Coulter Counter. *J. Bacteriol.* **1986**, *168*, 1466−1467.
(51) Wang, L.; Zhou, Y. J.; Ji, D.; Zhao, Z. K. An Accurate Method for Estimation of the Intracellular Aqueous Volume of *Escherichia coli* Cells. *J. Microbiol. Methods* **2013**, *93*, 73−76.
(52) Lin, J.-L.; Palomec, L.; Wheeldon, I. Design and Analysis of Enhanced Catalysis in Scaffolded Multienzyme Cascade Reactions. *ACS Catal.* **2014**, *4*, 505−511.
(53) Buchner, A.; Tostevin, F.; Gerland, U. Clustering and Optimal Arrangement of Enzymes in Reaction-Diffusion Systems. *Phys. Rev. Lett.* **2013**, *110*, 208104.
(54) Poshyvailo, L.; von Lieres, E.; Kondrat, S. Does Metabolite Channeling Accelerate Enzyme-Catalyzed Cascade Reactions? *PLoS One* **2017**, *12*, e0172673.
(55) Huang, X.; Holden, H. M.; Raushel, F. M. Channeling of Substrates and Intermediates in Enzyme-Catalyzed Reactions. *Annu. Rev. Biochem.* **2001**, *70*, 149−180.
(56) Wilner, O. I.; Weizmann, Y.; Gill, R.; Lioubashevski, O.; Freeman, R.; Willner, I. Enzyme Cascades Activated on Topologically Programmed DNA Scaffolds. *Nat. Nanotechnol.* **2009**, *4*, 249−254.
(57) Lin, J.-L.; Wheeldon, I. Kinetic Enhancements in DNA−Enzyme Nanostructures Mimic the Sabatier Principle. *ACS Catal.* **2013**, *3*, 560−564.
(58) Knözinger, H.; Kochloefl, K. Heterogeneous Catalysis and Solid Catalysts. In *Ullmann's Encyclopedia of Industrial Chemistry*; Wiley-VCH: Weinheim, Germany, 2005.
(59) Delebecque, C. J.; Lindner, A. B.; Silver, P. A.; Aldaye, F. A. Organization of Intracellular Reactions with Rationally Designed RNA Assemblies. *Science* **2011**, *333*, 470−474.
(60) Castellana, M.; Wilson, M. Z.; Xu, Y.; Joshi, P.; Cristea, I. M.; Rabinowitz, J. D.; Gitai, Z.; Wingreen, N. S. Enzyme Clustering Accelerates Processing of Intermediates through Metabolic Channeling. *Nat. Biotechnol.* **2014**, *32*, 1011−1018.
(61) Vranish, J. N.; Ancona, M. G.; Oh, E.; Susumu, K.; Lasarte Aragonés, G.; Breger, J. C.; Walper, S. A.; Medintz, I. L. Enhancing Coupled Enzymatic Activity by Colocalization on Nanoparticle Surfaces: Kinetic Evidence for Directed Channeling of Intermediates. *ACS Nano* **2018**, *12*, 7911−7926.
(62) Liu, Y.; Hickey, D. P.; Guo, J.-Y.; Earl, E.; Abdellaoui, S.; Milton, R. D.; Sigman, M. S.; Minteer, S. D.; Calabrese Barton, S. Substrate Channeling in an Artificial Metabolon: A Molecular Dynamics Blueprint for an Experimental Peptide Bridge. *ACS Catal.* **2017**, *7*, 2486−2493.
(63) Vranish, J. N.; Ancona, M. G.; Oh, E.; Susumu, K.; Medintz, I. L. Enhancing Coupled Enzymatic Activity by Conjugating One Enzyme to a Nanoparticle. *Nanoscale* **2017**, *9*, 5172−5187.
(64) Zhao, Z.; Fu, J.; Dhakal, S.; Johnson-Buck, A.; Liu, M.; Zhang, T.; Woodbury, N. W.; Liu, Y.; Walter, N. G.; Yan, H. Nanocaged Enzymes with Enhanced Catalytic Activity and Increased Stability against Protease Digestion. *Nat. Commun.* **2016**, *7*, 10619.
(65) Haimovitz, R.; Barak, Y.; Morag, E.; Voronov-Goldman, M.; Shoham, Y.; Lamed, R.; Bayer, E. A. Cohesin-Dockerin Microarray: Diverse Specificities between Two Complementary Families of Interacting Protein Modules. *Proteomics* **2008**, *8*, 968−979.
(66) Pagès, S.; Bélaïch, A.; Bélaïch, J.-P.; Morag, E.; Lamed, R.; Shoham, Y.; Bayer, E. A. Species-Specificity of the Cohesin-Dockerin Interaction between *Clostridium thermocellum* and *Clostridium cellulolyticum*: Prediction of Specificity Determinants of the Dockerin Domain. *Proteins: Struct., Funct., Genet.* **1997**, *29*, 517−527.
(67) Pinheiro, A. V.; Han, D.; Shih, W. M.; Yan, H. Challenges and Opportunities for Structural DNA Nanotechnology. *Nat. Nanotechnol.* **2011**, *6*, 763−772.
(68) Tsai, S. L.; Oh, J.; Singh, S.; Chen, R.; Chen, W. Functional Assembly of Minicellulosomes on the *Saccharomyces cerevisiae* Cell Surface for Cellulose Hydrolysis and Ethanol Production. *Appl. Environ. Microbiol.* **2009**, *75*, 6087−6093.
(69) Wilner, O. I.; Shimron, S.; Weizmann, Y.; Wang, Z.-G.; Willner, I. Self-Assembly of Enzymes on DNA Scaffolds: En Route to


DOI: 10.1021/acscatal.9b02413
*ACS Catal.* 2019, 9, 10812−10869

Biocatalytic Cascades and the Synthesis of Metallic Nanowires. *Nano Lett.* **2009**, *9*, 2040−2043.
(70) Myung, S.; You, C.; Zhang, Y. H. P. Recyclable Cellulose-Containing Magnetic Nanoparticles: Immobilization of Cellulose-Binding Module-Tagged Proteins and a Synthetic Metabolon Featuring Substrate Channeling. *J. Mater. Chem. B* **2013**, *1*, 4419−4427.
(71) Goldstein, D. E.; Little, R. R.; Lorenz, R. A.; Malone, J. I.; Nathan, D.; Peterson, C. M.; Sacks, D. B. Tests of Glycemia in Diabetes. *Diabetes Care* **2004**, *27*, 1761−1773.
(72) Müller, J.; Niemeyer, C. M. DNA-Directed Assembly of Artificial Multienzyme Complexes. *Biochem. Biophys. Res. Commun.* **2008**, *377*, 62−67.
(73) Nguyen, L. T.; Yang, K. L. Combined Cross-Linked Enzyme Aggregates of Horseradish Peroxidase and Glucose Oxidase for Catalyzing Cascade Chemical Reactions. *Enzyme Microb. Technol.* **2017**, *100*, 52−59.
(74) Gao, Y.; Roberts, C. C.; Zhu, J.; Lin, J.-L.; Chang, C.-e. A.; Wheeldon, I. Tuning Enzyme Kinetics through Designed Intermolecular Interactions Far from the Active Site. *ACS Catal.* **2015**, *5*, 2149−2153.
(75) Pal, S. K.; Peon, J.; Zewail, A. H. Biological Water at the Protein Surface: Dynamical Solvation Probed Directly with Femtosecond Resolution. *Proc. Natl. Acad. Sci. U. S. A.* **2002**, *99*, 1763−1768.
(76) Pal, S. K.; Zhao, L.; Zewail, A. H. Water at DNA Surfaces: Ultrafast Dynamics in Minor Groove Recognition. *Proc. Natl. Acad. Sci. U. S. A.* **2003**, *100*, 8113−8118.
(77) Alves, N. J.; Turner, K. B.; Medintz, I. L.; Walper, S. A. Protecting Enzymatic Function through Directed Packaging into Bacterial Outer Membrane Vesicles. *Sci. Rep.* **2016**, *6*, 24866.
(78) Xin, L.; Zhou, C.; Yang, Z.; Liu, D. Regulation of an Enzyme Cascade Reaction by a DNA Machine. *Small* **2013**, *9*, 3088−3091.
(79) Linko, V.; Eerikäinen, M.; Kostiainen, M. A. A Modular DNA Origami-Based Enzyme Cascade Nanoreactor. *Chem. Commun.* **2015**, *51*, 5351−5354.
(80) Zhou, L.; Liu, Y.; Shi, H.; Yang, X.; Huang, J.; Liu, S.; Chen, Q.; Liu, J.; Wang, K. Flexible Assembly of Cascade Enzyme on DNA Triangle Prism Nanostructure for Controlled Biomimetic Generation of Nitric Oxide. *ChemBioChem* **2018**, *19*, 2099−2106.
(81) Vogele, K.; List, J.; Simmel, F. C.; Pirzer, T. Enhanced Efficiency of an Enzyme Cascade on DNA-Activated Silica-Surfaces. *Langmuir* **2018**, *34*, 14780−14786.
(82) Freeman, R.; Sharon, E.; Tel-Vered, R.; Willner, I. Supramolecular Cocaine-Aptamer Complexes Activate Biocatalytic Cascades. *J. Am. Chem. Soc.* **2009**, *131*, 5028−5029.
(83) Wang, Z.-G.; Wilner, O. I.; Willner, I. Self-Assembly of Aptamer-Circular DNA Nanostructures for Controlled Biocatalysis. *Nano Lett.* **2009**, *9*, 4098−4102.
(84) You, M.; Wang, R.-W.; Zhang, X.; Chen, Y.; Wang, K.; Peng, L.; Tan, W. Photon-Regulated DNA-Enzymatic Nanostructures by Molecular Assembly. *ACS Nano* **2011**, *5*, 10090−10095.
(85) Freeman, R.; Sharon, E.; Teller, C.; Willner, I. Control of Biocatalytic Transformations by Programmed DNA Assemblies. *Chem. - Eur. J.* **2010**, *16*, 3690−3698.
(86) Fu, Y.; Zeng, D.; Chao, J.; Jin, Y.; Zhang, Z.; Liu, H.; Li, D.; Ma, H.; Huang, Q.; Gothelf, K. V.; Fan, C. Single-Step Rapid Assembly of DNA Origami Nanostructures for Addressable Nanoscale Bioreactors. *J. Am. Chem. Soc.* **2013**, *135*, 696−702.
(87) Chen, W.-H.; Vázquez-González, M.; Zoabi, A.; Abu-Reziq, R.; Willner, I. Biocatalytic Cascades Driven by Enzymes Encapsulated in Metal−Organic Framework Nanoparticles. *Nat. Catal.* **2018**, *1*, 689−695.
(88) Rajendran, A.; Nakata, E.; Nakano, S.; Morii, T. Nucleic-Acid-Templated Enzyme Cascades. *ChemBioChem* **2017**, *18*, 696−716.
(89) Hermanson, G. T. *Bioconjugate Techniques*, 3rd ed.; Academic Press: San Diego, 2013.
(90) Medintz, I. Universal Tools for Biomolecular Attachment to Surfaces. *Nat. Mater.* **2006**, *5*, 842−842.
(91) Algar, W. R.; Prasuhn, D. E.; Stewart, M. H.; Jennings, T. L.; Blanco-Canosa, J. B.; Dawson, P. E.; Medintz, I. L. The Controlled Display of Biomolecules on Nanoparticles: A Challenge Suited to Bioorthogonal Chemistry. *Bioconjugate Chem.* **2011**, *22*, 825−858.
(92) Sapsford, K. E.; Algar, W. R.; Berti, L.; Gemmill, K. B.; Casey, B. J.; Oh, E.; Stewart, M. H.; Medintz, I. L. Functionalizing Nanoparticles with Biological Molecules: Developing Chemistries That Facilitate Nanotechnology. *Chem. Rev.* **2013**, *113*, 1904−2074.
(93) Algar, W. R.; Dawson, P. E.; Medintz, I. L. *Chemoselective and Bioorthogonal Ligation Reactions: Concepts and Applications*; Wiley-VCH: Weinheim, Germany, 2017.
(94) Boeneman Gemmill, K.; Deschamps, J. R.; Delehanty, J. B.; Susumu, K.; Stewart, M. H.; Glaven, R. H.; Anderson, G. P.; Goldman, E. R.; Huston, A. L.; Medintz, I. L. Optimizing Protein Coordination to Quantum Dots with Designer Peptidyl Linkers. *Bioconjugate Chem.* **2013**, *24*, 269−281.
(95) Jin, X.; Park, O.-J.; Hong, S. H. Incorporation of Non-Standard Amino Acids into Proteins: Challenges, Recent Achievements, and Emerging Applications. *Appl. Microbiol. Biotechnol.* **2019**, *103*, 2947−2958.
(96) Boeneman, K.; Deschamps, J. R.; Buckhout-White, S.; Prasuhn, D. E.; Blanco-Canosa, J. B.; Dawson, P. E.; Stewart, M. H.; Susumu, K.; Goldman, E. R.; Ancona, M.; Medintz, I. L. Quantum Dot DNA Bioconjugates: Attachment Chemistry Strongly Influences the Resulting Composite Architecture. *ACS Nano* **2010**, *4*, 7253−7266.
(97) Medintz, I. L.; Goldman, E. R.; Lassman, M. E.; Hayhurst, A.; Kusterbeck, A. W.; Deschamps, J. R. Self-Assembled TNT Biosensor Based on Modular Multifunctional Surface-Tethered Components. *Anal. Chem.* **2005**, *77*, 365−372.
(98) Brown, C. W., III; Samanta, A.; Díaz, S. A.; Buckhout-White, S.; Walper, S. A.; Goldman, E. R.; Medintz, I. L. Dendrimeric DNA Nanostructures as Scaffolds for Efficient Bidirectional BRET−FRET Cascades. *Adv. Opt. Mater.* **2017**, *5*, 1700181−1700193.
(99) Ding, S. W.; Cargill, A. A.; Medintz, I. L.; Claussen, J. C. Increasing the Activity of Immobilized Enzymes with Nanoparticle Conjugation. *Curr. Opin. Biotechnol.* **2015**, *34*, 242−250.
(100) Fu, J.; Yang, Y. R.; Johnson-Buck, A.; Liu, M.; Liu, Y.; Walter, N. G.; Woodbury, N. W.; Yan, H. Multi-enzyme Complexes on DNA Scaffolds Capable of Substrate Channelling with an Artificial Swinging Arm. *Nat. Nanotechnol.* **2014**, *9*, 531−531.
(101) Walper, S. A.; Turner, K. B.; Medintz, I. L. Enzymatic Bioconjugation of Nanoparticles: Developing Specificity and Control. *Curr. Opin. Biotechnol.* **2015**, *34*, 232−241.
(102) Chen, H.; Ullah, J.; Jia, J. Progress in *Bacillus subtilis* Spore Surface Display Technology Towards Environment, Vaccine Development, and Biocatalysis. *J. Mol. Microbiol. Biotechnol.* **2017**, *27*, 159−167.
(103) Iwanicki, A.; Piątek, I.; Stasiłojć, M.; Grela, A.; Łęga, T.; Obuchowski, M.; Hinc, K. A System of Vectors for *Bacillus subtilis* Spore Surface Display. *Microb. Cell Fact.* **2014**, *13*, 30.
(104) Bugada, L. F.; Smith, M. R.; Wen, F. Engineering Spatially Organized Multienzyme Assemblies for Complex Chemical Transformation. *ACS Catal.* **2018**, *8*, 7898−7906.
(105) Chen, Y. P.; Hwang, I. E.; Lin, C. J.; Wang, H. J.; Tseng, C. P. Enhancing the Stability of Xylanase from *Cellulomonas fimi* by Cell-Surface Display on *Escherichia coli*. *J. Appl. Microbiol.* **2012**, *112*, 455−463.
(106) Liu, Z.; Inokuma, K.; Ho, S. H.; den Haan, R.; van Zyl, W. H.; Hasunuma, T.; Kondo, A. Improvement of Ethanol Production from Crystalline Cellulose Via Optimizing Cellulase Ratios in Cellulolytic *Saccharomyces cerevisiae*. *Biotechnol. Bioeng.* **2017**, *114*, 1201−1207.
(107) Ryu, S.; Karim, M. N. A Whole Cell Biocatalyst for Cellulosic Ethanol Production from Dilute Acid-Pretreated Corn Stover Hydrolyzates. *Appl. Microbiol. Biotechnol.* **2011**, *91*, 529−542.
(108) Schüürmann, J.; Quehl, P.; Festel, G.; Jose, J. Bacterial Whole-Cell Biocatalysts by Surface Display of Enzymes: Toward Industrial Application. *Appl. Microbiol. Biotechnol.* **2014**, *98*, 8031−8046.


DOI: 10.1021/acscatal.9b02413
*ACS Catal.* 2019, 9, 10812−10869

(109) Su, G. D.; Zhang, X.; Lin, Y. Surface Display of Active Lipase in *Pichia pastoris* Using Sed1 as an Anchor Protein. *Biotechnol. Lett.* **2010**, *32*, 1131−1136.
(110) Tabañag, I. D. F.; Chu, I. M.; Wei, Y.-H.; Tsai, S.-L. The Role of Yeast-Surface-Display Techniques in Creating Biocatalysts for Consolidated Bioprocessing. *Catalysts* **2018**, *8*, 94−129.
(111) Ueda, M. Establishment of Cell Surface Engineering and Its Development. *Biosci., Biotechnol., Biochem.* **2016**, *80*, 1243−1253.
(112) Fan, L.-H.; Zhang, Z.-J.; Yu, X.-Y.; Xue, Y.-X.; Tan, T.-W. Self-Surface Assembly of Cellulosomes with Two Miniscaffoldins on *Saccharomyces cerevisiae* for Cellulosic Ethanol Production. *Proc. Natl. Acad. Sci. U. S. A.* **2012**, *109*, 13260−13265.
(113) Han, G. H.; Seong, W.; Fu, Y.; Yoon, P. K.; Kim, S. K.; Yeom, S. J.; Lee, D. H.; Lee, S. G. Leucine Zipper-Mediated Targeting of Multi-Enzyme Cascade Reactions to Inclusion Bodies in *Escherichia coli* for Enhanced Production of 1-Butanol. *Metab. Eng.* **2017**, *40*, 41−49.
(114) Jäger, V. D.; Lamm, R.; Kloß, R.; Kaganovitch, E.; Grünberger, A.; Pohl, M.; Büchs, J.; Jaeger, K. E.; Krauss, U. A Synthetic Reaction Cascade Implemented by Colocalization of Two Proteins within Catalytically Active Inclusion Bodies. *ACS Synth. Biol.* **2018**, *7*, 2282−2295.
(115) Liang, Y.; Si, T.; Ang, E. L.; Zhao, H. Engineered Pentafunctional Minicellulosome for Simultaneous Saccharification and Ethanol Fermentation in *Saccharomyces cerevisiae*. *Appl. Environ. Microbiol.* **2014**, *80*, 6677−6684.
(116) Liu, F.; Banta, S.; Chen, W. Functional Assembly of a Multi-Enzyme Methanol Oxidation Cascade on a Surface-Displayed Trifunctional Scaffold for Enhanced NADH Production. *Chem. Commun.* **2013**, *49*, 3766−3768.
(117) Park, M.; Sun, Q.; Liu, F.; DeLisa, M. P.; Chen, W. Positional Assembly of Enzymes on Bacterial Outer Membrane Vesicles for Cascade Reactions. *PLoS One* **2014**, *9*, e97103.
(118) Price, J. V.; Chen, L.; Whitaker, W. B.; Papoutsakis, E.; Chen, W. Scaffoldless Engineered Enzyme Assembly for Enhanced Methanol Utilization. *Proc. Natl. Acad. Sci. U. S. A.* **2016**, *113*, 12691−12696.
(119) Tang, H.; Wang, J.; Wang, S.; Shen, Y.; Petranovic, D.; Hou, J.; Bao, X. Efficient Yeast Surface-Display of Novel Complex Synthetic Cellulosomes. *Microb. Cell Fact.* **2018**, *17*, 122.
(120) Tippmann, S.; Anfelt, J.; David, F.; Rand, J. M.; Siewers, V.; Uhlen, M.; Nielsen, J.; Hudson, E. P. Affibody Scaffolds Improve Sesquiterpene Production in *Saccharomyces cerevisiae*. *ACS Synth. Biol.* **2017**, *6*, 19−28.
(121) Wang, Y.; Heermann, R.; Jung, K. CipA and CipB as Scaffolds to Organize Proteins into Crystalline Inclusions. *ACS Synth. Biol.* **2017**, *6*, 826−836.
(122) Yang, Z.; Wang, H.; Wang, Y.; Ren, Y.; Wei, D. Manufacturing Multienzymatic Complex Reactors in Vivo by Self-Assembly to Improve the Biosynthesis of Itaconic Acid in *Escherichia coli*. *ACS Synth. Biol.* **2018**, *7*, 1244−1250.
(123) Zhang, G.; Quin, M. B.; Schmidt-Dannert, C. Self-Assembling Protein Scaffold System for Easy *in Vitro* Coimmobilization of Biocatalytic Cascade Enzymes. *ACS Catal.* **2018**, *8*, 5611−5620.
(124) Lin, J. L.; Zhu, J.; Wheeldon, I. Synthetic Protein Scaffolds for Biosynthetic Pathway Colocalization on Lipid Droplet Membranes. *ACS Synth. Biol.* **2017**, *6*, 1534−1544.
(125) Myhrvold, C.; Polka, J. K.; Silver, P. A. Synthetic Lipid-Containing Scaffolds Enhance Production by Colocalizing Enzymes. *ACS Synth. Biol.* **2016**, *5*, 1396−1403.
(126) Brady, D.; Jordaan, J. Advances in Enzyme Immobilisation. *Biotechnol. Lett.* **2009**, *31*, 1639−1650.
(127) Sheldon, R. A. Characteristic Features and Biotechnological Applications of Cross-Linked Enzyme Aggregates (CLEAs). *Appl. Microbiol. Biotechnol.* **2011**, *92*, 467−477.
(128) Sheldon, R. A.; Schoevaart, R.; Van Langen, L. M. Cross-Linked Enzyme Aggregates (CLEAs): A Novel and Versatile Method for Enzyme Immobilization (a Review). *Biocatal. Biotransform.* **2005**, *23*, 141−147.
(129) Chiswell, D. J.; McCaffery, J. Phage Antibodies: Will New 'Coliclonal' Antibodies Replace Monoclonal Antibodies? *Trends Biotechnol.* **1992**, *10*, 80−84.
(130) Scott, J. K.; Smith, G. P. Searching for Peptide Ligands with an Epitope Library. *Science* **1990**, *249*, 386−390.
(131) Murai, T.; Ueda, M.; Shibasaki, Y.; Kamasawa, N.; Osumi, M.; Imanaka, T.; Tanaka, A. Development of an Arming Yeast Strain for Efficient Utilization of Starch by Co-Display of Sequential Amylolytic Enzymes on the Cell Surface. *Appl. Microbiol. Biotechnol.* **1999**, *51*, 65−70.
(132) Ueda, M.; Tanaka, A. Cell Surface Engineering of Yeast: Construction of Arming Yeast with Biocatalyst. *J. Biosci. Bioeng.* **2000**, *90*, 125−136.
(133) Adachi, T.; Ito, J.; Kawata, K.; Kaya, M.; Ishida, H.; Sahara, H.; Hata, Y.; Ogino, C.; Fukuda, H.; Kondo, A. Construction of an *Aspergillus oryzae* Cell-Surface Display System Using a Putative GPI-anchored Protein. *Appl. Microbiol. Biotechnol.* **2008**, *81*, 711−719.
(134) Georgiou, G.; Poetschke, H. L.; Stathopoulos, C.; Francisco, J. A. Practical Applications of Engineering Gram-Negative Bacterial Cell Surfaces. *Trends Biotechnol.* **1993**, *11*, 6−10.
(135) Georgiou, G.; Stathopoulos, C.; Daugherty, P. S.; Nayak, A. R.; Iverson, B. L.; Curtiss, R., III. III Display of Heterologous Proteins on the Surface of Microorganisms: From the Screening of Combinatorial Libraries to Live Recombinant Vaccines. *Nat. Biotechnol.* **1997**, *15*, 29−34.
(136) Little, M.; Fuchs, P.; Breitling, F.; Dübel, S. Bacterial Surface Presentation of Proteins and Peptides: An Alternative to Phage Technology? *Trends Biotechnol.* **1993**, *11*, 3−5.
(137) Tabuchi, S.; Ito, J.; Adachi, T.; Ishida, H.; Hata, Y.; Okazaki, F.; Tanaka, T.; Ogino, C.; Kondo, A. Display of Both N- and C-Terminal Target Fusion Proteins on the *Aspergillus oryzae* Cell Surface Using a Chitin-Binding Module. *Appl. Microbiol. Biotechnol.* **2010**, *87*, 1783−1789.
(138) Tanino, T.; Fukuda, H.; Kondo, A. Construction of a *Pichia pastoris* Cell-Surface Display System Using Flo1p Anchor System. *Biotechnol. Prog.* **2006**, *22*, 989−993.
(139) Wang, Q.; Li, L.; Chen, M.; Qi, Q.; Wang, P. G. Construction of a Novel System for Cell Surface Display of Heterologous Proteins on *Pichia pastoris*. *Biotechnol. Lett.* **2007**, *29*, 1561−1566.
(140) Wang, Q.; Li, L.; Chen, M.; Qi, Q.; Wang, P. G. Construction of a Novel *Pichia pastoris* Cell-Surface Display System Based on the Cell Wall Protein Pir1. *Curr. Microbiol.* **2008**, *56*, 352−357.
(141) Yuzbasheva, E. Y.; Yuzbashev, T. V.; Laptev, I. A.; Konstantinova, T. K.; Sineoky, S. P. Efficient Cell Surface Display of Lip2 Lipase Using C-Domains of Glycosylphosphatidylinositol-Anchored Cell Wall Proteins of *Yarrowia lipolytica*. *Appl. Microbiol. Biotechnol.* **2011**, *91*, 645−654.
(142) Saccharomyces Genome Database. http://www.yeastgenome.org (accessed Jan 31, 2018).
(143) Cherry, J. M.; Hong, E. L.; Amundsen, C.; Balakrishnan, R.; Binkley, G.; Chan, E. T.; Christie, K. R.; Costanzo, M. C.; Dwight, S. S.; Engel, S. R.; Fisk, D. G.; Hirschman, J. E.; Hitz, B. C.; Karra, K.; Krieger, C. J.; Miyasato, S. R.; Nash, R. S.; Park, J.; Skrzypek, M. S.; Simison, M.; Weng, S.; Wong, E. D. *Saccharomyces* Genome Database: The Genomics Resource of Budding Yeast. *Nucleic Acids Res.* **2012**, *40*, D700−D705.
(144) Tanaka, T.; Kondo, A. Cell-Surface Display of Enzymes by the Yeast *Saccharomyces cerevisiae* for Synthetic Biology. *FEMS Yeast Res.* **2014**, *15*, 1−9.
(145) Tanaka, T.; Yamada, R.; Ogino, C.; Kondo, A. Recent Developments in Yeast Cell Surface Display toward Extended Applications in Biotechnology. *Appl. Microbiol. Biotechnol.* **2012**, *95*, 577−591.
(146) Himmel, M. E.; Ding, S.-Y.; Johnson, D. K.; Adney, W. S.; Nimlos, M. R.; Brady, J. W.; Foust, T. D. Biomass Recalcitrance: Engineering Plants and Enzymes for Biofuels Production. *Science* **2007**, *315*, 804−807.


DOI: 10.1021/acscatal.9b02413
*ACS Catal.* 2019, 9, 10812−10869

(147) Lynd, L. R.; Weimer, P. J.; van Zyl, W. H.; Pretorius, I. S. Microbial Cellulose Utilization: Fundamentals and Biotechnology. *Microbiol. Mol. Biol. Rev.* **2002**, *66*, 506−577.
(148) Thygesen, A.; Oddershede, J.; Lilholt, H.; Thomsen, A. B.; Ståhl, K. On the Determination of Crystallinity and Cellulose Content in Plant Fibres. *Cellulose* **2005**, *12*, 563−576.
(149) Fields, M. W.; Russell, J. B.; Wilson, D. B. The Role of Ruminal Carboxymethylcellulases in the Degradation of $\beta$-Glucans from Cereal Grain. *FEMS Microbiol. Ecol.* **1998**, *27*, 261−268.
(150) Liu, Z.; Ho, S. H.; Hasunuma, T.; Chang, J. S.; Ren, N. Q.; Kondo, A. Recent Advances in Yeast Cell-Surface Display Technologies for Waste Biorefineries. *Bioresour. Technol.* **2016**, *215*, 324−333.
(151) Zhang, Y. H.; Lynd, L. R. Toward an Aggregated Understanding of Enzymatic Hydrolysis of Cellulose: Noncomplexed Cellulase Systems. *Biotechnol. Bioeng.* **2004**, *88*, 797−824.
(152) Krässig, H. A. *Cellulose: Structure, Accessibility, and Reactivity*; Gordon & Breach: Yverdon, Switzerland, 1993.
(153) Yamada, R.; Hasunuma, T.; Kondo, A. Endowing Non-Cellulolytic Microorganisms with Cellulolytic Activity Aiming for Consolidated Bioprocessing. *Biotechnol. Adv.* **2013**, *31*, 754−763.
(154) Yamada, R.; Tanaka, T.; Ogino, C.; Fukuda, H.; Kondo, A. Novel Strategy for Yeast Construction Using $\delta$-Integration and Cell Fusion to Efficiently Produce Ethanol from Raw Starch. *Appl. Microbiol. Biotechnol.* **2010**, *85*, 1491−1498.
(155) Yamada, R.; Taniguchi, N.; Tanaka, T.; Ogino, C.; Fukuda, H.; Kondo, A. Cocktail $\delta$-Integration: A Novel Method to Construct Cellulolytic Enzyme Expression Ratio-Optimized Yeast Strains. *Microb. Cell Fact.* **2010**, *9*, 32−39.
(156) Merino, S. T.; Cherry, J. Progress and Challenges in Enzyme Development for Biomass Utilization. *Adv. Biochem. Eng./Biotechnol.* **2007**, *108*, 95−120.
(157) Binder, U.; Matschiner, G.; Theobald, I.; Skerra, A. High-Throughput Sorting of an Anticalin Library Via EspP-mediated Functional Display on the *Escherichia coli* Cell Surface. *J. Mol. Biol.* **2010**, *400*, 783−802.
(158) Jose, J.; Meyer, T. F. The Autodisplay Story, from Discovery to Biotechnical and Biomedical Applications. *Microbiol. Mol. Biol. Rev.* **2007**, *71*, 600−619.
(159) Quehl, P.; Hollender, J.; Schüürmann, J.; Brossette, T.; Maas, R.; Jose, J. Co-Expression of Active Human Cytochrome P450 1A2 and Cytochrome P450 Reductase on the Cell Surface of *Escherichia coli*. *Microb. Cell Fact.* **2016**, *15*, 26.
(160) Chen, W.; Georgiou, G. Cell-Surface Display of Heterologous Proteins: From High-Throughput Screening to Environmental Applications. *Biotechnol. Bioeng.* **2002**, *79*, 496−503.
(161) Gao, F.; Ding, H.; Xu, X.; Zhao, Y. A Self-Sufficient System for Removal of Synthetic Dye by Coupling of Spore-Displayed Triphenylmethane Reductase and Glucose 1-Dehydrogenase. *Environ. Sci. Pollut. Res.* **2016**, *23*, 21319−21326.
(162) Michon, C.; Langella, P.; Eijsink, V. G. H.; Mathiesen, G.; Chatel, J. M. Display of Recombinant Proteins at the Surface of Lactic Acid Bacteria: Strategies and Applications. *Microb. Cell Fact.* **2016**, *15*, 70.
(163) Hinc, K.; Isticato, R.; Dembek, M.; Karczewska, J.; Iwanicki, A.; Peszyńska-Sularz, G.; De Felice, M.; Obuchowski, M.; Ricca, E. Expression and Display of UreA of *Helicobacter acinonychis* on the Surface of *Bacillus subtilis* Spores. *Microb. Cell Fact.* **2010**, *9*, 2.
(164) Fierobe, H.-P.; Gaudin, C.; Belaich, A.; Loutfi, M.; Faure, E.; Bagnara, C.; Baty, D.; Belaich, J.-P. Characterization of Endoglucanase a from *Clostridium cellulolyticum*. *J. Bacteriol.* **1991**, *173*, 7956−7962.
(165) Gaudin, C.; Belaich, A.; Champ, S.; Belaich, J.-P. CelE, a Multidomain Cellulase from *Clostridium cellulolyticum*: A Key Enzyme in the Cellulosome? *J. Bacteriol.* **2000**, *182*, 1910−1915.
(166) Narita, J.; Okano, K.; Kitao, T.; Ishida, S.; Sewaki, T.; Sung, M. H.; Fukuda, H.; Kondo, A. Display of $\alpha$-Amylase on the Surface of *Lactobacillus casei* Cells by Use of the PgsA Anchor Protein, and Production of Lactic Acid from Starch. *Appl. Environ. Microbiol.* **2006**, *72*, 269−275.
(167) Narita, J.; Okano, K.; Tateno, T.; Tanino, T.; Sewaki, T.; Sung, M. H.; Fukuda, H.; Kondo, A. Display of Active Enzymes on the Cell Surface of *Escherichia coli* Using PgsA Anchor Protein and Their Application to Bioconversion. *Appl. Microbiol. Biotechnol.* **2006**, *70*, 564−572.
(168) Lu, Y.; Zhang, Y.-H. P.; Lynd, L. R. Enzyme−Microbe Synergy During Cellulose Hydrolysis by *Clostridium thermocellum*. *Proc. Natl. Acad. Sci. U. S. A.* **2006**, *103*, 16165−16169.
(169) Bayer, E. A.; Belaich, J. P.; Shoham, Y.; Lamed, R. The Cellulosomes: Multienzyme Machines for Degradation of Plant Cell Wall Polysaccharides. *Annu. Rev. Microbiol.* **2004**, *58*, 521−554.
(170) Doi, R. H.; Kosugi, A. Cellulosomes: Plant-Cell-Wall-Degrading Enzyme Complexes. *Nat. Rev. Microbiol.* **2004**, *2*, 541−551.
(171) Fontes, C. M.; Gilbert, H. J. Cellulosomes: Highly Efficient Nanomachines Designed to Deconstruct Plant Cell Well Complex Carbohydrates. *Annu. Rev. Biochem.* **2010**, *79*, 655−681.
(172) Demain, A. L.; Newcomb, M.; Wu, J. H. Cellulase, Clostridia, and Ethanol. *Microbiol. Mol. Biol. Rev.* **2005**, *69*, 124−154.
(173) Kipper, K.; Väljamäe, P.; Johansson, G. Processive Action of Cellobiohydrolase Cel7a from *Trichoderma reesei* Is Revealed as 'Burst' Kinetics on Fluorescent Polymeric Model Substrates. *Biochem. J.* **2005**, *385*, 527−535.
(174) Cappellaro, C.; Baldermann, C.; Rachel, R.; Tanner, W. Mating Type-Specific Cell-Cell Recognition of *Saccharomyces cerevisiae*: Cell Wall Attachment and Active Sites of a- and $\alpha$-Agglutinin. *EMBO J.* **1994**, *13*, 4737−4744.
(175) de Nobel, H.; Pike, J.; Lipke, P. N.; Kurjan, J. Genetics of a-Agglutunin Function in *Saccharomyces cerevisiae*. *Mol. Gen. Genet.* **1995**, *247*, 409−415.
(176) Wang, B.; Lee, C. H.; Johnson, E. L.; Kluwe, C. A.; Cunningham, J. C.; Tanno, H.; Crooks, R. M.; Georgiou, G.; Ellington, A. D. Discovery of High Affinity Anti-Ricin Antibodies by B Cell Receptor Sequencing and by Yeast Display of Combinatorial VH:VL Libraries from Immunized Animals. *MAbs* **2016**, *8*, 1035−1044.
(177) Yang, J.; Dang, H.; Lu, J. R. Improving Genetic Immobilization of a Cellulase on Yeast Cell Surface for Bioethanol Production Using Cellulose. *J. Basic Microbiol.* **2013**, *53*, 381−389.
(178) Yuan, X.; Chen, X.; Yang, M.; Hu, J.; Yang, W.; Chen, T.; Wang, Q.; Zhang, X.; Lin, R.; Zhao, A. Efficient Construct of a Large and Functional Scfv Yeast Display Library Derived from the Ascites B Cells of Ovarian Cancer Patients by Three-Fragment Transformation-Associated Recombination. *Appl. Microbiol. Biotechnol.* **2016**, *100*, 4051−4061.
(179) Kim, Y. H.; Campbell, E.; Yu, J.; Minteer, S. D.; Banta, S. Complete Oxidation of Methanol in Biobattery Devices Using a Hydrogel Created from Three Modified Dehydrogenases. *Angew. Chem., Int. Ed.* **2013**, *52*, 1437−1440.
(180) Palmore, G. T. R.; Bertschy, H.; Bergens, S. H.; Whitesides, G. M. A Methanol/Dioxygen Biofuel Cell That Uses $NAD^+$-Dependent Dehydrogenases as Catalysts: Application of an Electro-Enzymatic Method to Regenerate Nicotinamide Adenine Dinnucleotide at Low Overpotentials. *J. Electroanal. Chem.* **1998**, *443*, 155−161.
(181) Sokic-Lazic, D.; Arechederra, R. L.; Treu, B. L.; Minteer, S. D. Oxidation of Biofuels: Fuel Diversity and Effectiveness of Fuel Oxidation through Multiple Enzyme Cascades. *Electroanalysis* **2010**, *22*, 757−764.
(182) Tsai, S. L.; Goyal, G.; Chen, W. Surface Display of a Functional Minicellulosome by Intracellular Complementation Using a Synthetic Yeast Consortium and Its Application to Cellulose Hydrolysis and Ethanol Production. *Appl. Environ. Microbiol.* **2010**, *76*, 7514−7520.
(183) Ito, K.; Takahashi, M.; Yoshimoto, T.; Tsuru, D. Cloning and High-Level Expression of the Glutathione-Independent Formaldehyde Dehydrogenase Gene from *Pseudomonas putida*. *J. Bacteriol.* **1994**, *176*, 2483−2491.
(184) Beveridge, T. J. Structures of Gram-Negative Cell Walls and Their Derived Membrane Vesicles. *J. Bacteriol.* **1999**, *181*, 4725−4733.
(185) Kuehn, M. J.; Kesty, N. C. Baceterial Outer Membrane Vesicles and the Host-Pathogen Interaction. *Genes Dev.* **2005**, *19*, 2645−2655.


DOI: 10.1021/acscatal.9b02413
*ACS Catal.* 2019, 9, 10812−10869

(186) Kulp, A.; Kuehn, M. J. Biological Functions and Biogenesis of Secreted Bacterial Outer Membrane Vesicles. *Annu. Rev. Microbiol.* **2010**, *64*, 163−184.
(187) Bae, W.; Mulchandani, A.; Chen, W. Cell Surface Display of Synthetic Phytochelatins Using Ice Nucleation Protein for Enhanced Heavy Metal Bioaccumulation. *J. Inorg. Biochem.* **2002**, *88*, 223−227.
(188) Bernadac, A.; Gavioli, M.; Lazzaroni, J.-C.; Raina, S.; Lloubès, R. *Escherichia coli Tol-Pal* Mutants Form Outer Membrane Vesicles. *J. Bacteriol.* **1998**, *180*, 4872−4878.
(189) Eklund, M.; Axelsson, L.; Uhlen, M.; Nygren, P. A. Anti-Idiotypic Protein Domains Selected from Protein a-Based Affibody Libraries. *Proteins: Struct., Funct., Genet.* **2002**, *48*, 454−462.
(190) Nilsson, B.; Moks, T.; Jansson, B.; Abrahmsén, L.; Elmblad, A.; Holmgren, E.; Henrichson, C.; Jones, T. A.; Uhlén, M. A Synthetic IgG-binding Domain Based on Staphylococcal Protein A. *Protein Eng., Des. Sel.* **1987**, *1*, 107−113.
(191) Nord, K.; Gunneriusson, E.; Ringdahl, J.; Ståhl, S.; Uhlén, M.; Nygren, P.-Å. Binding Proteins Selected from Combinatorial Libraries of an α-Helical Bacterial Receptor Domain. *Nat. Biotechnol.* **1997**, *15*, 772−777.
(192) Nord, K.; Nilsson, J.; Nilsson, B.; Uhlén, M.; Nygren, P. Å. A Combinatorial Library of an Alpha-Helical Bacterial Receptor Domain. *Protein Eng., Des. Sel.* **1995**, *8*, 601−608.
(193) What Is an Anti-Idiotypic Antibody? https://www.genscript.com/antibody-news/what-is-an-anti-Idiotypic-antibody.html (accessed Dec 14, 2018).
(194) Wahlberg, E.; Härd, T. Conformational Stabilitzation of an Engineered Binding Protein. *J. Am. Chem. Soc.* **2006**, *128*, 7651−7660.
(195) Gao, X.; Chen, J. C.; Wu, Q.; Chen, G. Q. Polyhydroxyalkanoates as a Source of Chemicals, Polymers, and Biofuels. *Curr. Opin. Biotechnol.* **2011**, *22*, 768−774.
(196) Kim, E.-J.; Kim, K.-J. Crystal Structure and Biochemical Characterization of PhaA from *Ralstonia eutropha*, a Polyhydroxyalkanoate-Producing Bacterium. *Biochem. Biophys. Res. Commun.* **2014**, *452*, 124−129.
(197) Matsumoto, K.; Tanaka, Y.; Watanabe, T.; Motohashi, R.; Ikeda, K.; Tobitani, K.; Yao, M.; Tanaka, I.; Taguchi, S. Directed Evolution and Structural Analysis of NADPH-Dependent Acetoacetyl Coenzyme a (Acetoacetyl-CoA) Reductase from *Ralstonia eutropha* Reveals Two Mutations Responsible for Enhanced Kinetics. *Appl. Environ. Microbiol.* **2013**, *79*, 6134−6139.
(198) Pitts, A. C.; Tuck, L. R.; Faulds-Pain, A.; Lewis, R. J.; Marles-Wright, J. Structural Insight into the *Clostridium difficile* Ethanolamine Utilisation Microcompartment. *PLoS One* **2012**, *7*, e48360.
(199) Takenoya, M.; Nikolakakis, K.; Sagermann, M. Crystallographic Insights into the Pore Structures and Mechanisms of the EutL and EutM Shell Proteins of the Ethanolamine-Utilizing Microcompartment of *Escherichia coli*. *J. Bacteriol.* **2010**, *192*, 6056−6063.
(200) Tanaka, S.; Sawaya, M. R.; Yeates, T. O. Structure and Mechanisms of a Protein-Based Organelle in *Escherichia coli*. *Science* **2010**, *327*, 81−84.
(201) Zakeri, B.; Fierer, J. O.; Celik, E.; Chittock, E. C.; Schwarz-Linek, U.; Moy, V. T.; Howarth, M. Peptide Tag Forming a Rapid Covalent Bond to a Protein, through Engineering a Bacterial Adhesin. *Proc. Natl. Acad. Sci. U. S. A.* **2012**, *109*, E690−E697.
(202) Mutti, F. G.; Knaus, T.; Scrutton, N. S.; Breuer, M.; Turner, N. J. Conversion of Alcohols to Enantiopure Amines through Dual-Enzyme Hydrogen-Borrowing Cascades. *Science* **2015**, *349*, 1525−1529.
(203) Bommarius, B. R.; Schürmann, M.; Bommarius, A. S. A Novel Chimeric Amine Dehydrogenase Shows Altered Substrate Specificity Compared to Its Parent Enzymes. *Chem. Commun.* **2014**, *50*, 14953−14955.
(204) Dudzik, A.; Snoch, W.; Borowiecki, P.; Opalinska-Piskorz, J.; Witko, M.; Heider, J.; Szaleniec, M. Asymmetric Reduction of Ketones and B-Keto Esters by (S)-1-Phenylethanol Dehydrogenase from Denitrifying Bacterium *Aromatoleum aromaticum*. *Appl. Microbiol. Biotechnol.* **2015**, *99*, 5055−5069.
(205) Höffken, H. W.; Duong, M.; Friedrich, T.; Breuer, M.; Hauer, B.; Reinhardt, R.; Rabus, R.; Heider, J. Crystal Structure and Enzyme Kinetics of the (S)-Specific 1-Phenylethanol Dehydrogenase of the Denitrifying Bacterium Strain EbN1. *Biochemistry* **2006**, *45*, 82−93.
(206) Brunhuber, N. M. W.; Thoden, J. B.; Blanchard, J. S.; Vanhooke, J. L. *Rhodococcus* L-Phenylalanine Dehydrogenase: Kinetics, Mechanism, and Structural Basis for Catalytic Specifity. *Biochemistry* **2000**, *39*, 9174−9187.
(207) Vanhooke, J. L.; Thoden, J. B.; Brunhuber, N. M. W.; Blanchard, J. S.; Holden, H. M. Phenylalanine Dehydrogenase from *Rhodococcus* Sp. M4: High-Resolution X-Ray Analyses of Inhibitory Ternary Complexes Reveal Key Features in the Oxidative Deamination Mechanism. *Biochemistry* **1999**, *38*, 2326−2339.
(208) Schmidt-Dannert, S.; Zhang, G.; Johnston, T.; Quin, M. B.; Schmidt-Dannert, C. Building a Toolbox of Protein Scaffolds for Future Immobilization of Biocatalysts. *Appl. Microbiol. Biotechnol.* **2018**, *102*, 8373−8388.
(209) Eun, C.; Kekenes-Huskey, P. M.; Metzger, V. T.; McCammon, J. A. A Model Study of Sequential Enzyme Reactions and Electrostatic Channeling. *J. Chem. Phys.* **2014**, *140*, 105101.
(210) Miall, L. Organic Acids. *Econ. Microbiol.* **1978**, *2*, 48−119.
(211) Nuss, P.; Gardner, K. H. Attributional Life Cycle Assessment (ALCA) of Polyitaconic Acid Production from Northeast Us Softwood Biomass. *Int. J. Life Cycle Assess.* **2013**, *18*, 603−612.
(212) Okabe, M.; Lies, D.; Kanamasa, S.; Park, E. Y. Biotechnological Production of Itaconic Acid and Its Biosynthesis in *Aspergillus terreus*. *Appl. Microbiol. Biotechnol.* **2009**, *84*, 597−606.
(213) Yang, Z.; Gao, X.; Xie, H.; Wang, F.; Ren, Y.; Wei, D. Enhanced Itaconic Acid Production by Self-Assembly of Two Biosynthetic Enzymes in *Escherichia coli*. *Biotechnol. Bioeng.* **2017**, *114*, 457−462.
(214) Schmidtmann, E.; König, A. C.; Orwat, A.; Leister, D.; Hartl, M.; Finkemeier, I. Redox Regulation of Arabidopsis Mitochondrial Citrate Synthase. *Mol. Plant* **2014**, *7*, 156−169.
(215) Gao, X.; Yang, S.; Zhao, C.; Ren, Y.; Wei, D. Artificial Multienzyme Supramolecular Device: Highly Ordered Self-Assembly of Oligomeric Enzymes in Vitro and in Vivo. *Angew. Chem., Int. Ed.* **2014**, *53*, 14027−14030.
(216) Sivaramakrishnan, S.; Sung, J.; Ali, M.; Doniach, S.; Flyvbjerg, H.; Spudich, J. A. Combining Single-Molecule Optical Trapping and Small-Angle X-Ray Scattering Measurements to Compute the Persistence Length of a Protein ER/K Alpha-Helix. *Biophys. J.* **2009**, *97*, 2993−2999.
(217) Brautaset, T.; Jakobsen, Ø. M.; Flickinger, M. C.; Valla, S.; Ellingsen, T. E. Plasmid-Dependent Methylotrophy in Thermotolerant *Bacillus methanolicus*. *J. Bacteriol.* **2004**, *186*, 1229−1238.
(218) Hektor, H. J.; Kloosterman, H.; Dijkhuizen, L. Identification of a Magnesium-Dependent Nad(P)(H)-Binding Domain in the Nicotinoprotein Methanol Dehydrogenase from *Bacillus methanolicus*. *J. Biol. Chem.* **2002**, *277*, 46966−46973.
(219) Kato, N.; Yurimoto, H.; Thauer, R. K. The Physiological Role of the Ribulose Monophosphate Pathway in Bacteria and Archaea. *Biosci., Biotechnol., Biochem.* **2006**, *70*, 10−21.
(220) Krog, A.; Heggeset, T. M. B.; Müller, J. E. N.; Kupper, C. E.; Schneider, O.; Vorholt, J. A.; Ellingsen, T. E.; Brautaset, T. Methylotrophic *Bacillus methanolicus* Encodes Two Chromosomal and One Plasmid Born $NAD^+$ Dependent Methanol Dehydrogenase Paralogs with Different Catalytic and Biochemical Properties. *PLoS One* **2013**, *8*, e59188.
(221) Mitsui, R.; Sakai, Y.; Yasueda, H.; Kato, N. A Novel Operon Encoding Formaldehyde Fixation: The Ribulose Monophosphate Pathway in the Gram-Positive Facultative Methylotrophic Bacterium *Mycobacterium gastri* MB19. *J. Bacteriol.* **2000**, *182*, 944−948.
(222) Vonck, J.; Arfman, N.; De Vries, G. E.; Van Beeumen, J.; Van Bruggen, E. F. J.; Dijkhuizen, L. Electron Microscopic Analysis and Biochemical Characterization of a Novel Methanol Dehydrogenase from the Thermotolerant *Bacillus* Sp. C1. *J. Biol. Chem.* **1991**, *266*, 3949−3954.


DOI: 10.1021/acscatal.9b02413
*ACS Catal.* 2019, 9, 10812−10869

(223) Orita, I.; Sakamoto, N.; Kato, N.; Yurimoto, H.; Sakai, Y. Bifunctional Enzyme Fusion of 3-Hexulose-6-Phosphate Synthase and 6-Phospho-3-Hexuloisomerase. *Appl. Microbiol. Biotechnol.* **2007**, *76*, 439−445.
(224) Moon, T. S.; Dueber, J. E.; Shiue, E.; Prather, K. L. Use of Modular, Synthetic Scaffolds for Improved Production of Glucaric Acid in Engineered *E. coli*. *Metab. Eng.* **2010**, *12*, 298−305.
(225) Bai, Y.; Luo, Q.; Zhang, W.; Miao, L.; Xu, J.; Li, H.; Liu, J. Highly Ordered Protein Nanorings Designed by Accurate Control of Glutathione S-Transferase Self-Assembly. *J. Am. Chem. Soc.* **2013**, *135*, 10966−10969.
(226) Anderson, G. P.; Shriver-Lake, L. C.; Liu, J. L.; Goldman, E. R. Orthogonal Synthetic Zippers as Protein Scaffolds. *ACS Omega* **2018**, *3*, 4810−4815.
(227) Reinke, A. W.; Grant, R. A.; Keating, A. E. A Synthetic Coiled-Coil Interactome Provides Heterospecific Modules for Molecular Engineering. *J. Am. Chem. Soc.* **2010**, *132*, 6025−6031.
(228) Thomas, F.; Boyle, A. L.; Burton, A. J.; Woolfson, D. N. A Set of *De Novo* Designed Parallel Heterodimeric Coiled Coils with Quantified Dissociation Constants in the Micromolar to Sub-Nanomolar Regime. *J. Am. Chem. Soc.* **2013**, *135*, 5161−5166.
(229) Bromley, E. H. C.; Sessions, R. B.; Thomson, A. R.; Woolfson, D. N. Designed $\alpha$-Helical Tectons for Constructing Multicomponent Synthetic Biological Systems. *J. Am. Chem. Soc.* **2009**, *131*, 928−930.
(230) Fletcher, J. M.; Boyle, A. L.; Bruning, M.; Bartlett, G. J.; Vincent, T. L.; Zaccai, N. R.; Armstrong, C. T.; Bromley, E. H.; Booth, P. J.; Brady, R. L.; Thomson, A. R.; Woolfson, D. N. A Basis Set of De Novo Coiled-Coil Peptide Oligomers for Rational Protein Design and Synthetic Biology. *ACS Synth. Biol.* **2012**, *1*, 240−250.
(231) Gradišar, H.; Jerala, R. De Novo Design of Orthogonal Peptide Pairs Forming Parallel Coiled-Coil Heterodimers. *J. Pept. Sci.* **2011**, *17*, 100−106.
(232) Thompson, K. E.; Bashor, C. J.; Lim, W. A.; Keating, A. E. SYNZIP Protein Interaction Toolbox: *In Vitro* and *in Vivo* Specifications of Heterospecific Coiled-Coil Interaction Domains. *ACS Synth. Biol.* **2012**, *1*, 118−129.
(233) Arié, J. P.; Miot, M.; Sassoon, N.; Betton, J. M. Formation of Active Inclusion Bodies in the Periplasm of *Escherichia coli*. *Mol. Microbiol.* **2006**, *62*, 427−437.
(234) Kopito, R. R. Aggresomes, Inclusion Bodies, and Protein Aggregation. *Trends Cell Biol.* **2000**, *10*, 524−530.
(235) Choi, S.-L.; Lee, S. J.; Yeom, S. J.; Kim, H. J.; Rhee, Y. H.; Jung, H. C.; Lee, S. G. Controlled Localization of Functionally Active Proteins to Inclusion Bodies Using Leucine Zippers. *PLoS One* **2014**, *9*, e97093.
(236) Choi, S.-L.; Lee, S. J.; Ha, J.-S.; Song, J. J.; Rhee, Y. H.; Lee, S.-G. Generation of Catalytic Protein Particles in *Escherichia coli* Cells Using the Cellulose-Binding Domain from *Cellulomonas fimi* as a Fusion Partner. *Biotechnol. Bioprocess Eng.* **2011**, *16*, 1173−1179.
(237) Baek, J. M.; Mazumdar, S.; Lee, S. W.; Jung, M. Y.; Lim, J. H.; Seo, S. W.; Jung, G. Y.; Oh, M. K. Butyrate Production in Engineered *Escherichia coli* with Synthetic Scaffolds. *Biotechnol. Bioeng.* **2013**, *110*, 2790−2794.
(238) Diener, M.; Kopka, B.; Pohl, M.; Jaeger, K.-E.; Krauss, U. Fusion of a Coiled-Coil Domain Facilitates the High-Level Production of Catalytically Active Enzyme Inclusion Bodies. *ChemCatChem* **2016**, *8*, 142−152.
(239) Stetefeld, J.; Jenny, M.; Schulthess, T.; Landwehr, R.; Engel, J.; Kammerer, R. A. Crystal Structure of a Naturally Occurring Parallel Right-Handed Coiled Coil Tetramer. *Nat. Struct. Biol.* **2000**, *7*, 772−776.
(240) Choudary, B. M.; Chowdari, N. S.; Madhi, S.; Kantam, M. L. A Trifunctional Catalyst for One-Pot Synthesis of Chiral Diols Via Heck Coupling−N-oxidation−Asymmetric Dihydroxylation: Application for the Synthesis of Diltiazem and Taxol Side Chain. *J. Org. Chem.* **2003**, *68*, 1736−1746.
(241) González, B.; Vicuña, R. Benzaldehyde Lyase, a Novel Thiamine PPi-Requiring Enzyme, from *Pseudomonas fluorescens* Biovar I. *J. Bacteriol.* **1989**, *171*, 2401−2405.
(242) Kulig, J.; Frese, A.; Kroutil, W.; Pohl, M.; Rother, D. Biochemical Characterization of an Alcohol Dehydrogenase from *Ralstonia* Sp. *Biotechnol. Bioeng.* **2013**, *110*, 1838−1848.
(243) Kulig, J.; Simon, R. C.; Rose, C. A.; Husain, S. M.; Häckh, M.; Lüdeke, S.; Zeitler, K.; Kroutil, W.; Pohl, M.; Rother, D. Stereoselective Synthesis of Bulky 1,2-Diols with Alcohol Dehydrogenases. *Catal. Sci. Technol.* **2012**, *2*, 1580−1589.
(244) Man, H.; Kędziora, K.; Kulig, J.; Frank, A.; Lavandera, I.; Gotor-Fernández, V.; Rother, D.; Hart, S.; Turkenburg, J. P.; Grogan, G. Structures of Alcohol Dehydrogenases from *Ralstonia* and *Sphingobium* Spp. Reveal the Molecular Basis for Their Recognition of 'Bulky−Bulky' Ketones. *Top. Catal.* **2014**, *57*, 356−365.
(245) Mosbacher, T. G.; Mueller, M.; Schulz, G. E. Structure and Mechanism of the Thdp-Dependent Benzaldehyde Lyase from *Pseudomonas fluorescens*. *FEBS J.* **2005**, *272*, 6067−6076.
(246) Bintrim, S. B.; Ensign, J. C. Insertional Inactivation of Genes Encoding the Crystalline Inclusion Proteins of *Photorhabdus luminescens* Results in Mutants with Pleiotropic Phenotypes. *J. Bacteriol.* **1998**, *180*, 1261−1269.
(247) Bowen, D. J.; Ensign, J. C. Isolation and Characterization of Intracellular Protein Inclusions Produced by the Entomopathogenic Bacterium *Photorhabdus luminescens*. *Appl. Environ. Microbiol.* **2001**, *67*, 4834−4841.
(248) Hoshino, T. Violacein and Related Tryptophan Metabolites Produced by *Chromobacterium violaceum*: Biosynthetic Mechanism and Pathway for Construction of Violacein Core. *Appl. Microbiol. Biotechnol.* **2011**, *91*, 1463−1475.
(249) Sánchez, C.; Braña, A. F.; Méndez, C.; Salas, J. A. Reevaluation of the Violacein Biosynthetic Pathway and Its Relationship to Indolocarbazole Biosynthesis. *ChemBioChem* **2006**, *7*, 1231−1240.
(250) Yamaguchi, H.; Kiyota, Y.; Miyazaki, M. Techniques for Preparation of Cross-Linked Enzyme Aggregates and Their Applications in Bioconversions. *Catalysts* **2018**, *8*, 174.
(251) Cao, L.; van Langen, L.; Sheldon, R. A. Immobilised Enzymes: Carrier-Bound or Carrier-Free? *Curr. Opin. Biotechnol.* **2003**, *14*, 387−394.
(252) Perzon, A.; Dicko, C.; Çobanoğlu, Ö.; Yükselen, O.; Eryilmaz, J.; Dey, E. S. Cellulase Cross-Linked Enzyme aggregates(CLEA) Activities Can Be Modulated and Enhanced by Precipitant Selection. *J. Chem. Technol. Biotechnol.* **2017**, *92*, 1645−1649.
(253) Shah, S.; Sharma, A.; Gupta, M. N. Preparation of Cross-Linked Enzyme Aggregates by Using Bovine Serum Albumin as a Proteic Feeder. *Anal. Biochem.* **2006**, *351*, 207−213.
(254) López-Gallego, F.; Betancor, L.; Hidalgo, A.; Alonso, N.; Fernández-Lafuente, R.; Guisán, J. M. Co-Aggregation of Enzymes and Polyethyleneimine: A Simple Method to Prepare Stable and Immobilized Derivatives of Glutaryl Acylase. *Biomacromolecules* **2005**, *6*, 1839−1842.
(255) Wilson, L.; Illanes, A.; Abián, O.; Pessela, B. C. C.; Fernández-Lafuente, R.; Guisán, J. M. Co-Aggregation of Penicillin G Acylase and Polyionic Polymers: An Easy Methodology to Prepare Enzyme Biocatalysts Stable in Organic Media. *Biomacromolecules* **2004**, *5*, 852−857.
(256) Zheng, J.; Chen, Y.; Yang, L.; Li, M.; Zhang, J. Preparation of Cross-Linked Enzyme Aggregates of Trehalose Synthase Via Co-Aggregation with Polyethyleneimine. *Appl. Biochem. Biotechnol.* **2014**, *174*, 2067−2078.
(257) Rehman, S.; Bhatti, H. N.; Bilal, M.; Asgher, M. Cross-Linked Enzyme Aggregates (CLEAs) of Pencilluim Notatum Lipase Enzyme with Improved Activity, Stability and Reusability Characteristics. *Int. J. Biol. Macromol.* **2016**, *91*, 1161−1169.
(258) Cao, L. Immobilised Enzymes: Science or Art? *Curr. Opin. Chem. Biol.* **2005**, *9*, 217−226.
(259) Kim, M. I.; Kim, J.; Lee, J.; Jia, H.; Na, H. B.; Youn, J. K.; Kwak, J. H.; Dohnalkova, A.; Grate, J. W.; Wang, P.; Hyeon, T.; Park, H. G.; Chang, H. N. Crosslinked Enzyme Aggregates in Hierarchically-Ordered Mesoporous Silica: A Simple and Effective Method for Enzyme Stabilization. *Biotechnol. Bioeng.* **2007**, *96*, 210−218.


DOI: 10.1021/acscatal.9b02413
*ACS Catal.* 2019, 9, 10812−10869

(260) Xu, D. Y.; Yang, Z. Cross-Linked Tyrosinase Aggregates for Elimination of Phenolic Compounds from Wastewater. *Chemosphere* **2013**, *92*, 391−398.
(261) Talekar, S.; Ghodake, V.; Ghotage, T.; Rathod, P.; Deshmukh, P.; Nadar, S.; Mulla, M.; Ladole, M. Novel Magnetic Cross-Linked Enzyme Aggregates (Magnetic CLEAs) of Alpha Amylase. *Bioresour. Technol.* **2012**, *123*, 542−547.
(262) Cabirol, F. L.; Tan, P. L.; Tay, B.; Cheng, S.; Hanefeld, U.; Sheldon, R. A. *Linum Usitatissimum* Hydroxynitrile Lyase Cross-Linked Enzyme Aggregates: A Recyclable Enantioselective Catalyst. *Adv. Synth. Catal.* **2008**, *350*, 2329−2338.
(263) Verheyen, E.; Schillemans, J. P.; van Wijk, M.; Demeniex, M. A.; Hennink, W. E.; van Nostrum, C. F. Challenges for the Effective Molecular Imprinting of Proteins. *Biomaterials* **2011**, *32*, 3008−3020.
(264) Honda, T.; Miyazaki, M.; Nakamura, H.; Maeda, H. Immobilization of Enzymes on a Microchannel Surface through Cross-Linking Polymerization. *Chem. Commun.* **2005**, 5062−5064.
(265) Honda, T.; Miyazaki, M.; Nakamura, H.; Maeda, H. Facile Preparation of an Enzyme-Immobilized Microreactor Using a Cross-Linking Enzyme Membrane on a Microchannel Surface. *Adv. Synth. Catal.* **2006**, *348*, 2163−2171.
(266) Nguyen, L. T.; Neo, K. R.; Yang, K. L. Continuous Hydrolysis of Carboxymethyl Cellulose with Cellulase Aggregates Trapped inside Membranes. *Enzyme Microb. Technol.* **2015**, *78*, 34−39.
(267) Nguyen, L. T.; Yang, K. L. Uniform Cross-Linked Cellulase Aggregates Prepared in Millifluidic Reactors. *J. Colloid Interface Sci.* **2014**, *428*, 146−151.
(268) Nguyen, L. T.; Seow, N.; Yang, K. L. Hollow Cross-Linked Enzyme Aggregates (h-CLEA) of Laccase with High Uniformity and Activity. *Colloids Surf., B* **2017**, *151*, 88−94.
(269) Rodrigues, R. C.; Ortiz, C.; Berenguer-Murcia, A.; Torres, R.; Fernández-Lafuente, R. Modifying Enzyme Activity and Selectivity by Immobilization. *Chem. Soc. Rev.* **2013**, *42*, 6290−6307.
(270) Taboada-Puig, R.; Junghanns, C.; Demarche, P.; Moreira, M. T.; Feijoo, G.; Lema, J. M.; Agathos, S. N. Combined Cross-Linked Enzyme Aggregates from Versatile Peroxidase and Glucose Oxidase: Production, Partial Characterization and Application for the Elimination of Endocrine Disruptors. *Bioresour. Technol.* **2011**, *102*, 6593−6599.
(271) Zhang, Y.; Yong, Y.; Ge, J.; Liu, Z. Lectin Agglutinated Multienzyme Catalyst with Enhanced Substrate Affinity and Activity. *ACS Catal.* **2016**, *6*, 3789−3795.
(272) Gonzalez, C. F.; Langenberg, W. G.; Van Etten, J. L.; Vidaver, A. K. Ultrastructure of Bacteriophage $\phi$6: Arrangement of the Double-Stranded RNA and Envelope. *J. Gen. Virol.* **1977**, *35*, 353−359.
(273) Sinclair, J. F.; Tzagoloff, A.; Levine, D.; Mindich, L. Proteins of Bacteriophage $\phi$6. *J. Virol.* **1975**, *16*, 685−695.
(274) Johnson, M. D., III; Mindich, L. Plasmid-Directed Assembly of the Lipid-Containing Membrane of Bacteriophage $\phi$6. *J. Bacteriol.* **1994**, *176*, 4124−4132.
(275) Stitt, B. L.; Mindich, L. Morphogenesis of Bacteriophage $\phi$6: A Presumptive Viral Membrane Precursor. *Virology* **1983**, *127*, 446−458.
(276) Lin, J. L.; Wheeldon, I. Dual N- and C-Terminal Helices Are Required for Endoplasmic Reticulum and Lipid Droplet Association of Alcohol Acetyltransferases in *Saccharomyces cerevisiae*. *PLoS One* **2014**, *9*, e104141.
(277) Verstrepen, K. J.; Van Laere, S. D. M.; Vanderhaegen, B. M. P.; Derdelinckx, G.; Dufour, J.-P.; Pretorius, I. S.; Winderickx, J.; Thevelein, J. M.; Delvaux, F. R. Expression Levels of the Yeast Alcohol Acetyltransferase Genes ATF1, Lg-ATF1, and ATF2 Control the Formation of a Broad Range of Volatile Esters. *Appl. Environ. Microbiol.* **2003**, *69*, 5228−5237.
(278) Chen, Y.; Siewers, V.; Nielsen, J. Profiling of Cytosolic and Peroxisomal acetyl-CoA Metabolism in *Saccharomyces cerevisiae*. *PLoS One* **2012**, *7*, e42475.
(279) Meaden, P. G.; Dickinson, F. M.; Mifsud, A.; Tessier, W.; Westwater, J.; Bussey, H.; Midgley, M. The ALD6 Gene of *Saccharomyces cerevisiae* Encodes a Cytosolic, Mg2+-Activated Acetaldehyde Dehydrogenase. *Yeast* **1997**, *13*, 1319−1327.
(280) Sickmann, A.; Reinders, J.; Wagner, Y.; Joppich, C.; Zahedi, R.; Meyer, H. E.; Schönfisch, B.; Perschil, I.; Chacinska, A.; Guiard, B.; Rehling, P.; Pfanner, N.; Meisinger, C. The Proteome of *Saccharomyces cerevisiae* Mitochondria. *Proc. Natl. Acad. Sci. U. S. A.* **2003**, *100*, 13207−13212.
(281) Qu, R.; Huang, A. H. C. Oleosin KD 18 on the Surface of Oil Bodies in Maize—Genomic and cDNA Sequences and the Deduced Protein Structure. *J. Biol. Chem.* **1990**, *265*, 2238−2243.
(282) Jogl, G.; Tong, L. Crystal Structure of Yeast Acetyl-Coenzyme a Synthetase in Complex with AMP. *Biochemistry* **2004**, *43*, 1425−1431.
(283) Adams, J. J.; Gregg, K.; Bayer, E. A.; Boraston, A. B.; Smith, S. P. Structural Basis of *Clostridium perfringens* Toxin Complex Formation. *Proc. Natl. Acad. Sci. U. S. A.* **2008**, *105*, 12194−12199.
(284) Carvalho, A. L.; Dias, F. M.; Prates, J. A.; Nagy, T.; Gilbert, H. J.; Davies, G. J.; Ferreira, L. M.; Romão, M. J.; Fontes, C. M. Cellulosome Assembly Revealed by the Crystal Structure of the Cohesin-Dockerin Complex. *Proc. Natl. Acad. Sci. U. S. A.* **2003**, *100*, 13809−13814.
(285) Bauler, P.; Huber, G.; Leyh, T.; McCammon, J. A. Channeling by Proximity: The Catalytic Advantages of Active Site Colocalization Using Brownian Dynamics. *J. Phys. Chem. Lett.* **2010**, *1*, 1332−1335.
(286) Bai Flagfeldt, D.; Siewers, V.; Huang, L.; Nielsen, J. Characterization of Chromosomal Integration Sites for Heterologous Gene Expression in *Saccharomyces cerevisiae*. *Yeast* **2009**, *26*, 545−551.
(287) Gao, S.; Tong, Y.; Zhu, L.; Ge, M.; Zhang, Y.; Chen, D.; Jiang, Y.; Yang, S. Iterative Integration of Multiple-Copy Pathway Genes in *Yarrowia lipolytica* for Heterologous $\beta$-Carotene Production. *Metab. Eng.* **2017**, *41*, 192−201.
(288) Linko, V.; Nummelin, S.; Aarnos, L.; Tapio, K.; Toppari, J. J.; Kostiainen, M. A. DNA-Based Enzyme Reactors and Systems. *Nanomaterials* **2016**, *6*, 139−139.
(289) Saccà, B.; Niemeyer, C. M. Functionalization of DNA Nanostructures with Proteins. *Chem. Soc. Rev.* **2011**, *40*, 5910−5921.
(290) Sun, Q.; Tsai, S.-L.; Chen, W. Chapter Fourteen - Artificial Scaffolds for Enhanced Biocatalysis. *Methods Enzymol.* **2019**, *617*, 363−383.
(291) Seeman, N. C.; Sleiman, H. F. DNA Nanotechnology. *Nat. Rev. Mater.* **2018**, *3*, 17068.
(292) Seeman, N. C. Nucleic-Acid Junctions and Lattices. *J. Theor. Biol.* **1982**, *99*, 237−247.
(293) Fu, J.; Yang, Y. R.; Dhakal, S.; Zhao, Z.; Liu, M.; Zhang, T.; Walter, N. G.; Yan, H. Assembly of Multienzyme Complexes on DNA Nanostructures. *Nat. Protoc.* **2016**, *11*, 2243−2243.
(294) Timm, C.; Niemeyer, C. M. Assembly and Purification of Enzyme-Functionalized DNA Origami Structures. *Angew. Chem., Int. Ed.* **2015**, *54*, 6745−6750.
(295) Shih, W. M.; Quispe, J. D.; Joyce, G. F. A 1.7-Kilobase Single-Stranded DNA That Folds into a Nanoscale Octahedron. *Nature* **2004**, *427*, 618−621.
(296) Ke, G.; Liu, M.; Jiang, S.; Qi, X.; Yang, Y. R.; Wootten, S.; Zhang, F.; Zhu, Z.; Liu, Y.; Yang, C. J.; Yan, H. Directional Regulation of Enzyme Pathways through the Control of Substrate Channeling on a DNA Origami Scaffold. *Angew. Chem., Int. Ed.* **2016**, *55*, 7483−7486.
(297) Liu, M.; Fu, J.; Qi, X.; Wootten, S.; Woodbury, N. W.; Liu, Y.; Yan, H. A Three-Enzyme Pathway with an Optimised Geometric Arrangement to Facilitate Substrate Transfer. *ChemBioChem* **2016**, *17*, 1097−1101.
(298) Yang, Y. R.; Fu, J.; Wootten, S.; Qi, X.; Liu, M.; Yan, H.; Liu, Y. 2D Enzyme Cascade Network with Efficient Substrate Channeling by Swinging Arms. *ChemBioChem* **2018**, *19*, 212−216.
(299) Niemeyer, C. M.; Koehler, J.; Wuerdemann, C. DNA-Directed Assembly of Bienzymic Complexes from *in Vivo* Biotinylated NAD(P)H:FMN Oxidoreductase and Luciferase. *ChemBioChem* **2002**, *3*, 242−245.
(300) Ngo, T. A.; Nakata, E.; Saimura, M.; Morii, T. Spatially Organized Enzymes Drive Cofactor-Coupled Cascade Reactions. *J. Am. Chem. Soc.* **2016**, *138*, 3012−3021.


DOI: 10.1021/acscatal.9b02413
*ACS Catal.* 2019, 9, 10812−10869

(301) Rothemund, P. W. K. Folding DNA to Create Nanoscale Shapes and Patterns. *Nature* **2006**, *440*, 297−302.
(302) Douglas, S. M.; Dietz, H.; Liedl, T.; Högberg, B.; Graf, F.; Shih, W. M. Self-Assembly of DNA into Nanoscale Three-Dimensional Shapes. *Nature* **2009**, *459*, 414−418.
(303) Lin, C.; Liu, Y.; Yan, H. Designer DNA Nanoarchitectures. *Biochemistry* **2009**, *48*, 1663−1674.
(304) *NanoEngineer-1: 3D Multi-Scale Modeling and Simulation Program for Nano-Composites with Special Support for Structural DNA Nanotechnology*; Nanorex, Inc., 2015.
(305) Benson, E.; Mohammed, A.; Gardell, J.; Masich, S.; Czeizler, E.; Orponen, P.; Högberg, B. DNA Rendering of Polyhedral Meshes at the Nanoscale. *Nature* **2015**, *523*, 441−444.
(306) Veneziano, R.; Ratanalert, S.; Zhang, K.; Zhang, F.; Yan, H.; Chiu, W.; Bathe, M. Designer Nanoscale DNA Assemblies Programmed from the Top Down. *Science* **2016**, *352*, 1534−1534.
(307) Kim, D. N.; Kilchherr, F.; Dietz, H.; Bathe, M. Quantitative Prediction of 3D Solution Shape and Flexibility of Nucleic Acid Nanostructures. *Nucleic Acids Res.* **2012**, *40*, 2862−2868.
(308) Feldkamp, U.; Niemeyer, C. M. Rational Design of DNA Nanoarchitectures. *Angew. Chem., Int. Ed.* **2006**, *45*, 1856−1876.
(309) Niemeyer, C. M. Semisynthetic DNA−Protein Conjugates for Biosensing and Nanofabrication. *Angew. Chem., Int. Ed.* **2010**, *49*, 1200−1216.
(310) Yang, Y. R.; Liu, Y.; Yan, H. DNA Nanostructures as Programmable Biomolecular Scaffolds. *Bioconjugate Chem.* **2015**, *26*, 1381−1395.
(311) Niemeyer, C. M.; Sano, T.; Smith, C. L.; Cantor, C. R. Oligonucleotide-Directed Self-Assembly of Proteins: Semisynthetic DNA—Streptavidin Hybrid Molecules as Connectors for the Generation of Macroscopic Arrays and the Construction of Supramolecular Bioconjugates. *Nucleic Acids Res.* **1994**, *22*, 5530−5539.
(312) Thomsen, R. P. Engineering Peptides, Proteins, and Lipid Bilayers with DNA Nanotechnology. Ph.D. Thesis, Aarhus University, Aarhus, Denmark, 2018.
(313) Goodman, R. P.; Erben, C. M.; Malo, J.; Ho, W. M.; McKee, M. L.; Kapanidis, A. N.; Turberfield, A. J. A Facile Method for Reversibly Linking a Recombinant Protein to DNA. *ChemBioChem* **2009**, *10*, 1551−1557.
(314) Liu, C. C.; Schultz, P. Adding New Chemistries to the Genetic Code. *Annu. Rev. Biochem.* **2010**, *79*, 413−444.
(315) Keppler, A.; Gendreizig, S.; Gronemeyer, T.; Pick, H.; Vogel, H.; Johnsson, K. A General Method for the Covalent Labeling of Fusion Proteins with Small Molecules *in Vivo*. *Nat. Biotechnol.* **2003**, *21*, 86−86.
(316) Los, G. V.; Encell, L. P.; McDougall, M. G.; Hartzell, D. D.; Karassina, N.; Zimprich, C.; Wood, M. G.; Learish, R.; Ohana, R. F.; Urh, M.; Simpson, D.; Mendez, J.; Zimmerman, K.; Otto, P.; Vidugiris, G.; Zhu, J.; Darzins, A.; Klaubert, D. H.; Bulleit, R. F.; Wood, K. V. HaloTag: A Novel Protein Labeling Technology for Cell Imaging and Protein Analysis. *ACS Chem. Biol.* **2008**, *3*, 373−382.
(317) Rosen, C. B.; Kodal, A. L. B.; Nielsen, J. S.; Schaffert, D. H.; Scavenius, C.; Okholm, A. H.; Voigt, N. V.; Enghild, J. J.; Kjems, J.; Tørring, T.; Gothelf, K. V. Template-Directed Covalent Conjugation of DNA to Native Antibodies, Transferrin and Other Metal-Binding Proteins. *Nat. Chem.* **2014**, *6*, 804−809.
(318) Kodal, A. L. B.; Rosen, C. B.; Mortensen, M. R.; Tørring, T.; Gothelf, K. V. DNA-Templated Introduction of an Aldehyde Handle in Proteins. *ChemBioChem* **2016**, *17*, 1338−1342.
(319) Praetorius, F.; Dietz, H. Self-Assembly of Genetically Encoded DNA-Protein Hybrid Nanoscale Shapes. *Science* **2017**, *355*, eaam5488.
(320) Chen, R. P.; Blackstock, D.; Sun, Q.; Chen, W. Dynamic Protein Assembly by Programmable DNA Strand Displacement. *Nat. Chem.* **2018**, *10*, 474−481.
(321) Sheldon, R. A.; van Pelt, S. Enzyme Immobilisation in Biocatalysis: Why, What and How. *Chem. Soc. Rev.* **2013**, *42*, 6223−6235.
(322) Zdarta, J.; Meyer, A.; Jesionowski, T.; Pinelo, M. A General Overview of Support Materials for Enzyme Immobilization: Characteristics, Properties, Practical Utility. *Catalysts* **2018**, *8*, 92−118.
(323) Sheldon, R. A. Enzyme Immobilization: The Quest for Optimum Performance. *Adv. Synth. Catal.* **2007**, *349*, 1289−1307.
(324) Wu, C. S.; Wu, C. T.; Yang, Y. S.; Ko, F. H. An Enzymatic Kinetics Investigation into the Significantly Enhanced Activity of Functionalized Gold Nanoparticles. *Chem. Commun.* **2008**, 5327−5329.
(325) Dutta, N.; Mukhopadhyay, A.; Dasgupta, A. K.; Chakrabarti, K. Nanotechnology Enabled Enhancement of Enzyme Activity and Thermostability: Study on Imparied Pectate Lyase from Attenuated *Macrophomina phaseolina* in Presence of Hydroxyapatite Nanoparticle. *PLoS One* **2013**, *8*, e63567.
(326) Feng, W.; Ji, P. Enzymes Immobilized on Carbon Nanotubes. *Biotechnol. Adv.* **2011**, *29*, 889−895.
(327) Prlainović, N. Ž.; Bezbradica, D. I.; Rogan, J. R.; Uskoković, P. S.; Mijin, D. Ž.; Marinković, A. D. Surface Functionalization of Oxidized Multi-Walled Carbon Nanotubes: *Candida rugosa* Lipase Immobilization. *C. R. Chim.* **2016**, *19*, 363−370.
(328) Cang-Rong, J. T.; Pastorin, G. The Influence of Carbon Nanotubes on Enzyme Activity and Structure: Investigation of Different Immobilization Procedures through Enzyme Kinetics and Circular Dichroism Studies. *Nanotechnology* **2009**, *20*, 255102.
(329) Gong, A.; Zhu, C. T.; Xu, Y.; Wang, F. Q.; Tsabing, D. K.; Wu, F. A.; Wang, J. Moving and Unsinkable Graphene Sheets Immobilized Enzyme for Microfluidic Biocatalysis. *Sci. Rep.* **2017**, *7*, 4309.
(330) Devadoss, A.; Forsyth, R.; Bigham, R.; Abbasi, H.; Ali, M.; Tehrani, Z.; Liu, Y.; Guy, O. J. Ultrathin Functional Polymer Modified Graphene for Enhanced Enzymatic Electrochemical Sensing. *Biosensors* **2019**, *9*, 16.
(331) Silvera Batista, C. A.; Larson, R. G.; Kotov, N. A. Nonadditivity of Nanoparticle Interactions. *Science* **2015**, *350*, 1242477.
(332) Susumu, K.; Oh, E.; Delehanty, J. B.; Pinaud, F.; Gemmill, K. B.; Walper, S.; Breger, J.; Schroeder, M. J.; Stewart, M. H.; Jain, V.; Whitaker, C. M.; Huston, A. L.; Medintz, I. L. A New Family of Pyridine-Appended Multidentate Polymers as Hydrophilic Surface Ligands for Preparing Stable Biocompatible Quantum Dots. *Chem. Mater.* **2014**, *26*, 5327−5344.
(333) Kudr, J.; Haddad, Y.; Richtera, L.; Heger, Z.; Cernak, M.; Adam, V.; Zitka, O. Magnetic Nanoparticles: From Design and Synthesis to Real World Applications. *Nanomaterials* **2017**, *7*, 243−271.
(334) Serrano García, R.; Stafford, S.; Gun'ko, Y. K. Recent Progress in Synthesis and Functionalization of Multimodal Fluorescent-Magnetic Nanoparticles for Biological Applications. *Appl. Sci.* **2018**, *8*, 172−194.
(335) Cahyana, A. H.; Pratiwi, D.; Ardiansah, B. Citrate-Capped Superparamagnetic Iron Oxide (Fe3O4-CA) Nanocatalyst for Synthesis of Pyrimidine Derivative Compound as Antioxidative Agent. *IOP Conf. Ser.: Mater. Sci. Eng.* **2017**, *188*, 012008.
(336) Phan, C. M.; Nguyen, H. M. Role of Capping Agent in Wet Synthesis of Nanoparticles. *J. Phys. Chem. A* **2017**, *121*, 3213−3219.
(337) Netto, C. G. C. M.; Toma, H. E.; Andrade, L. H. Superparamagnetic Nanoparticles as Versatile Carriers and Supporting Materials for Enzymes. *J. Mol. Catal. B: Enzym.* **2013**, *85*−*86*, 71−92.
(338) Yildiz, I. Applications of Magnetic Nanoparticles in Biomedical Separation and Purification. *Nanotechnol. Rev.* **2016**, *5*, 331−340.
(339) Franzreb, M.; Siemann-Herzberg, M.; Hobley, T. J.; Thomas, O. R. Protein Purification Using Magnetic Adsorbent Particles. *Appl. Microbiol. Biotechnol.* **2006**, *70*, 505−516.
(340) Chen, Y. T.; Kolhatkar, A. G.; Zenasni, O.; Xu, S.; Lee, T. R. Biosensing Using Magnetic Particle Detection Techniques. *Sensors* **2017**, *17*, 2300−2335.
(341) Koh, I.; Josephson, L. Magnetic Nanoparticle Sensors. *Sensors* **2009**, *9*, 8130−8145.
(342) Mukai, C.; Gao, L.; Nelson, J. L.; Lata, J. P.; Cohen, R.; Wu, L.; Hinchman, M. M.; Bergkvist, M.; Sherwood, R. W.; Zhang, S.; Travis, A. J. Biomimicry Promotes the Efficiency of a 10-Step Sequential


DOI: 10.1021/acscatal.9b02413
*ACS Catal.* 2019, 9, 10812−10869

Enzymatic Reaction on Nanoparticles, Converting Glucose to Lactate. *Angew. Chem., Int. Ed.* **2017**, *56*, 235−238.
(343) Marques Netto, C. G. C.; Andrade, L. H.; Toma, H. E. Carbon Dioxide/Methanol Conversion Cycle Based on Cascade Enzymatic Reactions Supported on Superparamagnetic Nanoparticles. *An. Acad. Bras. Cienc.* **2018**, *90*, 593−606.
(344) Dong, Q.; Ouyang, L. M.; Yu, H. L.; Xu, J. H. Efficient Biosynthesis of Uridine Diphosphate Glucose from Maltodextrin by Multiple Enzymes Immobilized on Magnetic Nanoparticles. *Carbohydr. Res.* **2010**, *345*, 1622−1626.
(345) Jefferis, R. Review of Glycosylation Engineering of Biopharmaceuticals: Methods and Protocols. *mAbs* **2013**, *5*, 638−640.
(346) Moradi, S. V.; Hussein, W. M.; Varamini, P.; Simerska, P.; Toth, I. Glycosylation, an Effective Synthetic Strategy to Improve the Bioavailability of Therapeutic Peptides. *Chem. Sci.* **2016**, *7*, 2492−2500.
(347) Moretti, R.; Thorson, J. S. Enhancing the Latent Nucleotide Triphosphate Flexibility of the Glucose-1-Phosphate Thymidylyltransferase RmlA. *J. Biol. Chem.* **2007**, *282*, 16942−16947.
(348) Jiang, J.; Biggins, J. B.; Thorson, J. S. Expanding the Pyrimidine Diphosphosugar Repertoire: The Chemoenzymatic Synthesis of Amino- and Acetamidoglucopyranosyl Derivatives. *Angew. Chem., Int. Ed.* **2001**, *40*, 1502−1505.
(349) Yang, K.; Xu, N. S.; Su, W. W. Co-Immobilized Enzymes in Magnetic Chitosan Beads for Improved Hydrolysis of Macromolecular Substrates under a Time-Varying Magnetic Field. *J. Biotechnol.* **2010**, *148*, 119−127.
(350) Bera, D.; Qian, L.; Tseng, T.-K.; Holloway, P. H. Quantum Dots and Their Multimodal Applications: A Review. *Materials* **2010**, *3*, 2260−2345.
(351) Green, M. The Nature of Quantum Dot Capping Ligands. *J. Mater. Chem.* **2010**, *20*, 5797−5809.
(352) Kuo, W.-H. K.; Chase, H. A. Exploiting the Interactions between Poly-Histidine Fusion Tags and Immobilized Metal Ions. *Biotechnol. Lett.* **2011**, *33*, 1075−1084.
(353) Medintz, I. L.; Uyeda, H. T.; Goldman, E. R.; Mattoussi, H. Quantum Dot Bioconjugates for Imaging, Labelling, and Sensing. *Nat. Mater.* **2005**, *4*, 435−446.
(354) Kang, W.; Liu, J.; Wang, J.; Nie, Y.; Guo, Z.; Xia, J. Cascade Biocatalysis by Multienzyme-Nanoparticle Assemblies. *Bioconjugate Chem.* **2014**, *25*, 1387−1394.
(355) Breger, J. C.; Ancona, M. G.; Walper, S. A.; Oh, E.; Susumu, K.; Stewart, M. H.; Deschamps, J. R.; Medintz, I. L. Understanding How Nanoparticle Attachment Enhances Phosphotriesterase Kinetic Efficiency. *ACS Nano* **2015**, *9*, 8491−8503.
(356) Claussen, J. C.; Malanoski, A.; Breger, J. C.; Oh, E.; Walper, S. A.; Susumu, K.; Goswami, R.; Deschamps, J. R.; Medintz, I. L. Probing the Enzymatic Activity of Alkaline Phosphatase within Quantum Dot Bioconjugates. *J. Phys. Chem. C* **2015**, *119*, 2208−2221.
(357) Brown, C. W., III; Oh, E.; Hastman, D. A., Jr; Walper, S. A.; Susumu, K.; Stewart, M. H.; Deschamps, J. R.; Medintz, I. L. Kinetic Enhancement of the Diffusion-Limited Enzyme Beta-Galactosidase When Displayed with Quantum Dots. *RSC Adv.* **2015**, *5*, 93089−93094.
(358) Griffin, J. H.; Criddle, R. S. Substrate-Inhibited Lactate Dhydrogenase, Reaction Mechanism and Essential Role of Dissociated Subunits. *Biochemistry* **1970**, *9*, 1195−1205.
(359) Alves, N. J.; Moore, M.; Johnson, B. J.; Dean, S. N.; Turner, K. B.; Medintz, I. L.; Walper, S. A. Environmental Decontamination of a Chemical Warfare Simulant Utilizing a Membrane Vesicle-Encapsulated Phosphotriesterase. *ACS Appl. Mater. Interfaces* **2018**, *10*, 15712−15719.
(360) Alves, N. J.; Turner, K. B.; Daniele, M. A.; Oh, E.; Medintz, I. L.; Walper, S. A. Bacterial Nanobioreactors–Directing Enzyme Packaging into Bacterial Outer Membrane Vesicles. *ACS Appl. Mater. Interfaces* **2015**, *7*, 24963−24972.
(361) Breger, J.; Walper, S.; Ancona, M.; Stewart, M.; Oh, E.; Susumu, K.; Medintz, I. Understanding the Enhanced Kinetics of Enzyme-Quantum Dot Constructs. *MRS Adv.* **2016**, *1*, 3831−3836.
(362) Breger, J. C.; Sapsford, K. E.; Ganek, J.; Susumu, K.; Stewart, M. H.; Medintz, I. L. Detecting Kallikrein Proteolytic Activity with Peptide-Quantum Dot Nanosensors. *ACS Appl. Mater. Interfaces* **2014**, *6*, 11529−11535.
(363) Breger, J. C.; Walper, S. A.; Oh, E.; Susumu, K.; Stewart, M. H.; Deschamps, J. R.; Medintz, I. L. Quantum Dot Display Enhances Activity of a Phosphotriesterase Trimer. *Chem. Commun.* **2015**, *51*, 6403−6406.
(364) Diaz, S. A.; Breger, J. C.; Medintz, I. L. Monitoring Enzymatic Proteolysis Using Either Enzyme- or Substrate Bioconjugated Quantum Dots. *Methods Enzymol.* **2016**, *571*, 19−54.
(365) Hondred, J. A.; Breger, J. C.; Alves, N. J.; Trammell, S. A.; Walper, S. W.; Medintz, I. L.; Claussen, J. C. Printed Graphene Electrochemical Biosensors Fabricated by Inkjet Maskless Lithography for Rapid and Sensitive Detection of Organophosphates. *ACS Appl. Mater. Interfaces* **2018**, *10*, 11125−11134.
(366) Hondred, J. A.; Breger, J. C.; Garland, N. T.; Oh, E.; Susumu, K.; Walper, S. A.; Medintz, I. L.; Claussen, J. C. Enhanced Enzyme Activity of Phosphotriesterase Trimer Conjugated on Gold Nanoparticles for Pesticide Detection. *Analyst* **2017**, *142*, 3261−3271.
(367) Hondred, J. A.; Medintz, I. L.; Claussen, J. C. Enhanced Electrochemical Biosensor and Supercapacitor with 3D Porous Architectured Graphene Via Salt Impregnated Inkjet Maskless Lithography. *Nanoscale Horiz* **2019**, *4*, 735−746.
(368) Malanoski, A. P.; Breger, J. C.; Brown, C. W. I.; Deschamps, J. R.; Susumu, K.; Oh, E.; Anderson, G. P.; Walper, S. A.; Medintz, I. L. Kinetic Enhancement in High-Activity Enzyme Complexes Attached to Nanoparticles. *Nanoscale Horiz* **2017**, *2*, 241−252.
(369) Medintz, I. L. Interesting Developments at the Nanoparticle-Protein Interface: Imprlications for Next Generation Drug Delivery. *Ther. Delivery* **2016**, *7*, 513−516.
(370) Samanta, A.; Breger, J. C.; Susumu, K.; Oh, E.; Walper, S. A.; Bassim, N.; Medintz, I. L. DNA-Nanoparticle Composites Synergistically Enhance Organophosphate Hydrolase Enzymatic Activity. *ACS Appl. Nano Mater.* **2018**, *1*, 3091−3097.
(371) Samanta, A.; Walper, S. A.; Susumu, K.; Dwyer, C. L.; Medintz, I. L. An Enzymatically-Sensitized Sequential and Concentric Energy Transfer Relay Self-Assembled around Semiconductor Quantum Dots. *Nanoscale* **2015**, *7*, 7603−7614.
(372) Vranish, J. N.; Ancona, M. G.; Walper, S. A.; Medintz, I. L. Pursuing the Promise of Enzymatic Enhancement with Nanoparticle Assemblies. *Langmuir* **2018**, *34*, 2901−2925.
(373) Huang, X.; Ren, J. Nanomaterial-Based Chemiluminescence Resonance Energy Transfer: A Strategy To Develop New Analytical Methods. *TrAC, Trends Anal. Chem.* **2012**, *40*, 77−89.
(374) Limoges, B.; Marchal, D.; Mavré, F.; Savéant, J.-M. High Amplification Rates from the Association of Two Enzymes Confined within a Nanometric Layer Immobilized on an Electrode: Modeling and Illustrating Example. *J. Am. Chem. Soc.* **2006**, *128*, 6014−6015.
(375) Xu, S.; Li, X.; Li, C.; Li, J.; Zhang, X.; Wu, P.; Hou, X. In Situ Generation and Consumption of H2O2 by Bienzyme-Quantum Dots Bioconjugates for Improved Chemiluminescence Resonance Energy Transfer. *Anal. Chem.* **2016**, *88*, 6418−6424.
(376) Dykman, L. A.; Khlebtsov, N. G. Gold Nanoparticles in Biology and Medicine: Recent Advances and Prospects. *Acta Nat.* **2011**, *3*, 34−55.
(377) Tiwari, P. M.; Vig, K.; Dennis, V. A.; Singh, S. R. Functionalized Gold Nanoparticles and Their Biomedical Applications. *Nanomaterials* **2011**, *1*, 31−63.
(378) Zhou, J.; Ralston, J.; Sedev, R.; Beattie, D. A. Functionalized Gold Nanoparticles: Synthesis, Structure and Colloid Stability. *J. Colloid Interface Sci.* **2009**, *331*, 251−262.
(379) Grzelczak, M.; Pérez-Juste, J.; Mulvaney, P.; Liz-Marzán, L. M. Shape Control in Gold Nanoparticles. *Chem. Soc. Rev.* **2008**, *37*, 1783−1791.
(380) Lata, J. P.; Gao, L.; Mukai, C.; Cohen, R.; Nelson, J. L.; Anguish, L.; Coonrod, S.; Travis, A. J. Effects of Nanoparticle Size on Multilayer Formation and Kinetics of Tethered Enzymes. *Bioconjugate Chem.* **2015**, *26*, 1931−1938.


DOI: 10.1021/acscatal.9b02413
*ACS Catal.* 2019, 9, 10812−10869

(381) Rao, K. S.; El-Hami, K.; Kodaki, T.; Matsushige, K.; Makino, K. A. Novel Method for Synthesis of Silica Nanoparticles. *J. Colloid Interface Sci.* **2005**, *289*, 125−131.
(382) Wu, S. H.; Mou, C. Y.; Lin, H. P. Synthesis of Mesoporous Silica Nanoparticles. *Chem. Soc. Rev.* **2013**, *42*, 3862−3875.
(383) Liberman, A.; Mendez, N.; Trogler, W. C.; Kummel, A. C. Syntehsis and Surface Functionalization of Silica Nanoparticles for Nanomedicine. *Surf. Sci. Rep.* **2014**, *69*, 132−158.
(384) Furukawa, H.; Cordova, K. E.; O'Keeffe, M.; Yaghi, O. M. The Chemistry and Applications of Metal-Organic Frameworks. *Science* **2013**, *341*, 1230444.
(385) Yuan, S.; Feng, L.; Wang, K.; Pang, J.; Bosch, M.; Lollar, C.; Sun, Y.; Qin, J.; Yang, X.; Zhang, P.; Wang, Q.; Zou, L.; Zhang, Y.; Zhang, L.; Fang, Y.; Li, J.; Zhou, H.-C. Stable Metal−Organic Frameworks: Design, Synthesis, and Applications. *Adv. Mater.* **2018**, *30*, 1704303−1704337.
(386) Majewski, M. B.; Howarth, A. J.; Li, P.; Wasielewski, M. R.; Hupp, J. T.; Farha, O. K. Enzyme Encapsulation in Metal−Organic Frameworks for Applications in Catalysis. *CrystEngComm* **2017**, *19*, 4082−4091.
(387) Mehta, J.; Bhardwaj, N.; Bhardwaj, S. K.; Kim, K.-H.; Deep, A. Recent Advances in Enzyme Immobilization Techniques: Metal-Organic Frameworks as Novel Substrates. *Coord. Chem. Rev.* **2016**, *322*, 30−40.
(388) Li, P.; Chen, Q.; Wang, T. C.; Vermeulen, N. A.; Mehdi, B. L.; Dohnalkova, A.; Browning, N. D.; Shen, D.; Anderson, R.; Gómez-Gualdrón, D. A.; Cetin, F. M.; Jagiello, J.; Asiri, A. M.; Stoddart, J. F.; Farha, O. K. Hierarchically Engineered Mesoporous Metal-Organic Frameworks toward Cell-Free Immobilized Enzyme Systems. *Chem.* **2018**, *4*, 1022−1034.
(389) Howarth, A. J.; Liu, Y.; Li, P.; Li, Z.; Wang, T. C.; Hupp, J. T.; Farha, O. K. Chemical, Thermal and Mechanical Stabilities of Metal−Organic Frameworks. *Nat. Rev. Mater.* **2016**, *1*, 15018.
(390) Li, P.; Moon, S. Y.; Guelta, M. A.; Lin, L.; Gomez-Gualdron, D. A.; Snurr, R. Q.; Harvey, S. P.; Hupp, J. T.; Farha, O. K. Nanosizing a Metal-Organic Framework Enzyme Carrier for Accelerating Nerve Agent Hydrolysis. *ACS Nano* **2016**, *10*, 9174−9182.
(391) Lyu, F.; Zhang, Y.; Zare, R. N.; Ge, J.; Liu, Z. One-Pot Synthesis of Protein-Embedded Metal-Organic Frameworks with Enhanced Biological Activities. *Nano Lett.* **2014**, *14*, 5761−5765.
(392) Katyal, P.; Yang, Y.; Vinogradova, O.; Lin, Y. Expression of Cellulolytic Enzyme as a Fusion Protein That Reacts Specifically with a Polymeric Scaffold. *Methods Enzymol.* **2017**, *590*, 259−276.
(393) Schmidt-Dannert, C.; Lopez-Gallego, F. A Roadmap for Biocatalysis - Functional and Spatial Orchestration of Enzyme Cascades. *Microb. Biotechnol.* **2016**, *9*, 601−609.
(394) Ji, X.; Su, Z.; Wang, P.; Ma, G.; Zhang, S. Tethering of Nicotinamide Adenine Dinucleotide inside Hollow Nanofibers for High-Yield Synthesis of Methanol from Carbon Dioxide Catalyzed by Coencapsulated Multienzymes. *ACS Nano* **2015**, *9*, 4600−4610.
(395) Zore, O. V.; Pande, P.; Okifo, O.; Basu, A. K.; Kasi, R. M.; Kumar, C. V. Nanoarmoring: Strategies for Preparation of Multi-Catalytic Enzyme Polymer Conjugates and Enhancement of High Temperature Biocatalysis. *RSC Adv.* **2017**, *7*, 29563−29574.
(396) Ajayan, P. M. Nanotubes from Carbon. *Chem. Rev.* **1999**, *99*, 1787−1799.
(397) Zhang, Y.; Pan, D.; Zhou, Q.; Zhao, J.; Pan, N.; Zhang, Y.; Wang, L.-x.; Shen, Y. An Enzyme Cascade-Based Electrochemical Immunoassay Using a Polydopamine−Carbon Nanotube Nanocomposite for Signal Amplification. *J. Mater. Chem. B* **2018**, *6*, 8180−8187.
(398) Zhang, Y.; Arugula, M. A.; Williams, S. T.; Minteer, S. D.; Simonian, A. L. Layer-by-Layer Assembly of Carbon Nanotubes Modified with Invertase/Glucose Dehydrogenase Cascade for Sucrose/$O_2$ Biofuel Cell. *J. Electrochem. Soc.* **2016**, *163*, F449−F454.
(399) Varaprasad, K.; Raghavendra, G. M.; Jayaramudu, T.; Yallapu, M. M.; Sadiku, R. A Mini Review on Hydrogels Classification and Recent Developments in Miscellaneous Applications. *Mater. Sci. Eng., C* **2017**, *79*, 958−971.
(400) Laftah, W. A.; Hashim, S.; Ibrahim, A. N. Polymer Hydrogels: A Review. *Polym.-Plast. Technol. Eng.* **2011**, *50*, 1475−1486.
(401) Wu, Q.; He, Z.; Wang, X.; Zhang, Q.; Wei, Q.; Ma, S.; Ma, C.; Li, J.; Wang, Q. Cascade Enzymes within Self-Assembled Hybrid Nanogel Mimicked Neutrophil Lysosomes for Singlet Oxygen Elevated Cancer Therapy. *Nat. Commun.* **2019**, *10*, 240.
(402) Schmieg, B.; Dobber, J.; Kirschhofer, F.; Pohl, M.; Franzreb, M. Advantages of Hydrogel-Based 3D-Printed Enzyme Reactors and Their Limitations for Biocatalysis. *Front. Bioeng. Biotechnol.* **2019**, *6*, 211.
(403) Sapsford, K. E.; Tyner, K. M.; Dair, B. J.; Deschamps, J. R.; Medintz, I. L. Analyzing Nanomaterial Bioconjugates: A Review of Current and Emerging Purification and Characterization Techniques. *Anal. Chem.* **2011**, *83*, 4453−4488.
(404) Yang, J.; Kickhoefer, V. A.; Ng, B. C.; Gopal, A.; Bentolila, L. A.; John, S.; Tolbert, S. H.; Rome, L. H. Vaults Are Dynamically Unconstrained Cytoplasmic Nanoparticles Capable of Half Vault Exchange. *ACS Nano* **2010**, *4*, 7229−7240.
(405) Molinnus, D.; Poghossian, A.; Keusgen, M.; Katz, E.; Schöning, M. J. Coupling of Biomolecular Logic Gates with Electronic Transducers: From Single Enzyme Logic Gates to Sense/Act/Treat Chips. *Electroanalysis* **2017**, *29*, 1840−1849.
(406) Privman, M.; Guz, N.; Katz, E. Enzyme-Logic Digital Biosensors for Biomedical Applications. *Int. J. Unconv. Comput.* **2018**, *13*, 435−476.


DOI: 10.1021/acscatal.9b02413
*ACS Catal.* 2019, 9, 10812−10869